

Aus der Universitätsklinik für Thorax-, Herz- und
Gefäßchirurgie Tübingen
Sektion Medizinische Werkstoffkunde und Technologie

Peel Bond Strength between 3D-printing Tray Materials
and Elastomeric Impression/Adhesive Systems: A
Laboratory Study

Inaugural-Dissertation
zur Erlangung des Doktorgrades
der Zahnheilkunde

der Medizinischen Fakultät
der Eberhard Karls Universität
zu Tübingen

vorgelegt von
Xu, Yichen

2019

Dekan: Professor Dr. I. B. Autenrieth

1. Berichterstatter: Professor Dr. J. Geis-Gerstorfer

2. Berichterstatter: Professor Dr. D. Wolff

Tag der Disputation: 07.10.2019

Contents

Contents.....	I
List of Tables	III
List of Figures	IV
List of Abbreviations	X
1. Introduction	1
1.1 Custom trays	1
1.2 CAD and AM of custom trays.....	2
1.2.1 CAD.....	2
1.2.2 AM.....	3
1.2.3 Digital workflow of fabricating custom trays using CAD and AM	4
1.2.4 Available AM technologies and materials for custom tray fabrication	5
1.3 Bonding between custom trays and impression/adhesive systems	11
1.3.1 Impression materials.....	12
1.3.2 Adhesives.....	13
1.3.3 Custom tray materials.....	15
1.3.4 Surface treatments	16
1.4 Research aim.....	18
2. Materials and Methods	19
2.1 CAD of Test Blocks	19
2.2 AM of test blocks	20
2.2.1 Printing test blocks using FFF.....	20
2.2.2 Printing test blocks using SLA.....	22
2.2.3 Printing blocks using DLP.....	25
2.3 Fabrication of reference test blocks	29
2.3.1 CAD and AM of molds used for fabricating wax spacer and reference test block	29
2.3.2 Fabrication process of reference test block	33
2.4 CAD and AM of carrier	37
2.5 SEM analysis.....	39
2.6 Roughness measurement.....	42
2.7 Peel bond strength test	43

2.8 Failure mode analysis.....	48
2.9 Statistical analysis	49
3. Results.....	50
3.1 SEM	50
3.2 Roughness measurement.....	53
3.3 Peel bond strength test	60
3.4 Failure mode	66
4. Discussion	72
5. Conclusion	88
6. Summary	90
7. Zusammenfassung	92
8. References.....	94
Appendix	XII

List of Tables

Table 1: Conventional and 3D-printing custom tray materials in this study.	11
Table 2: 3D roughness parameters that might be related to the bonding.	17
Table 3: Impression/adhesive systems used in the present study.	46
Table 4: Classification and definition of the failure mode.	48
Table 5: Mean (standard deviation) line peel bond strength (N/m) and areal peel bond strength (kPa) of each group (n = 12).	63
Table 6: Two-way ANOVA of peel bond strength.	63
Table 7: Different crosshead speeds used in the related studies.	82

List of Figures

Figure 1: A typical digital workflow of fabricating custom tray.	5
Figure 2: The working principle of FFF.	6
Figure 3: The working principle of SLA.	8
Figure 4: The working principle of DLP.	9
Figure 5: CAD of the test blocks in OpenSCAD. (a) The cuboid base; (b) A cuboid handle was added onto the top surface of the base with 45 degrees; (c) A connector was used to connect the base and the handle; (d) A centered hole was added on the handle with a diameter of 0.5 mm.	19
Figure 6: The printing direction and layout of the FFF-printed test blocks. Twenty samples were printed on the supporting raft layer with a margin width of 5 mm.	20
Figure 7: The FFF 3D printer and printing material. (a) The FFF 3D printer “Replicator+”; (b) The spool of PLA filament.	21
Figure 8: The FFF-printed test block (white scale: 10 mm).	21
Figure 9: The printing direction and layout of the SLA-printed test blocks. Twelve specimens were set to be printed directly on the printing platform without supporting material.	22
Figure 10: The SLA 3D printer and printing material. (a) The SLA 3D printer “Form 2”; (b) The light-curing resin “Dental LT Clear Resin”.	23
Figure 11: Post-processing devices of the SLA 3D printer. (a) Post-cleaning device “Form Wash”; (b) Post-curing device “Form Cure”.	24
Figure 12: The SLA-printed test block (white scale: 10 mm).	24
Figure 13: The printing direction and layout on the build platform in Netfabb.	25
Figure 14: The supporting grid and supporting materials of the test block.	26
Figure 15: The DPL 3D printer, printing material, and self-developed roller mixer. (a) The DLP 3D printer “SOLFLEX 170”; (b) The custom tray material “FREEPRINT tray”; (c) The self-developed roller mixer.	27

Figure 16: The flash-light polymerization device “Otoflash G171”. 28

Figure 17: The DLP-printed test block (white scale: 10 mm). 28

Figure 18: The mold of wax spacer. (a) The original prototype designed in OpenSCAD;
 (b) The mold size of wax spacer. 29

Figure 19: Molds of reference test block reserved 1.25 mm height for the baseplate wax,
 so the total height of the mold base was set to 7.25 mm. The reference custom
 tray material could polymerize against the 1.25 mm thick baseplate wax and
 maintain the base height of 6 mm. 30

Figure 20: Five CAD-designed molds of reference test block. (a) The design with the
 centered cylinder; (b) The design with the centered cylinder, without the upper
 border. (c) The design with upper border, without the centered cylinder; (d) The
 design without the centered cylinder and the upper border; (e) The design
 without the centered cylinder and the upper border, a portion of the posterior
 border was removed. 31

Figure 21: The cured test blocks cannot be removed from the molds with cylinder design.
 (a) The test block firmly remained in the mold designed in Figure 20a; (b)
 Excessive removal force resulted in the mold fracture, the cylinder remained in
 the test block (red arrow) (white scale: 10 mm). 32

Figure 22: The cured test blocks could be removed from the molds without cylinder
 design. The test block fabricated by the mold designed in Figure 20c showed the
 best accuracy (middle). The red circles showed the inaccurate parts of the other
 two test blocks. (white scale: 10 mm). 33

Figure 23: Fabrication of the wax spacer (white scale: 10 mm). 33

Figure 24: Vaseline was applied onto the inner walls of the mold. 34

Figure 25: The UV-light curing of the reference test block. (a) The first resin layer was
 cured by the UV-light device “Dentacolor XS”; (b) Rest of the resin layers were
 cured by the UV-light device “LML2000”. 35

Figure 26: Marking the centered hole (white scale: 10 mm). 35

Figure 27: Drilling the centered hole of the reference test block. (a) Reference test block was fixed on a universal vice; (b) The parameter setting of the drilling machine “B 13S”; (c) The centered hole was being drilled.	36
Figure 28: The fabricated reference test block.	37
Figure 29: CAD of the carrier. (a) The CAD model of the carrier; (b) Two lateral cubes of the carrier; (c) Upper sheet of the carrier; (d) The central void part of the carrier could accommodate the test block base.	38
Figure 30: The printing direction and layout of the carrier.	39
Figure 31: The SLA-printed carrier (white scale: 10 mm).	39
Figure 32: Sputter coater “BAL-TEC SCD 050”.	40
Figure 33: SEM system “Zeiss LEO 1430”.	40
Figure 34: Sample sputtering before SEM analysis. (a) The test surface and holder were connected with liquid silver paint to conduct electricity; (b) Au-Pd coating was sputtered on the test surface of each sample.	41
Figure 35: Devices used for roughness measurement. (a) The leveling device “Leitz Schliﬀpresse”; (b) The proliometer “Mahr S6P”.	42
Figure 36: Grouping of peel bond strength test.	43
Figure 37: Preparation of the universal adaptor. (a) Three screws were inserted into the adaptor; (b) The filling material was 3 mm from the top edge of the adaptor (white scale: 10 mm).	44
Figure 38: Preparation of the test block. (a) Vaseline was applied to the surrounding walls around the test surface; (b) The carrier and the test block were bonded by molten adhesive wax to construct a test complex; (c) A thin layer of the adhesive was smeared on the test surface (white scale: 10 mm).	45
Figure 39: The impression setting in the peel bond strength test. (a) The test complex was fixed by a custom-made loading device with a perpendicular weight of 1.4 kg; (b) The custom-made loading device was enclosed in a 37 °C incubator to simulate the intraoral temperature.	46

Figure 40: Peel bond strength test. (a) The universal testing machine; (b) A tensile load at a crosshead speed of 300 mm/min was applied to the test block; (c) The test block was detached from the impression material after peeling.	47
Figure 41: SEM images of the test surface of the SLA-printed Dental LT test block. (a) 100 × magnification; (b) 500 × magnification; (c) 1000 × magnification; (d) 2000 × magnification.	50
Figure 42: SEM images of the test surface of the DLP-printed FREEPRINT tray test block. (a) 100 × magnification; (b) 500 × magnification; (c) 1000 × magnification; (d) 2000 × magnification.	51
Figure 43: SEM images of the test surface of the FFF-printed PLA test block. (a) 100 × magnification; (b) 500 × magnification; (c) 1000 × magnification; (d) 2000 × magnification.....	52
Figure 44: SEM images of the test surface of the conventionally light-cured Zeta tray LC test block. (a) 100 × magnification; (b) 500 × magnification; (c) 1000 × magnification; (d) 2000 × magnification.	53
Figure 45: Mean (standard deviation) Sa values of all material groups (n = 7). * represents a statistically significant difference.	54
Figure 46: Mean (standard deviation) Ssk values of all material groups (n = 7). * represents a statistically significant difference.....	55
Figure 47: Mean (standard deviation) Vvc values of all material groups (n = 7). * represents a statistically significant difference.....	56
Figure 48: Mean (standard deviation) Vvv values of all material groups (n = 7). * represents a statistically significant difference.....	57
Figure 49: Mean (standard deviation) Sdr values of all material groups (n = 7). * represents a statistically significant difference.....	58
Figure 50: 3D-reconstructed surface topographies of the test blocks (15% vertical amplification). (a) Dental LT; (b) FREEPRINT tray; (c) PLA; (d) Reference.	59
Figure 51: Representative peeling force-distance curves of adhesive failure of each	

tray-impression material combination.....	60
Figure 52: Representative peeling force-distance curves of mixed failure of each tray-impression material combination.....	61
Figure 53: Representative peeling force-distance curves of cohesive failure of each tray material-VSXE combination.	62
Figure 54: Peel bond strength of each tray-impression material combination (grouped by impression/adhesive system, box plot, n = 12). + represents the mean value of each group. (a) Line peel bond strength; (b) Areal peel bond strength.	64
Figure 55: Peel bond strength of each tray-impression material combination (grouped by tray material, box plot, n = 12). + represents the mean value of each group. (a) Line peel bond strength; (b) Areal peel bond strength.	65
Figure 56: Representative light-microscopical images of test surfaces that adhesively failed after peeling (6.3 × and 32 × magnification).....	67
Figure 57: Representative light-microscopical images of test surfaces that mixedly failed after peeling (6.3 × and 32 × magnification).....	68
Figure 58: Representative light-microscopical images of test surfaces that cohesively failed after peeling (6.3 × and 32 × magnification).....	69
Figure 59: Constituent ratio of failure mode of each group (n = 12).	70
Figure 60: Representative light-microscopical images of adhesive failure between the VSXE impression and the Dental LT tray material (6.3 × and 32 × magnification). (a) VSXE impression surface after peeling; (b) Dental LT surface after peeling; (c) The detachment between adhesive and impression material resulted in the defect on the peeled impression surface, exposing the subjacent impression material (red arrow). The rupture within the adhesive layer led the adhesive remain on the peeled impression surface (green arrow); (d) The adhesive debonded with impression material integrally remained on the peeled tray material surface, which presented to be raised and highly transparent (red arrow). The ruptured adhesive remained on the peeled tray material surface and	

presented to be frosted (green arrow)..... 71

Figure 61: Coronal section of SLA- and FFF-printed layers. The unfilled areas existed between the FFF-printed layers..... 72

Figure 62: The generation of DLP-printed surface texture. The pattern of each layer is pixelated by the DMD. During this process, the edge could be turned from straight to stepped. Successive stepped edges accumulate layer by layer along the build direction, generating the observed surface texture on the test block. The orientation of the DLP-printed surface texture is the same as the build direction of the test block. 74

Figure 63: The schematic of V_{vc} and V_{vv} 77

Figure 64: Comparison of peel tests. (a) An example of standard peel test: a film is peeled from a rigid object; (b) The peel test performed between test block and elastic impression. 79

Figure 65: The adhesive of PE has a high elongation, which leads to the adhesive to be pulled into filament behind the peeling frontier. 80

Figure 66: Categorization of failure modes between tray and impression material..... 84

List of Abbreviations

3D	Three-dimensional
AM	Additive manufacturing
ANOVA	Analysis of variance
A-silicone	Addition silicone
CAD	Computer-aided design
CAM	Computer-aided manufacturing
C-silicone	Condensation silicone
DLP	Digital light processing
DMD	Digital micromirror device
FDM	Fused deposition modeling
FEA	Finite Element Analysis
FFF	Fused filament fabrication
IPA	Isopropyl alcohol
LEDs	Light-emitting diodes
PE	Polyether
PLA	Poly lactide
PS	Polysulfide
Sa	Arithmetic mean height
Sdr	Developed interfacial area ratio
SEM	Scanning electron microscopy
SLA	Stereolithography
SLM	Selective laser melting
SLS	Selective laser sintering
SM	Subtractive manufacturing
Ssk	Skewness
STL	Standard tessellation language
Svi	Valley fluid retention index

UV	Ultraviolet
VDFS	Vat Deflection Feedback System
VPS	Vinyl polysiloxane
VSXE	Vinylsiloxanether
V_{vc}	Core void volume
V_{vv}	Dales void volume

1. Introduction

1.1 Custom trays

Impression trays are used for supporting, confining and controlling impression materials while recording oral impressions. According to the fabrication method, impression trays are classified as stock trays and custom trays [1]. Stock trays are pre-made with a variety of sizes and shapes. According to the form of each patient's dental arch, the appropriate stock tray must be selected to achieve the best fit. Even so, the limited sizes and shapes of stock tray cannot fully meet clinical requirements because of intersubject variations of patients. Essential modifications of stock trays are usually performed for a better fit [2], such as adjusting the flange angle for a wide dentition and adding baseplate wax to extend the tray border for a deep vestibule. In contrast, custom trays have a better fit than stock trays since they are individually fabricated according to each patient's dentition and dental arch [3]. Since no additional modification is needed for custom trays after fabrication, custom trays are more manageable for dentists. The polymerization-induced shrinkage of elastomeric impression material is proportional to the impression thickness [4]. By providing a uniform thickness of impression material, custom trays minimize the inaccuracy of the final impressions, thus ensuring the precision of the working models and prostheses [5]. Compared to the stock tray, less impression material is used by the custom tray due to its more compatible size [6]. The saved expense of impression material may compensate for the cost of custom tray fabrication to some extent. In addition, streamline-designed custom trays can reduce the discomfort of patients, and appropriate flange extension of custom trays would minimize the tissue distortion.

Despite the abovementioned advantages, the frequency of utilizing custom trays is limited by some critical factors. In conventional techniques, custom trays need to be fabricated by technicians in a dental laboratory. The fabricating process is complex with quite a few steps, namely recording primary impression, perfusing primary cast,

blocking undercuts, marking relief areas and tray border, adapting relief wax, adapting wax spacer, making tissue stops, applying separating medium, adapting tray material on wax spacer, fabricating tray handle, trimming margin extension and molding tray border [7].

In addition to the need for specific equipment and materials, the fabricating process also takes a long time, which often results in more visits of patients. Unlike the reusable stock trays, custom trays are usually discarded after impression taking since they are designed only for an individual patient. The extra labor, economy and time costs on fabrication become the disadvantages of custom trays [8], which make custom trays less frequently used [4,9]. With the rapid development of digital technology in dentistry, computer-aided design (CAD) and additive manufacturing (AM) has shown promise to overcome these disadvantages and provide a feasible solution.

1.2 CAD and AM of custom trays

1.2.1 CAD

For dentistry, CAD is the term to describe designing dental products using a software system. First appeared in the 1980s [10], the early dental CAD software systems were mainly developed for dental prostheses, such as crowns, veneers, inlays, and bridges, but seldom for custom trays. The possible reason might be the initial computer-aided manufacturing (CAM) technique was based on subtractive manufacturing (SM), and to mill a bulky custom tray might induce a large amount of material wasted, thus significantly increasing the cost. With the application of AM in dentistry, newly developed CAD systems have added the function of custom tray design, such as 3shape and Zirkonzahn. To date, only a few studies are related to the custom trays fabricated by CAD and AM. Even so, attractive advantages of CAD/AM-fabricated custom trays have been reported. Huang et al. used a novel CAD method to design custom trays for maxillectomy patients, the result showed the impressions recorded by the CAD/AM-fabricated custom trays and by conventionally fabricated ones did not

statistically differ in thickness, but the thickness of the former was more even [11]. Chen et al. indicated the custom trays fabricated by CAD and AM for edentulous jaws showed better accuracy compared to the hand-made ones. They concluded CAD and AM are efficient to produce custom trays with reliable reproducibility and accuracy [8]. Through comparing the fabrication time, Wei et al. found that using CAD and AM to fabricate custom trays would consume less time than using conventional technique and improve the efficiency both in clinical and laboratory process [12]. A clinical evaluation from Sun et al. demonstrated impressions recorded by CAD/AM-fabricated custom trays had better thickness distribution than those recorded by conventionally fabricated custom trays [13]. Since the CAD process has a high degree of freedom, custom trays can be designed to explore novel impression techniques. For example, by CAD, custom trays can be modified to equip a Gothic arch, by this design the centric relation could be recorded during the impression taking [2,14], or to accommodate a 3D-printed splinting framework to record impression for edentulous jaw with multiple implants [15].

1.2.2 AM

Longly, CAM in dentistry is based on SM [16], which works through removing unwanted materials away from a material block until the final product is manufactured. The manufacturing process of SM is numerically controlled by a computer so that sophisticated dental products could be accurately manufactured with consistent quality [16]. In recent years, the explorations of AM for dental applications is fastly growing due to its unique advantages over SM: (1) AM is able to manufacture complex structures that are difficult for SM, such as hollow interior sections; (2) AM only uses the materials that are needed for manufacturing, rather than cutting materials away and discarding them, therefore there is almost no material wasted [17].

The concept of AM, also termed three-dimensional (3D) printing, was first introduced by Chuck Hull in the 1980s [18]. Being the opposite of subtractive manufacturing, AM

joins materials together to construct a 3D object. The printing process is achieved by a layering method: materials are selectively hardened within each layer, and successive layers are sequentially accumulated in the vertical axis [19].

In dentistry, there are many applications that need to be customized, such as trays, dentures, appliances, splints, surgical guides, abutments, and even implants. With the developments of 3D-printing technologies and available materials, increasing 3D-printed products are being explored for dental applications [20]. For custom tray fabrication, 3D printing seems promising due to its high resolution, rapid manufacturing and low waste of raw material.

1.2.3 Digital workflow of fabricating custom trays using CAD and AM

Using CAD and AM to fabricate custom trays primarily consists of three processes, namely data acquisition, data processing, and AM. A typical digital workflow for custom tray fabrication is shown in Figure 1. The purpose of data acquisition is to acquire a digitized primary cast, on which a custom tray can be designed. This process can be achieved by direct intraoral scanning or by indirect primary cast scanning. Afterward, the acquired data is then transmitted to a computer for data processing. With the help of CAD software, custom trays are designed on the digitized primary cast. The conventional procedure that needs to be manipulated by dental technicians is carried out virtually on a computer screen, such as blocking undercuts and marking tray border. By following the step-by-step instructions, dentists and dental technicians are able to create and modify the digital custom tray model easily and intuitively. The design can be highly customized to adjust details according to clinical requirements, such as modifying flange extension and controlling the distance from the custom tray to oral tissues.

After designing, the data of custom tray need to be saved as standard tessellation

language (SLT) format and then submitted to a 3D-printing preparing software. Most 3D printers in the market have their corresponding 3D-printing preparing software, only a small fraction of 3D-printing preparing software is embedded in the 3D printers. Unlike CAD software, 3D-printing preparing software does not have the function of designing or modifying the original data. However, it helps to build supporting materials and set printing parameters, such as layer thickness, layout, printing direction. According to the determined layer thickness, the digitized custom tray is automatically sliced into horizontal layers in the 3D-printing preparing software. The cross-section of each layer represents the pattern that would be solidified by the 3D printer. After preparing, the STL data of custom tray will eventually be translated into printing language that can be identified by the 3D printer. Compared with the conventional manual technique, the digital workflow of custom trays simplifies the fabrication process and saves the cost of labor and time.

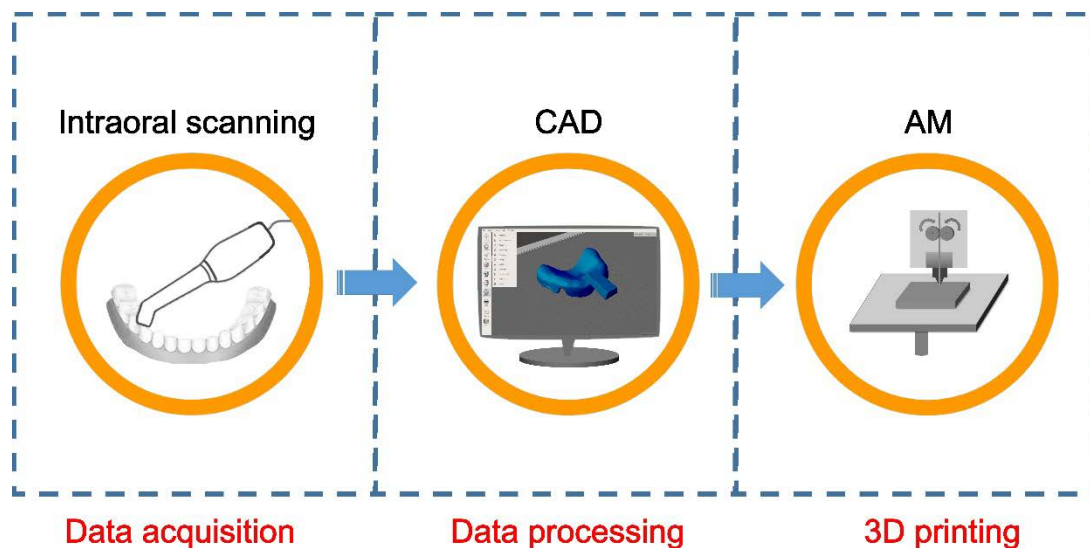


Figure 1: A typical digital workflow of fabricating custom tray.

1.2.4 Available AM technologies and materials for custom tray fabrication

For over 30 years, varieties of AM technologies and materials have been developed. Common AM technologies include stereolithography (SLA), fused filament fabrication (FFF), digital light processing (DLP), Polyjet, selective laser melting (SLM), and

selective laser sintering (SLS) [16,21], and the available 3D-printing materials include polymers, metals, and ceramics [22]. For custom tray fabrication, polymer seems a suitable material due to the relatively low cost. In the following sections, three common polymer-printing AM technologies and the corresponding tray materials investigated in the present study will be briefly introduced.

1.2.4.1 FFF

FFF, also known as fused deposition modeling (FDM), is an extrusion-deposition based AM technology. The basic working principle relies on the melting and solidification of thermoplastic materials [23].

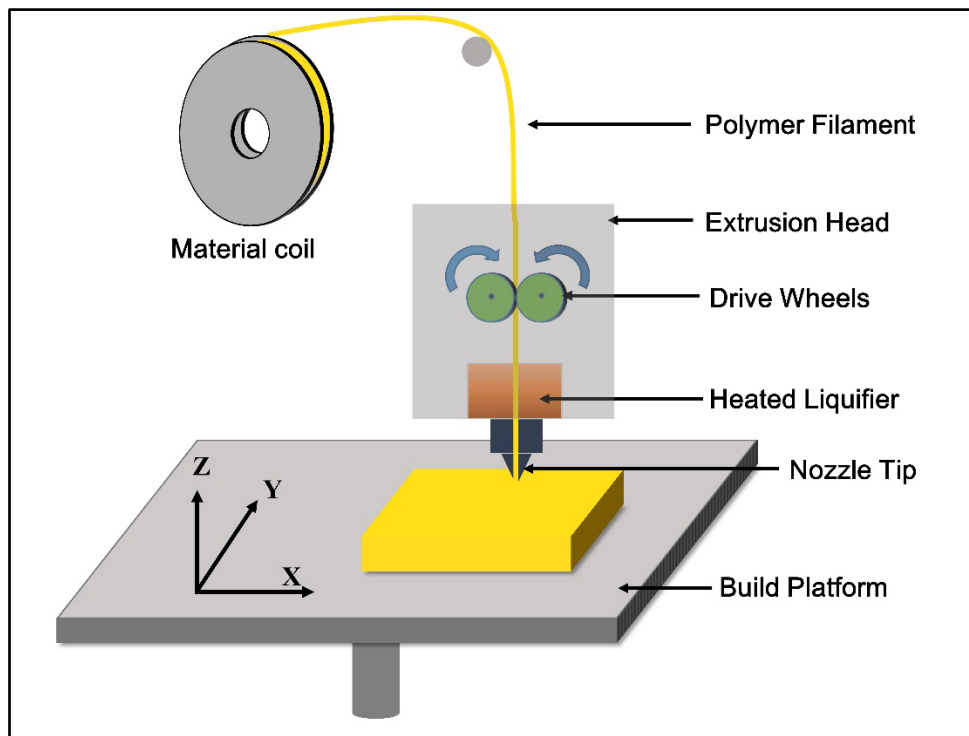


Figure 2: The working principle of FFF.

As illustrated in Figure 2, a thermoplastic polymer filament is continuously fed into the extrusion head from the material coil by the drive wheels. Inside the extrusion head, a heated liquifier is used to melt the polymer filament. When the molten polymer is being extruded out from the nozzle tip, the numerically controlled extrusion head moves

horizontally in X- and Y-axis to draw a cross-section of a specific layer. Due to the acute decrease of temperature, the extruded molten polymer is immediately solidified on the build platform. Once a layer is completed, either the build platform moves down or the extrusion head moves up in Z-axis to start a new layer. This process is repeated until the final product is constructed. Each time the distance moved in Z-axis equals to the layer thickness, which can be pre-determined in the 3D-printing preparing software. Increasing the layer thickness can decrease the resolution, accelerate the printing process and enhance the surface roughness. For FFF printers, the layer thickness approximately ranges from 0.10 mm to 0.33 mm, which is relatively higher than the photopolymerization AM technologies, such as SLA and DLP, resulting in the printed parts have a lower manufacturing accuracy and rougher surfaces [24]. For some engineering applications, the FFF-generated roughness needs to be eliminated by finishing processes [25].

However, for custom tray fabrication, FFF seems feasible due to the following reasons: FFF is a cost-effective technology that can be easily afforded by most dental clinics [26,27]; The accuracy of FFF is acceptable since the accuracy requirement of custom tray is not extremely high; In addition, the FFF-printed rough surfaces are beneficial for the bonding between the custom trays and the impression/adhesive systems [28].

1.2.4.2 SLA

Stereolithography or SLA is an early photopolymerization AM technology, the principle of which is based on the photochemical reaction: the photoinitiator react to the ultraviolet (UV) light, linking monomers and oligomers together to form a rigid network.

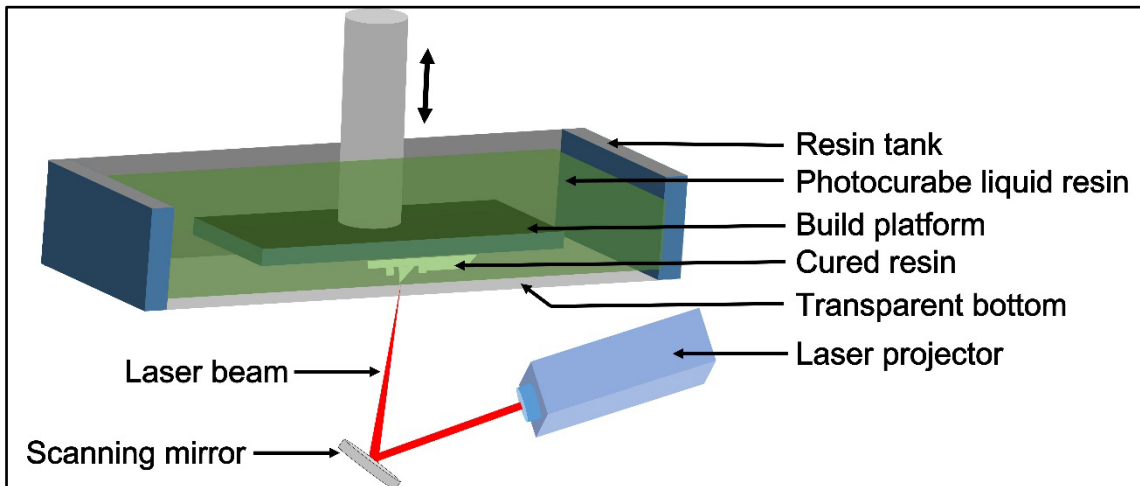


Figure 3: The working principle of SLA.

As shown in Figure 3, a movable build platform is immersed in the photocurable liquid resin. Between the build platform and the resin tank bottom, a tiny initial distance is remained. The laser beam emitted from the projector is reflected by a numerically controlled scanning mirror and passes through the transparent bottom, curing the focused liquid resin immediately. Through the rotation of the scanning mirror, the laser beam is guided to draw the cross-section of a layer. Once a layer is solidified, the build platform ascends by a distance equals to the layer thickness so that the uncured liquid resin can be refilled between the bottom and the previously solidified layer. This process is repeated until the final 3D object is printed.

SLA is deemed a relatively slow AM technology because the laser spot can only cure a small area [18]. The curing time can be one or two minutes for a layer, and several hours or even several days for a whole object [16]. After printing, the formed part needs to be washed to remove the uncured resin on its surface, and to be post-cured to enhance conversion rate [21]. The irritating resin monomer may cause skin sensitization, so the operator needs corresponding protections. In addition, SLA is relatively expensive because of the costly resin and the printing device. Nevertheless, SLA is still considered the gold standard because of the attractive advantages: complex and sophisticated structures can be built with high resolution, and the printed smooth surfaces do not

usually need finishing [21,29,30].

1.2.4.3 DLP

Being the “sister technology” of SLA, DLP is also a photopolymerization AM technology that works similarly except for the light curing process [18]. Instead of curing a small area and drawing the cross-section of a layer, the DLP laser cures a whole layer at a time. This improvement greatly improves the printing efficiency and shortens the printing time. To explain the working principle of DLP in detail, a schematic is shown in Figure 4.

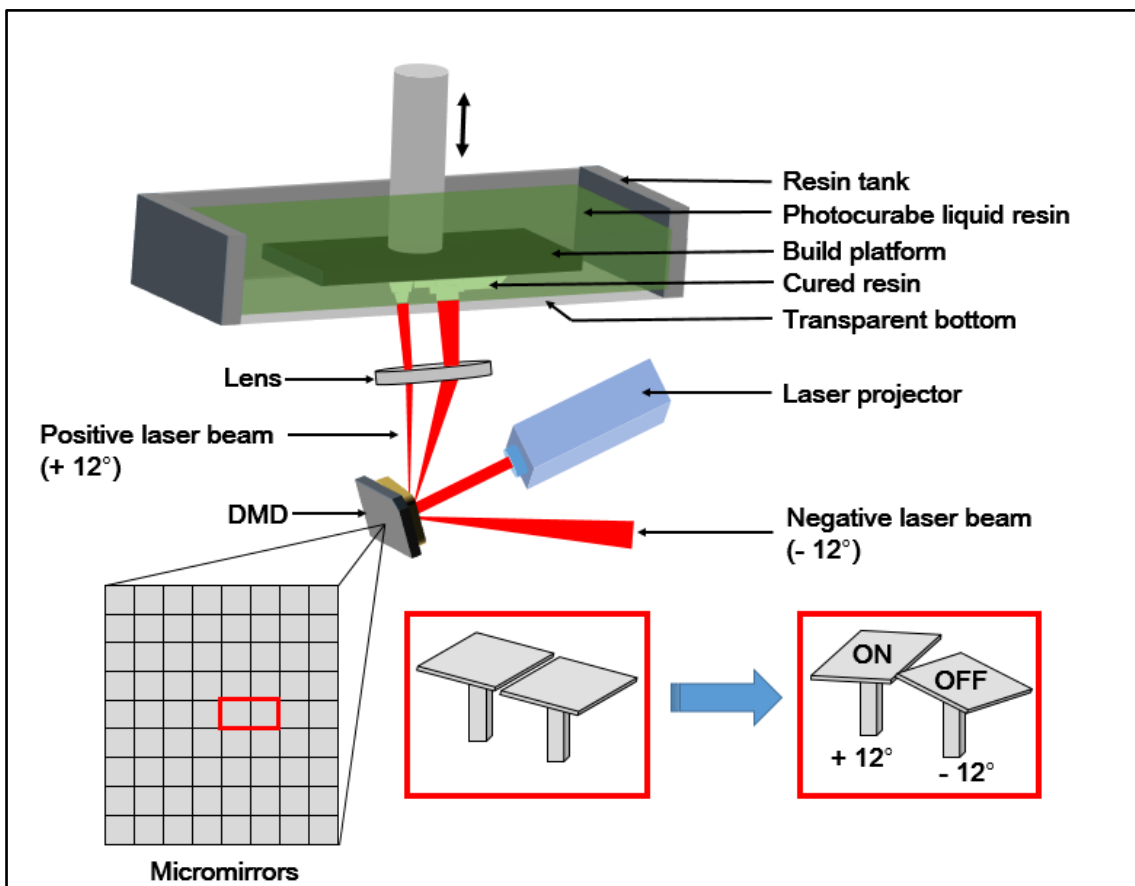


Figure 4: The working principle of DLP.

In a DLP 3D printer, the laser beam is reflected by a numerically controlled optical component named digital micromirror device (DMD). Being a chip developed by Texas

Instruments in 1987 [31], DMD has over a million tiny mirrors arrayed rectangularly on its surface. Each micromirror has a dimension less than $8\ \mu\text{m} \times 8\ \mu\text{m}$ and corresponds to a pixel. When the DMD is working, a tiny voltage converted from the digital signal can generate an electrostatic force, which rotates each micromirror plus or minus 12 degrees, turning the laser beam on or off. The turned-on laser beam is reflected into the lens, passes through the transparent bottom, and cure the liquid resin. Meanwhile, the turned-off laser beam is reflected elsewhere. In this way, the pattern of a layer is reflected onto the liquid resin, thus a whole layer is cured at a time. Since the micromirrors are very small, the DLP-printed parts have a relatively high resolution and smooth surfaces [32]. Compared to that of SLA, the printing speed of DLP has been greatly improved. However, the cost of DLP also increases because of the sophisticated optic system.

1.2.4.4 Conventional and 3D-printing custom tray materials

Conventionally, a variety of materials are available for custom tray fabrication, such as heat-activated, thermoplastic, autopolymerizing, and light-curing resins [33]. For fabricating custom trays, the materials should be rigid and dimensionally stable to ensure the accuracy of impressions [34]. Autopolymerizing resins were regarded as a less ideal tray material because of their unavoidable polymerization-induced shrinkage and residual stress relaxation [35]. It was suggested that using autopolymerizing resins to fabricate custom trays should be at least 24 hours before impression taking [36]. Thermoplastic resins were once recommended for their convenience. However, their thermoplasticity may result in insufficient material strength and possible deformation [37]. Studies indicated light-curing resins were better for custom tray fabrication since they were stiff and showed a low degree of polymerization-induced shrinkage. Wirz et al. suggested that light-curing resin trays can be directly used after fabrication, the additional storage time for polymerization completion was unnecessary [38]. Therefore, in the present study, a conventional light-curing resin, Zeta Tray LC, was used as the

reference tray material.

Currently, a variety of 3D-printing polymers can be used for custom tray fabrication, some of which are already commercially available. However, research on these new 3D-printing custom tray materials is still lacking. In this study, three 3D-printing custom tray materials were selected for investigation due to their rigidity and dimensional stability, i.e. Dental LT, FREEPRINT tray, and Polylactide (PLA), which are available for SLA, DLP, and FFF, respectively. Although the detailed components of each material are hidden because of commercial interest, the basic information of the investigated materials was found and introduced in Table 1.

Table 1: Conventional and 3D-printing custom tray materials in this study.

Tray material	Corresponding technique	Component	Solidifying method
Dental LT	SLA	(Meth)acrylate based	UV light: 405 nm
FREEPRINT tray	DLP	(Meth)acrylate based	UV light: 378 - 388 nm
PLA	FFF	Polylactic Acid	Cooling below melting point (150 °C)
Zeta Tray LC	Conventional method	(Meth)acrylate based	UV light: 350 – 400 nm

In addition to rigidity and dimensional stability, another significant requirement of custom tray materials is to provide sufficient retention for the impression. Therefore, the bonding between custom tray materials and impression/adhesive systems is crucial, which will be introduced in the following sections.

1.3 Bonding between custom trays and impression/adhesive systems

The precise fitness is one of the critical factors that determine the long-term clinical

success of oral restorations [39]. Thus, an accurate impression is of great importance to correctly replicate the oral tissues. During the impression taking, the flowable impression material enters the undercuts of teeth and soft tissues, which, after setting, resists the removal of impression from oral tissues [40]. If the bond strength between the custom tray and the impression is insufficient, detachment is liable to happen between the two during withdrawing the impression, resulting in the deformation of the impression, inaccuracy of the subsequent model, and even failure of the final prosthesis [41]. In addition to withstanding the removal force, the bonding between the impression and the tray was thought to ensure the uniform polymerization-induced shrinkage of the impression, thus further improving the accuracy [33].

To improve the bonding between tray and impression, either mechanical retention or chemical adhesion can be utilized. The factors that influence the bonding have been thoroughly researched in previous studies, including impression materials, adhesives, custom tray materials, and surface treatments. In the following sections, an overview of these factors will be given.

1.3.1 Impression materials

Among the various impression materials that are commercially available, the rubber-based elastomeric impression materials are generally preferred due to their accurate reproducibility, dimensional stability, and convenient manipulation [33,42]. Comparisons in bond strength between different elastomeric impression materials and custom tray materials have been well investigated. Generally, despite the different experimental conditions, polyether (PE) impression materials showed the highest bond strength, followed by the polysulfide (PS) impression materials, while the bond strength of condensation silicone (C-silicone) impression materials was the lowest [40,43–45]. However, a study from MacSween et al. exceptionally indicated that PE showed lower bond strength when compared to PS [46]. The bond strength of addition silicone (A-silicone) impression materials, or vinyl polysiloxane (VPS) [47], was reported

inconsistently. Most of the related studies indicated the bond strength of VPS was comparable to that of PE [39,43,45,48] and higher than that of PS [33,43,45]. However, exceptions can be found in the result reported by Marafie et al., stating that the bond strength of VPS was lower than that of PE [49], and that found by MacSween et al., who claimed the bond strength of VPS and PS was similar [46].

The bond strength depends on not only the type of elastomeric impression material but also the formulation provided by the manufacturer. Even for the same type of elastomeric impression material, significant difference in bond strength could be found among impressions provided by different manufacturers [40,45,46,50]. In clinical practice, choosing the type of elastomeric impression materials is mainly based on the indications. For instance, PE is more suitable for cases with poor moisture control. Other factors such as costs may also affect the choice of dentists. Therefore, the bonding properties of elastomeric impression materials do not seem to be the most important factor in material selection. At present, PS and C-silicone have become increasingly unpopular because of certain disadvantages, while PE and VPS are still commonly in use. Recently, a new elastomeric impression material, Vinylsiloxanether (VSXE), was marketed as a product having both the advantages of A-silicone and PE. Therefore, in the present study, VPS, PE, and VSXE were selected for investigation.

1.3.2 Adhesives

Since there is usually no chemical adhesion between elastomeric impression materials and tray materials [51,52], adhesives are recommended to be applied onto the inner surfaces of the tray to improve the impression retention [42]. Previous studies indicated that using tray adhesive could significantly increase the bond strength, accuracy, and consistency of the impressions [44,45,53–55]. Since little information is available regarding the chemical composition of the tray adhesive of elastomeric impression materials [56], the detailed working principle of the adhesive is still unclear. Studies

indicated that the solvent of the adhesive could slightly dissolve and swell the outermost polymer surface [43,44] so that the solute of the adhesive could penetrate into the superficial molecular networks [49]. Therefore, the bond strength between custom trays and elastomeric impression materials is related to the chemical compatibility between the adhesives and the tray materials [48].

The adhesive and impression material are usually regarded as an impression/adhesive system when they are supplied by the same manufacturer. However, there are also universal adhesives available in the market. Comparisons in the bond strength between manufacturer-supplied and universal adhesives were performed repeatedly but the results were not conclusive. Ramdev et al. indicated the tensile bond strength of two manufacturer-supplied adhesives was higher than that of a universal adhesive [57]. However, Peregrina et al. [50] and Ashwini et al. [41] reported the universal adhesives had higher tensile bond strength than the manufacturer-supplied ones. Furthermore, through exchanging manufacturer-supplied adhesives of two A-silicone impression materials, Bindra et al. found the bond strength increased significantly [58], Payne et al. stated that no statistical difference in bond strength was observed [48], while Yi et al. indicated the bond strength became significantly lower [42].

In addition, the adhesive drying time was also reported to strongly affect the bond strength. Generally, from the start of adhesive application, the bond strength seemed to rise with the increase of adhesive drying time in the initial period [39,40,42], after which the bond strength might reach the maximum value and tended to be stable [40,42]. However, when the drying time was exceedingly prolonged, such as to 7 days, the bond strength could slightly decrease [59]. To achieve the highest bond strength, the optimum adhesive drying time was recommended by each manufacturer. Therefore, for standardization, this study utilized the manufacturer-recommended adhesive for each investigated impression material, and the adhesive drying time was strictly obeyed

according to manufacturer's instruction.

1.3.3 Custom tray materials

As described in section 1.3.2, the surface chemistry of the custom tray material determines its solubility in the adhesive solvent and affects the bond strength. Previously, the comparisons in bond strength were mainly performed between autopolymerizing and light-curing resins. Dixon et al. [59] and Abdullah et al. [33] indicated the VPS impression/adhesive system exhibited significantly higher bond strength to the light-curing resin than to the autopolymerizing acrylic resin. However, this conclusion was contradictory to that reported by Kumar et al. [56] and Peregrina et al. [50], both studies found the light-curing and autopolymerizing resin did not differ in bond strength with VPS impression/adhesive system. Ashwini et al. investigated the bond strength of light-curing and autopolymerizing resin to three VPS impression/adhesive systems. Interestingly, the light-curing resin showed higher bond strength to two VPS impression/adhesive systems, but no significant difference was observed in bond strength between light-curing and autopolymerizing resin with the 3M ESPE VPS impression/adhesive system [41]. In addition, Payne et al. found two thermoplastic tray materials showed significant difference in bonding with PE and VPS impression/adhesive system [48]. Chai et al. compared the bond strength of autopolymerizing resin and polystyrene with VPS, PS, PE, and C-silicone impression/adhesive system, the results indicated polystyrene had higher bond strength to VPS but lower bond strength to PS and C-silicone, while no statistical difference were found in bond strength between the two tray materials with PE [43].

In the author's recent publication, the bond strength of three FFF custom tray materials with a C-silicone impression/adhesive system was measured and compared to that of a conventional light-curing resin. All investigated FFF custom tray materials showed good chemical compatibilities with the adhesive of the C-silicone system [28]. However,

the research on the compatibility between other 3D-printing custom tray materials and impression/adhesive systems remains untouched.

1.3.4 Surface treatments

In addition to the surface chemistry, the surface topography of the tray material also plays a vital role in the bonding between impressions and trays. The internal surface of the custom tray was suggested to be roughened to increase the adhesive retention [40]. Payne et al. roughened the tray material surface by the tungsten carbide bur, the result showed the bond strength of the tray material to a VPS impression/adhesive system significantly increased after surface preparation [60]. Craig et al. stated that roughening the custom tray surface by silicone carbide paper could significantly enhance the bond strength [61]. The study of Davis et al. exhibited that the acrylic resin abraded with silicon carbide paper adhered significantly better with a PS impression/adhesive system than the acrylic resin polymerized against wax [40]. Maruo et al. [39] and Payne et al. [48] found that the surface topography of the tray material significantly affected the bonding between the custom trays and the impression systems. However, the variance in bond strength depended on the tray-impression material combinations.

It should be noted that none of the abovementioned studies had examined the surface topography of the tray material before and after surface treatments, so it is not clear how these surface treatments influenced the surface roughness and which roughness parameter is related to the impression retention. The author's recent publication initially explored this field and found gritblasting could decrease the surface roughness of FFF-printed custom tray materials, thus weakening its bonding with the impression material. The result indicated that the roughness parameter valley fluid retention index (S_{vi}) might be related to the bonding between the impression material and the tray material [28]. For further confirmation, this study selected the 3D roughness parameters that might be related to the bonding for investigation (Table 2).

Table 2: 3D roughness parameters that might be related to the bonding.

Parameter	Type	Formula	Description
Arithmetic mean height (Sa)	Height	$S_a = \frac{1}{A} \iint_A Z(x, y) dx dy$	Sa is the most commonly used 3D roughness parameter defined as the average of the absolute value of the surface height.
Skewness (Ssk)	Height	$S_{sk} = \frac{1}{S_q^3} \left[\frac{1}{A} \iint_A Z^3(x, y) dx dy \right]$	Ssk describes the symmetry of the topography height distribution. Negative skewness indicates the existence of relatively deep valleys for fluid retention.
Core void volume (Vvc)	Functional	$V_{vc} = V_v(10\%) - V_v(80\%);$ $V_v(mr) = k \int_{mr}^{100\%} [S_{mc}(mr) - S_{mc}(q)] dq$	Vvc represents the void volume of the core section. A larger Vvc value indicates better fluid retention in the core zone.
Dales void volume (Vvv)	Functional	$V_{vv} = k \int_{80\%}^{100\%} [S_{mc}(mr) - S_{mc}(q)] dq$	Vvv represents the void volume of the valley section. A larger Vvv value indicates better fluid retention in the valley zone.
Developed interfacial area ratio (Sdr)	Hybrid	$S_{dr} = \frac{\sum \sum A_{ij} - A}{A} \times 100\%$	Sdr is the roughness parameter which is used to measure the surface complexity and provides correlations in adhesion applications.

1.4 Research aim

With the above background the present study aimed to evaluate the bonding of three 3D-printing custom tray materials (Dental LT, FREEPRINT tray, and PLA), which were respectively printed by three AM technologies (SLA, DLP, and FFF), to three elastomeric impression/adhesive systems (VSXE, VPS, and PE) by peel test. The peel bond strength of the 3D-printed custom tray materials was compared with that of a conventional light-curing resin (Zeta Tray LC). Through scanning electron microscopy (SEM) analyses and roughness measurements, the surface topographies of the four tray materials were investigated qualitatively and quantitatively. Additionally, the failure modes after peeling were microscopically studied.

It was hypothesized that:

- (1) The type of tray materials has no influence on the peel bond strength;
- (2) The type of impression/adhesive systems has no influence on the peel bond strength.

2. Materials and Methods

2.1 CAD of Test Blocks

The test block was designed in a CAD software (OpenSCAD, 2015.03-2 Windows, <http://www.openscad.org/>). The geometrical shape of the test block was designed to simulate the peeling action of the custom tray during the impression taking [28]: A cuboid base was designed with the dimension of 25.4 mm × 25.4 mm × 6 mm (Figure 5a). A cuboid handle with the dimension of 25.4 mm × 13 mm × 7 mm was added onto the top surface of the base at 45 degrees (Figure 5b). A cuboid connector was added to connect the base and handle (Figure 5c). At last, a centered hole was designed on the handle with a diameter of 0.5 mm (Figure 5d).

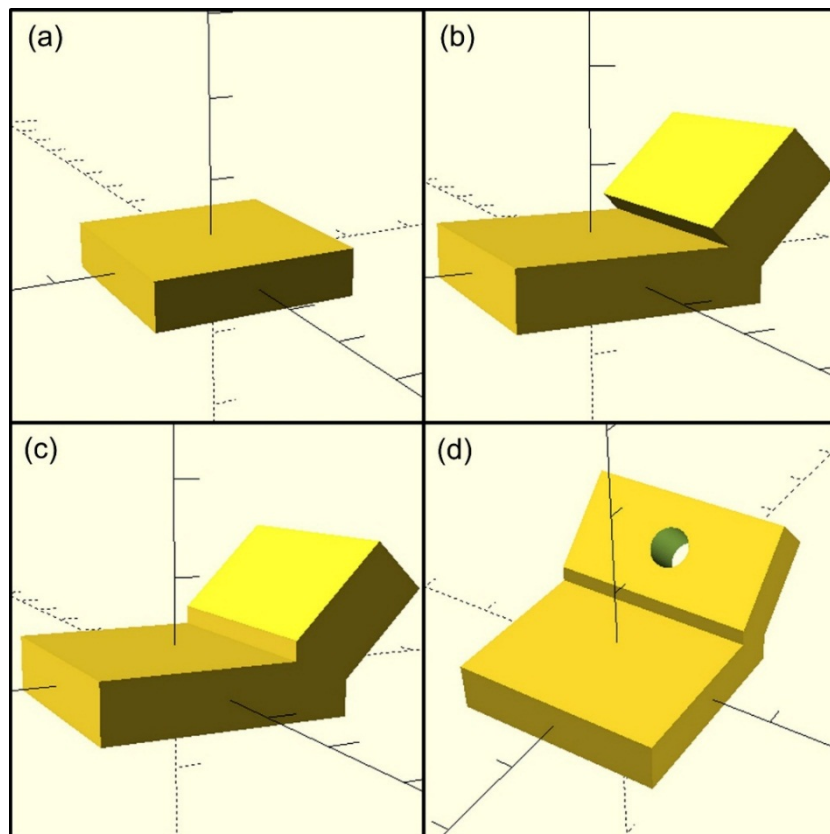


Figure 5: CAD of the test blocks in OpenSCAD. (a) The cuboid base; (b) A cuboid handle was added onto the top surface of the base with 45 degrees; (c) A connector was used to connect the base and the handle; (d) A centered hole was added on the handle with a diameter of 0.5 mm.

2.2 AM of test blocks

2.2.1 Printing test blocks using FFF

The designed test block data were saved as STL file format and transferred to a 3D-printing preparing software (MakerBot Print 3.4, MakerBot Industries, NY, USA). A raft layer was created to support the test blocks with a margin width of 5 mm. The printing layer thickness and infill density were set to 100 μm and 100% respectively. The balanced print mode was selected to ensure accuracy. The printing layout and build direction on the build platform are shown in Figure 6.

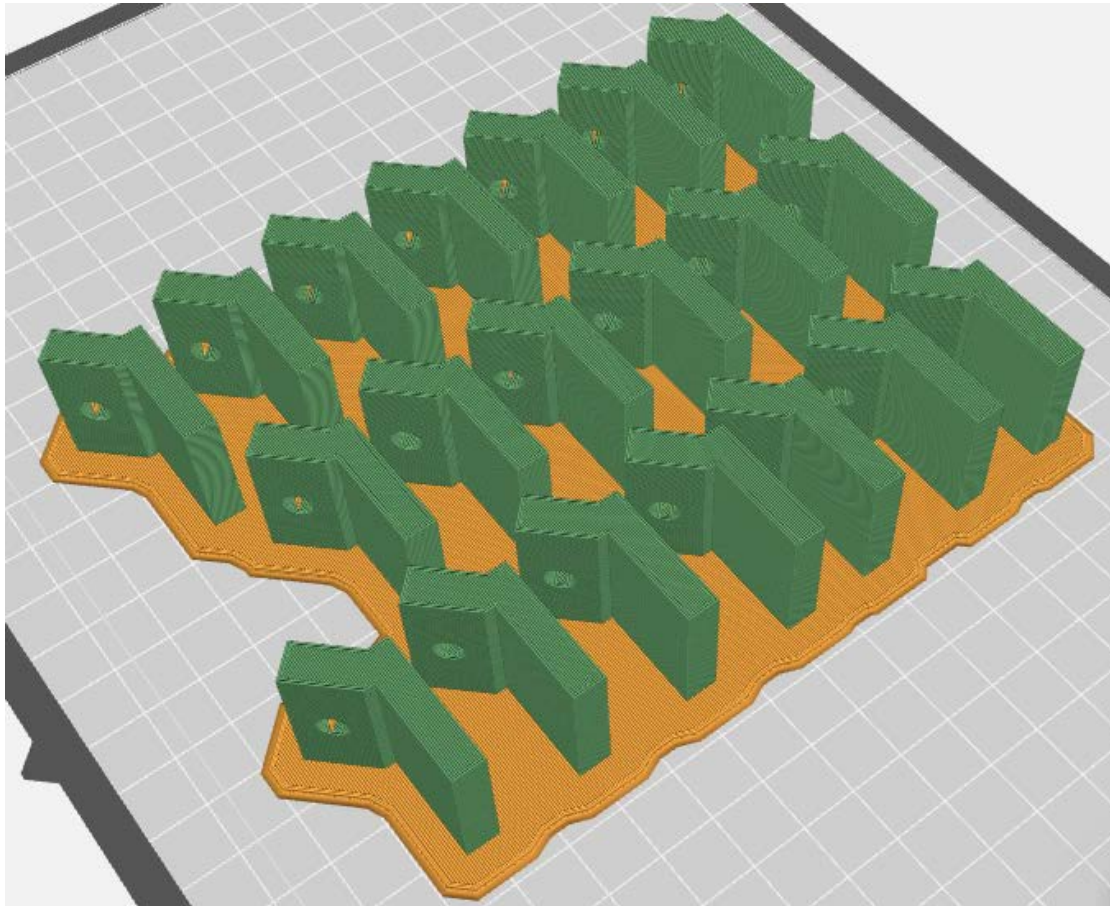


Figure 6: The printing direction and layout of the FFF-printed test blocks. Twenty samples were printed on the supporting raft layer with a margin width of 5 mm.

After setting the printing parameters, test blocks were printed with PLA (PLA Precision Material, MakerBot Industries, NY, USA) (Figure 7b) by a FFF 3D printer (Replicator+, MakerBot Industries, NY, USA) (Figure 7a). Twenty test blocks were printed each time

for 23 hours. After printing, the raft layer was removed, and the FFF-printed test blocks were collected for the subsequent peel bond strength test (Figure 8).

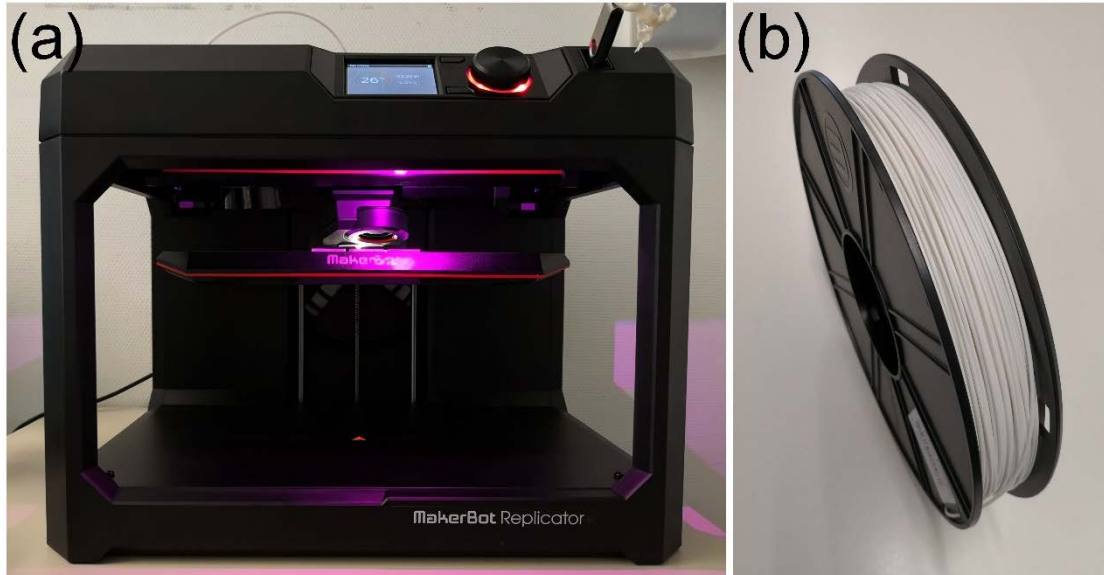


Figure 7: The FFF 3D printer and printing material. (a) The FFF 3D printer “Replicator+”; (b) The spool of PLA filament.

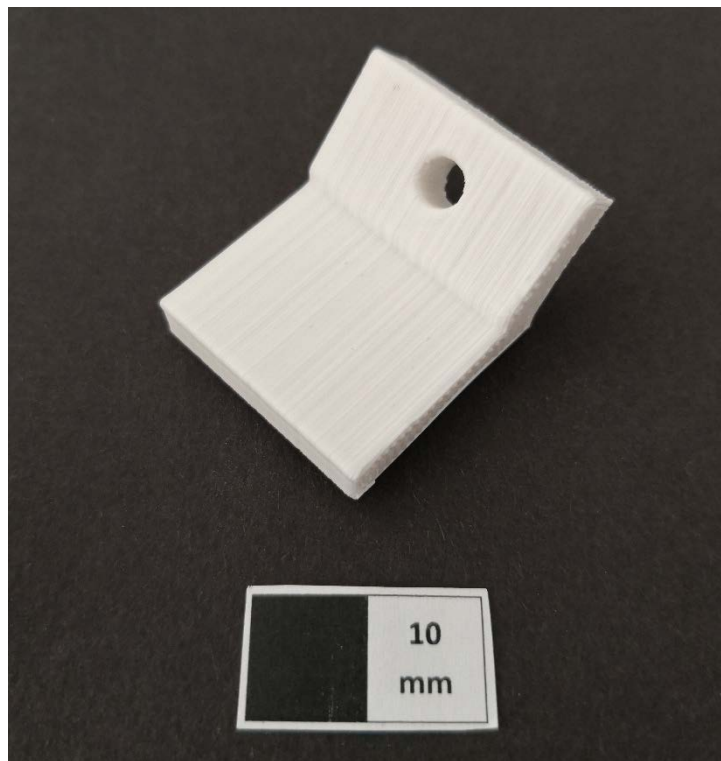


Figure 8: The FFF-printed test block (white scale: 10 mm).

2.2.2 Printing test blocks using SLA

The STL file of the test block was preprocessed in a 3D-printing preparing software (PreForm 2.18.0, Formlabs, Somerville, USA). The layer thickness was set to 100 μm . Figure 9 shows the direction and layout for printing. Since in the preliminary test, the test blocks printed with supporting materials were liable to be deformed, all the samples were set to be printed directly on the build platform of the SLA 3D printer.

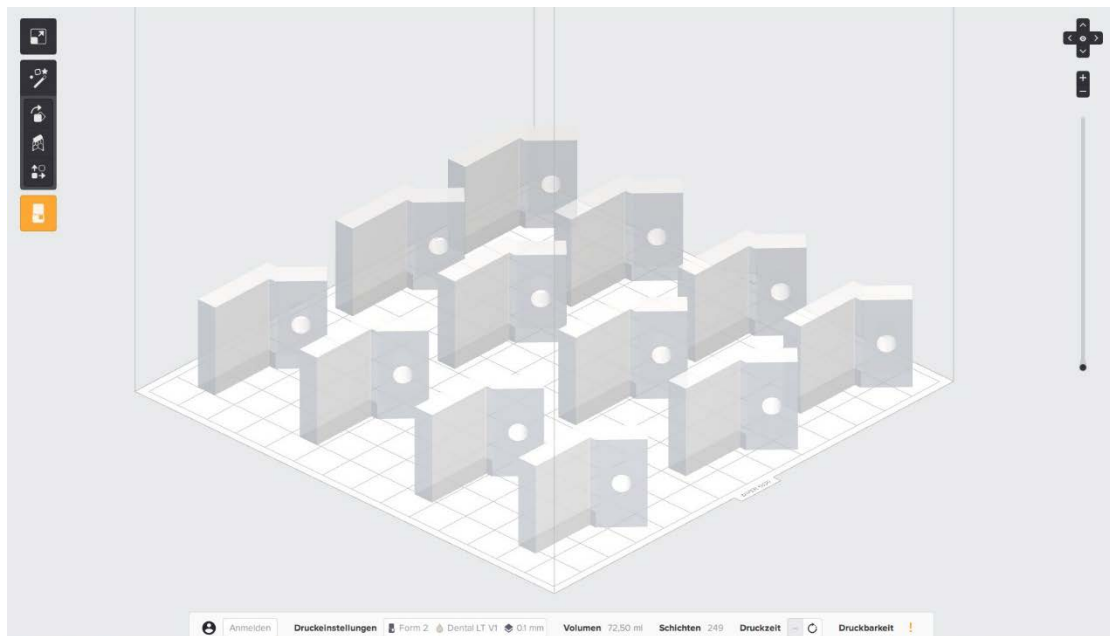


Figure 9: The printing direction and layout of the SLA-printed test blocks. Twelve specimens were set to be printed directly on the printing platform without supporting material.

After preparing, test blocks were printed with a light-curing resin (Dental LT Clear Resin, Formlabs, Somerville, USA) (Figure 10b) by an SLA 3D printer (Form 2, Formlabs, Somerville, USA) (Figure 10a). Twelve test blocks were printed each time for 2 hours and 20 minutes.

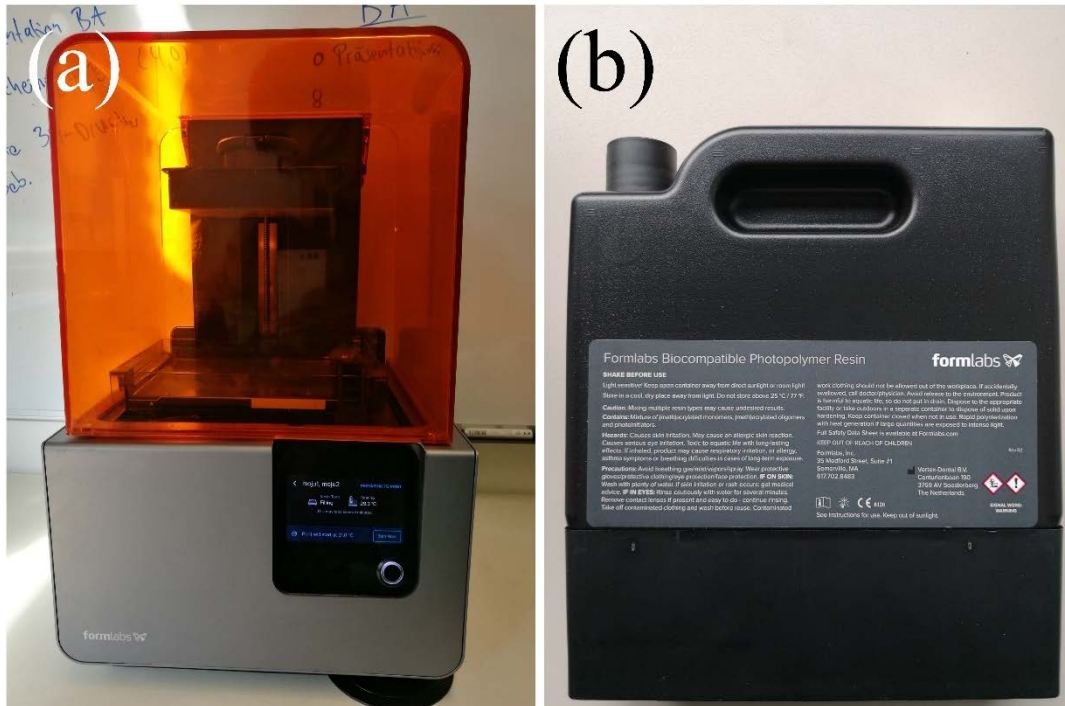


Figure 10: The SLA 3D printer and printing material. (a) The SLA 3D printer “Form 2”; (b) The light-curing resin “Dental LT Clear Resin”.

After printing, the build platform, with the printed test blocks still attached, was washed in a post-cleaning device (Form Wash, Formlabs, Somerville, USA) (Figure 11a) filled with isopropyl alcohol (Isopropanol 100%, SAV LP GmbH, Flintsbach am Inn, Germany) (IPA) for 5 minutes to remove the uncured liquid resin. Afterward, the test blocks were dried in air and removed from the build platform after ensuring the washed surface had no uncured resin. To achieve the optimal performance of Dental LT, the washed test blocks were then exposed to 405 nm light emitted from 13 multi-directional light-emitting diodes (LEDs) at 80 °C for 20 minutes in a post-curing device (Form Cure, Formlabs, Somerville, USA) (Figure 11b). After post-curing, the test blocks were collected (Figure 12) and stored in black plastic bags for light-sensitive sample storage (Whirl-Pak black bags, Nasco, Milton, USA).



Figure 11: Post-processing devices of the SLA 3D printer. (a) Post-cleaning device “Form Wash”; (b) Post-curing device “Form Cure”.

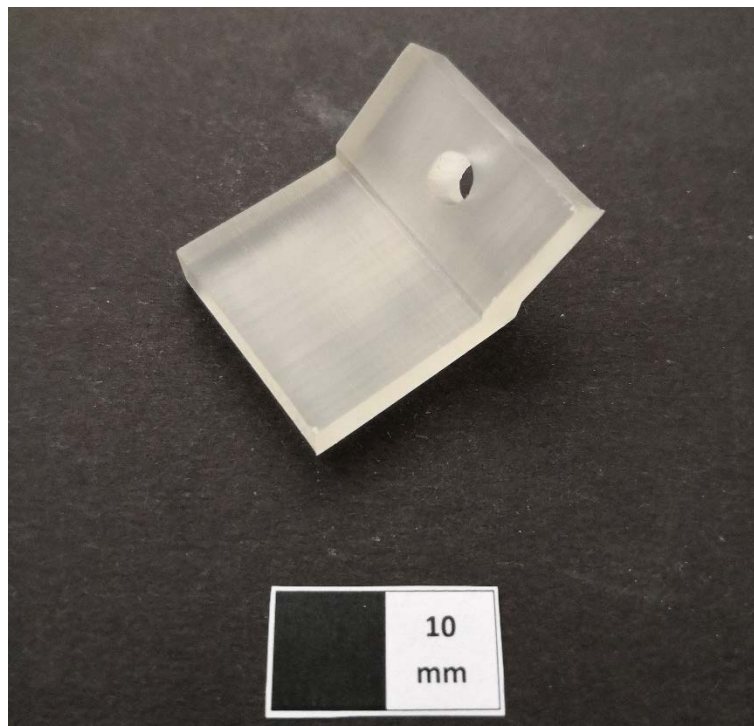


Figure 12: The SLA-printed test block (white scale: 10 mm).

2.2.3 Printing blocks using DLP

The STL file of the designed test block was sent to a 3D-printing preparing software (Netfabb premium 2019.0, AUTODESK, San Rafael, USA). It was known from the preliminary test that printing samples directly on the build platform, printing samples in the center of the platform, high printing speed and excessive samples per print would result in the deformation of the printed test block. Therefore, the number of test blocks per print was reduced to six. All test blocks were laid in the outermost positions of the platform to minimize peeling force (Figure 13). The build style was chosen as Dental Gentle Vat Deflection Feedback System (VDFS) 3 mm to reduce the printing speed.

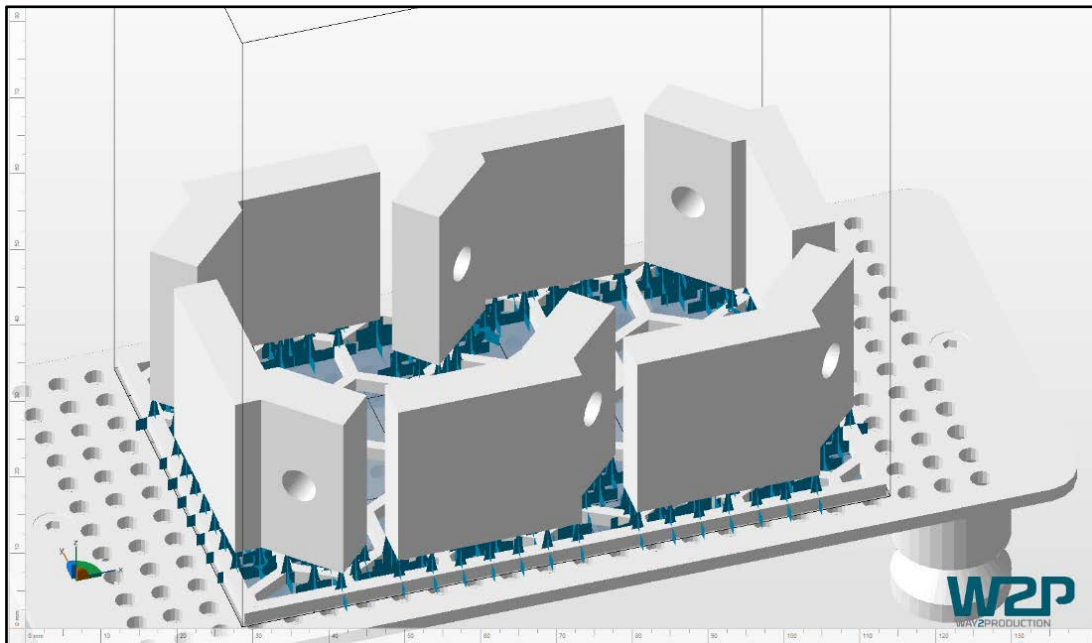


Figure 13: The printing direction and layout on the build platform in Netfabb.

To anchor the test blocks, a supporting grid with supporting materials was added on the build platform, the width of the supporting material on the test blocks was set to 0.5 mm (Figure 14). All test blocks were Z-compensated for better accuracy of the holes.

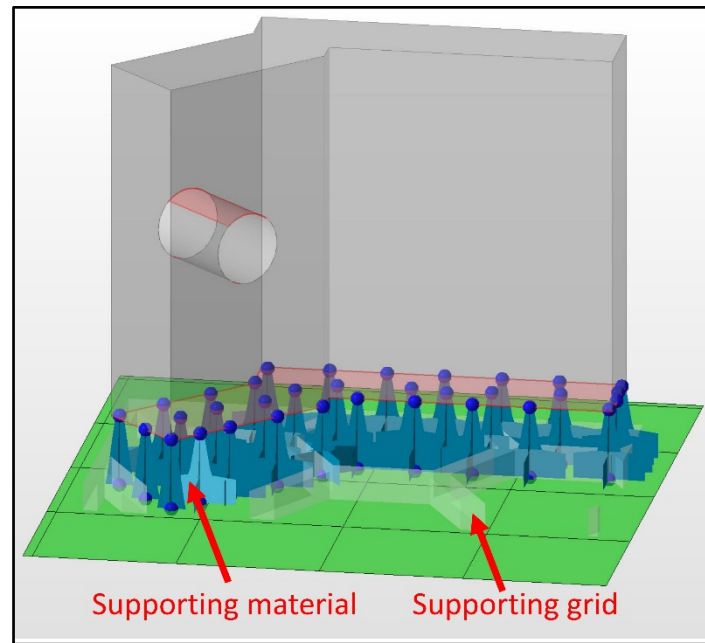


Figure 14: The supporting grid and supporting materials of the test block.

The print job file was created by Netfabb and sent to a DLP 3D printer (SOLFLEX 170, W2P Engineering, Vienna, Austria) (Figure 15a). Before printing, the custom tray material (FREEPRINT tray, DETAX, Ettlingen, Germany) (Figure 15b) was evenly mixed by a self-developed roller mixer (Figure 15c). For each print, six test blocks were printed with the layer thickness of 100 μm for about 53 minutes.



Figure 15: The DPL 3D printer, printing material, and self-developed roller mixer. (a) The DLP 3D printer “SOLFLEX 170”; (b) The custom tray material “FREEPRINT tray”; (c) The self-developed roller mixer.

After printing, the uncured resin was allowed to drip for 10 minutes. The printed parts were then removed from the build platform and pre-cleaned in a vessel filled with IPA (Isopropanol 100%, SAV LP GmbH, Flintsbach am Inn, Germany) using an ultrasonic cleaner (Ulsonix Proclean 10.0M ECO, Expondo, Berlin, Germany) for 3 minutes. Next, the DLP-printed test blocks were carefully removed from the supporting material and ultrasonically cleaned with IPA for another 3 minutes. After the cleaning process, the test blocks were dried by compressed air and post-cured in a flash-light polymerization

device (Otoflash G171, VOCO, Cuxhaven, Germany) (Figure 16) with 2×2000 flashes under protective nitrogen. The post-processed test blocks were then collected (Figure 17) and stored in black plastic bags.



Figure 16: The flash-light polymerization device “Otoflash G171”.

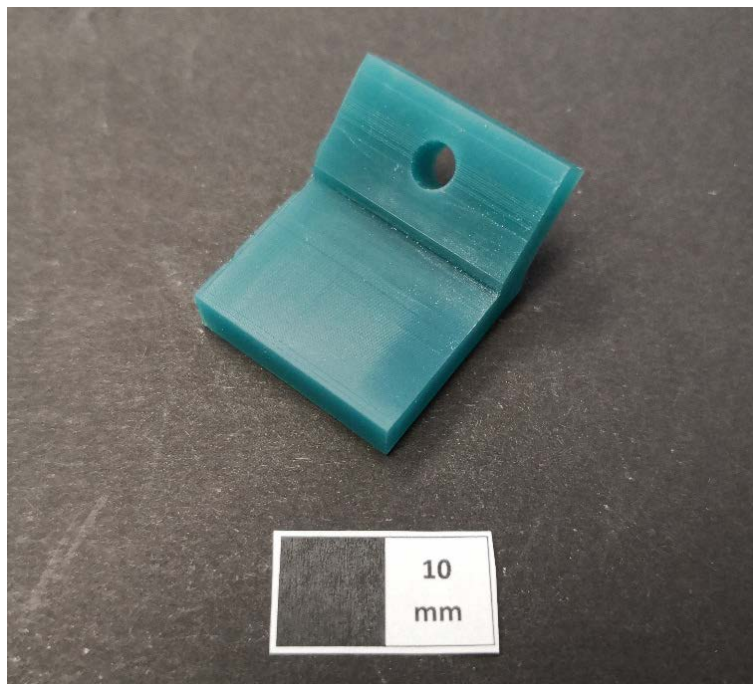


Figure 17: The DLP-printed test block (white scale: 10 mm).

2.3 Fabrication of reference test blocks

2.3.1 CAD and AM of molds used for fabricating wax spacer and reference test block

All molds were designed in a CAD software (OpenSCAD, 2015.03-2 Windows, <http://www.openscad.org/>) and analyzed in a 3D-printing preparing software (Netfabb premium 2019.0, AUTODESK, San Rafael, USA).

As shown in Figure 18a, the mold of wax spacer was designed as a $25.4 \text{ mm} \times 25.4 \text{ mm}$ square frame with one side deficient. To ensure the firmness, the lateral wall thickness was set to 2.3 mm and the height was set to 6 mm (Figure 18b).

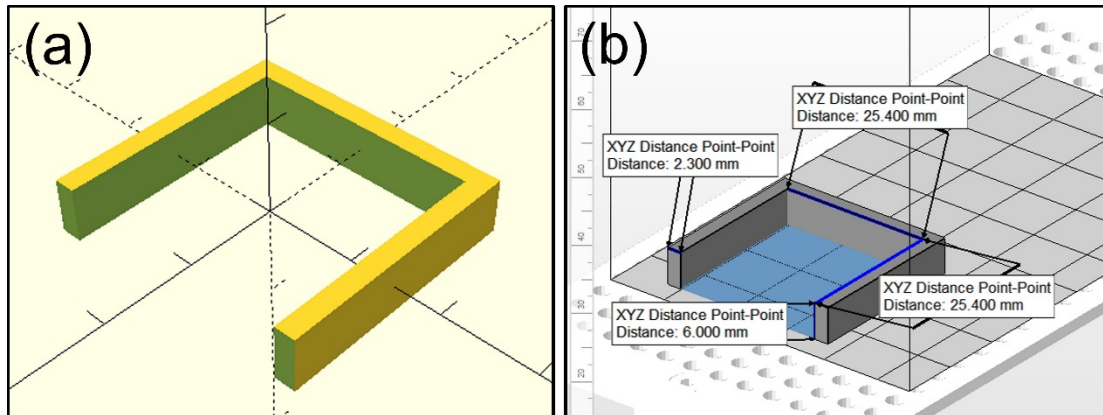


Figure 18: The mold of wax spacer. (a) The original prototype designed in OpenSCAD; (b) The mold size of wax spacer.

As shown in Figure 19, the mold of reference test block was the negative imprint of the test block designed in Section 2.1. However, since the custom tray was fabricated on the wax spacer in the conventional technique, the molds of reference test block also reserved an extra space with 1.25 mm in height to allow the conventional light-curing resin polymerize against baseplate wax. The total height of the mold base was 7.25 mm, the height of 1.25 mm at the bottom was reserved for the baseplate wax, and the height of the upper 6 mm was the same as the height of the test block base.

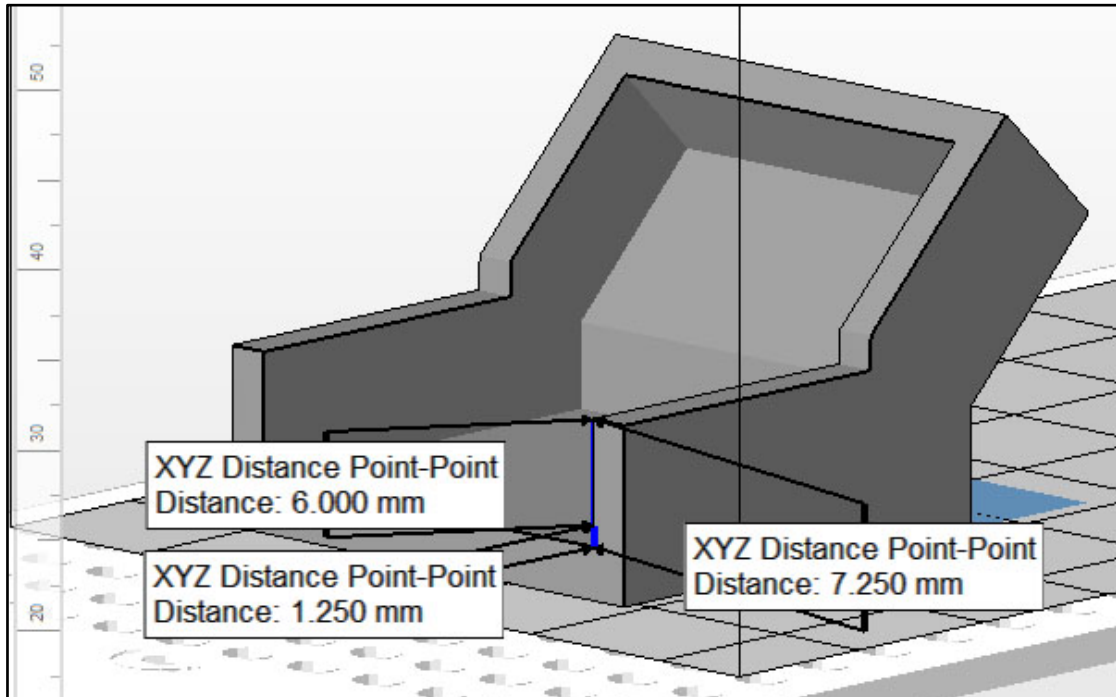


Figure 19: Molds of reference test block reserved 1.25 mm height for the baseplate wax, so the total height of the mold base was set to 7.25 mm. The reference custom tray material could polymerize against the 1.25 mm thick baseplate wax and maintain the base height of 6 mm.

Considering the difficulty of removing the fabricated reference test block out of the mold, five molds were designed. The mold in Figure 20a had a cylinder so that the fabricated reference test block would have a hole in the center of the handle. However, the cylinder might increase the difficulty of removing the light-cured reference test block out from the mold. In order to reduce the removal resistance, minor modifications were made according to the design in Figure 20a. In Figure 20b, the upper border of the mold was deleted. In Figure 20c, 20d and 20e, the cylinder design was removed. Compared to the mold designed in Figure 20c, the design in Figure 20d removed the upper border, and the design in Figure 20e further removed a portion of the posterior border, so that the fabricated test block could be held by finger during removal. Reducing the mold structure would make the fabricated test block easier to be removed, but the fabrication accuracy would also decrease at the same time. Therefore, it was necessary to select an optimal mode design that could enable the removal of fabricated

reference test block and maintain its maximum accuracy.

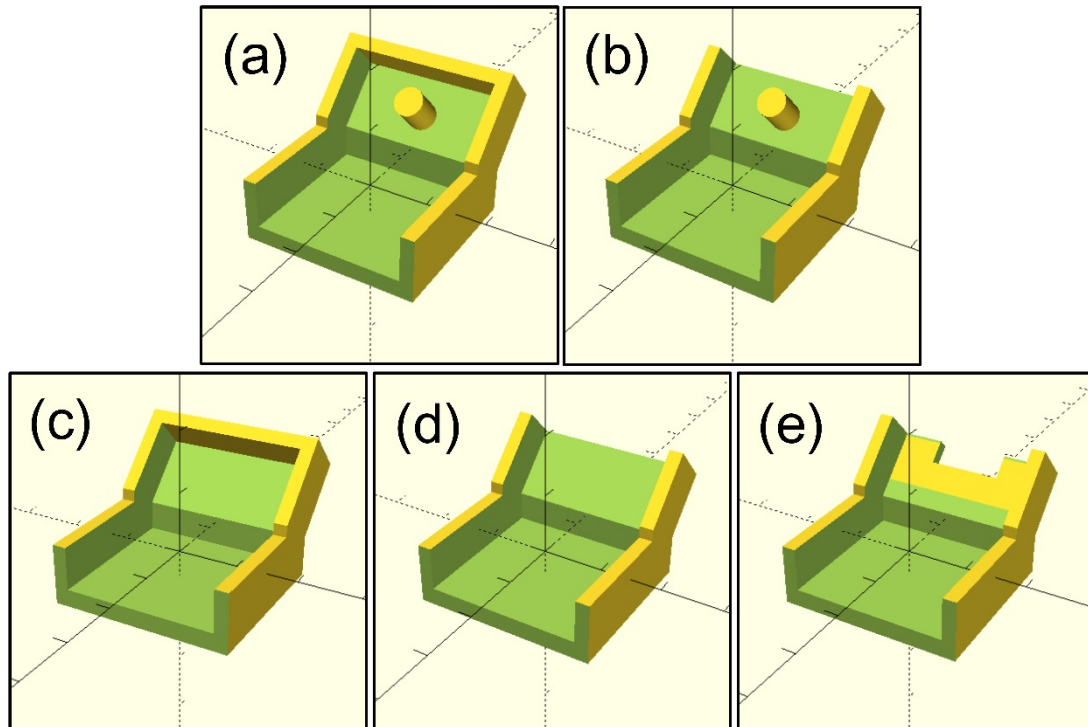


Figure 20: Five CAD-designed molds of reference test block. (a) The design with the centered cylinder; (b) The design with the centered cylinder, without the upper border. (c) The design with upper border, without the centered cylinder; (d) The design without the centered cylinder and the upper border; (e) The design without the centered cylinder and the upper border, a portion of the posterior border was removed.

With the above purpose, a pilot test was conducted. All CAD-designed molds of reference test block and the mold of wax spacer were printed by the SLA printer (Form 2, Formlabs, Somerville, USA) with a light-curing material (Grey V4, Formlabs, Somerville, USA). The layer thickness was set to 50 μm . After printing, the molds were post-cleaned by Form Wash with IPA for 15 minutes and then post-cured by Form Cure at 60 $^{\circ}\text{C}$ for 60 minutes. After postprocessing, the supporting materials were removed, and the molds were collected. A conventional light-curing resin (Lichtwachs, Wegold Edelmetalle, Wendelstein, Germany) was applied into each printed mold to fabricate the reference test block. After light curing, the solidified test blocks could not be removed out from the molds designed in Figure 20a and 20b (Figure 21a), and excessive removal

force could result in mold fracture (Figure 21b). In contrast, the reference test blocks could be removed out from the molds designed in Figure 20c, 20d and 20e. By inspection, the test block fabricated by the mold designed in Figure 20c was found to possess the best accuracy (Figure 22). Therefore, the mold design in Figure 20c was selected to fabricate the reference test blocks in this study.

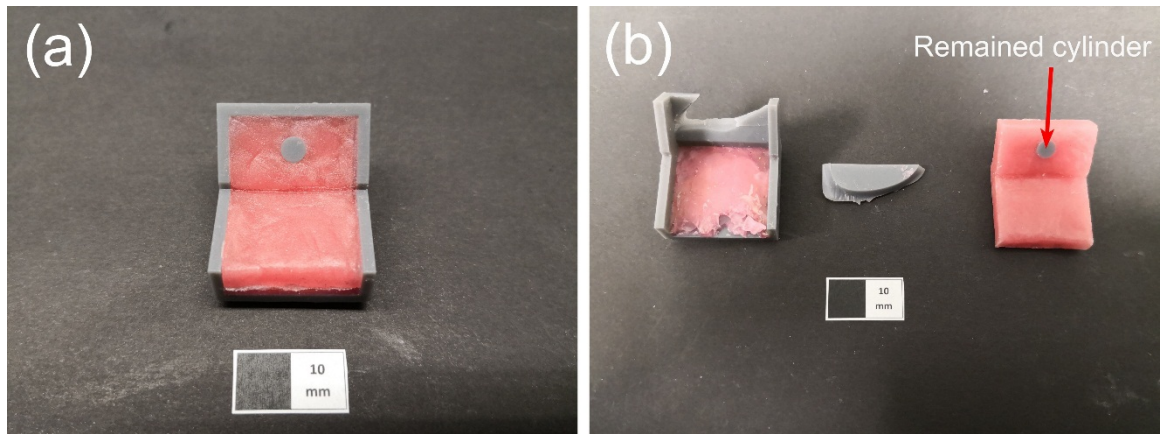


Figure 21: The cured test blocks cannot be removed from the molds with cylinder design. (a) The test block firmly remained in the mold designed in Figure 20a; (b) Excessive removal force resulted in the mold fracture, the cylinder remained in the test block (red arrow) (white scale: 10 mm).

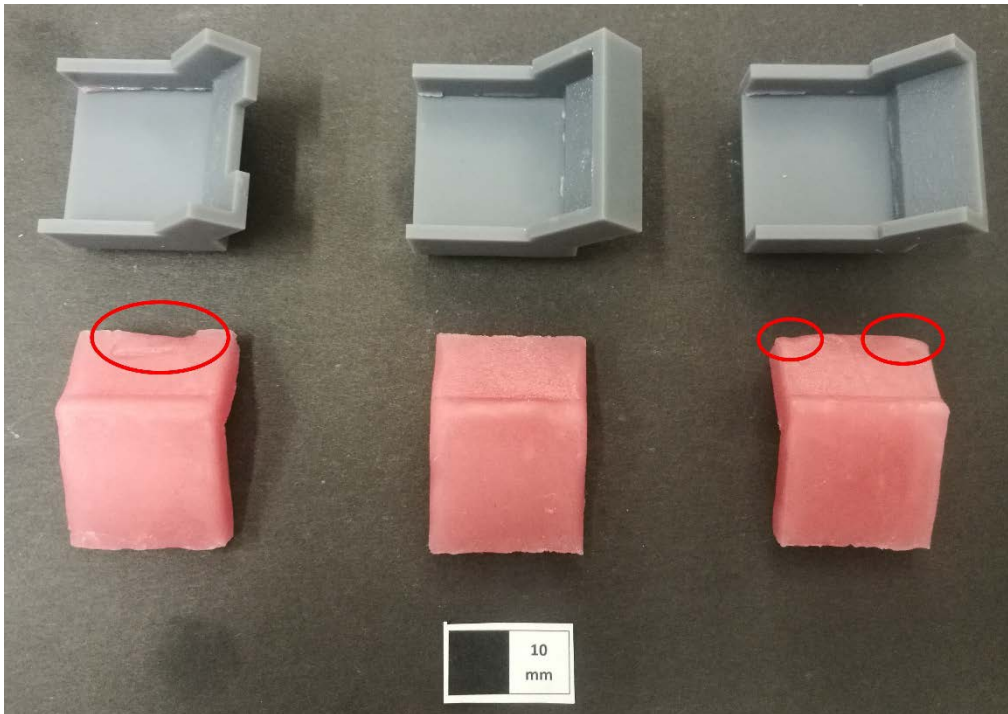


Figure 22: The cured test blocks could be removed from the molds without cylinder design. The test block fabricated by the mold designed in Figure 20c showed the best accuracy (middle). The red circles showed the inaccurate parts of the other two test blocks. (white scale: 10 mm).

2.3.2 Fabrication process of reference test block

The wax spacer was cut from the base plate wax (Modellierwachs rosa special, OMNI DENT, Rodgau Nieder-Roden, Germany) using a scalpel guided by the mold of wax spacer (Figure 23).

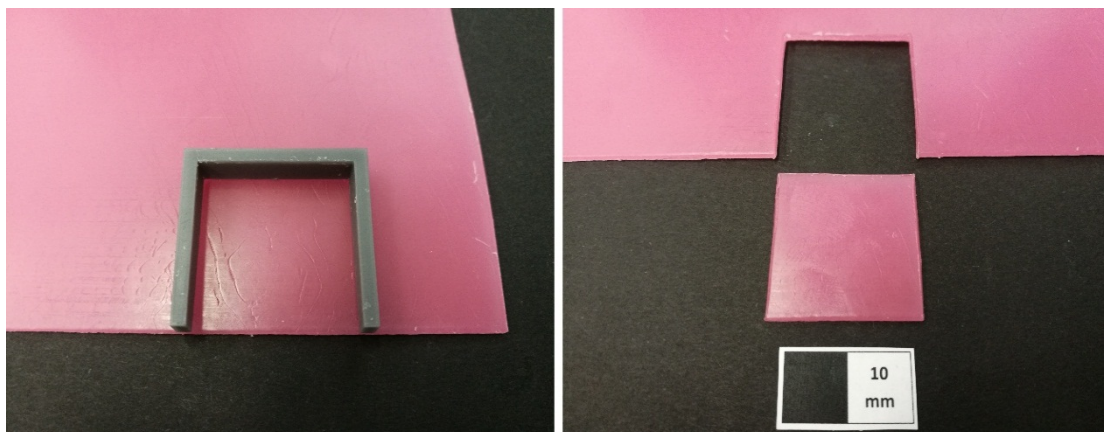


Figure 23: Fabrication of the wax spacer (white scale: 10 mm).

Next, the wax spacer was adapted at the bottom of the mold. A thin layer of vaseline was evenly applied to the inner walls of the mold (Figure 24).

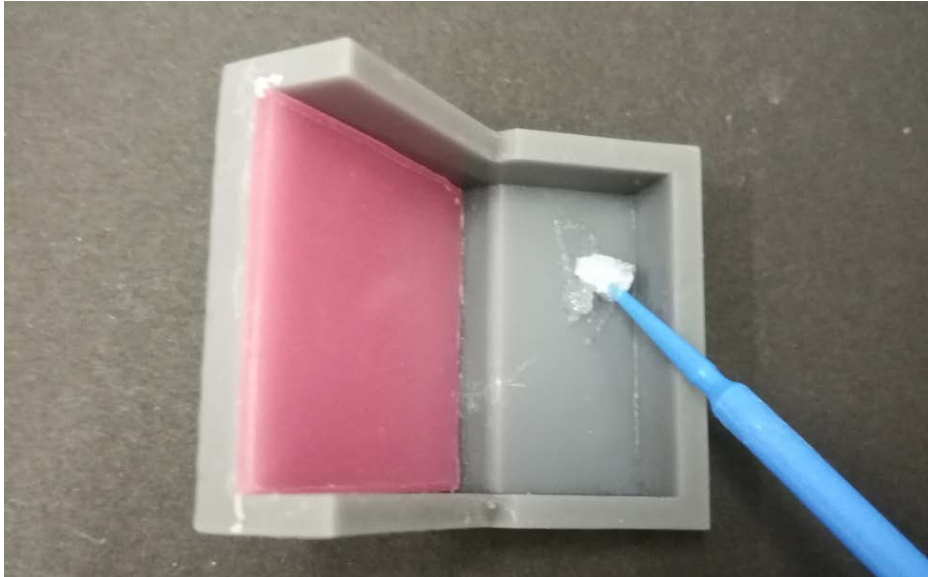


Figure 24: Vaseline was applied onto the inner walls of the mold.

A layer of a conventional light-curing custom tray material (Zeta Tray LC, Zhermack, Marl, Germany) was adapted into the mold against the wax spacer. A UV-light device (Dentacolor XS, Kulzer, Hanau, Germany) was used to cure the first resin layer for 3 minutes (Figure 25a). Afterward, the light-curing resin was adapted into the mold layer by layer until the mold was fully filled. Another UV-light device (LML2000, Wilde, Walluf, Germany) was used to cure the subsequently adapted resin for 4 minutes in atmospheric pressure and another 4 minutes in vacuum (Figure 25b).

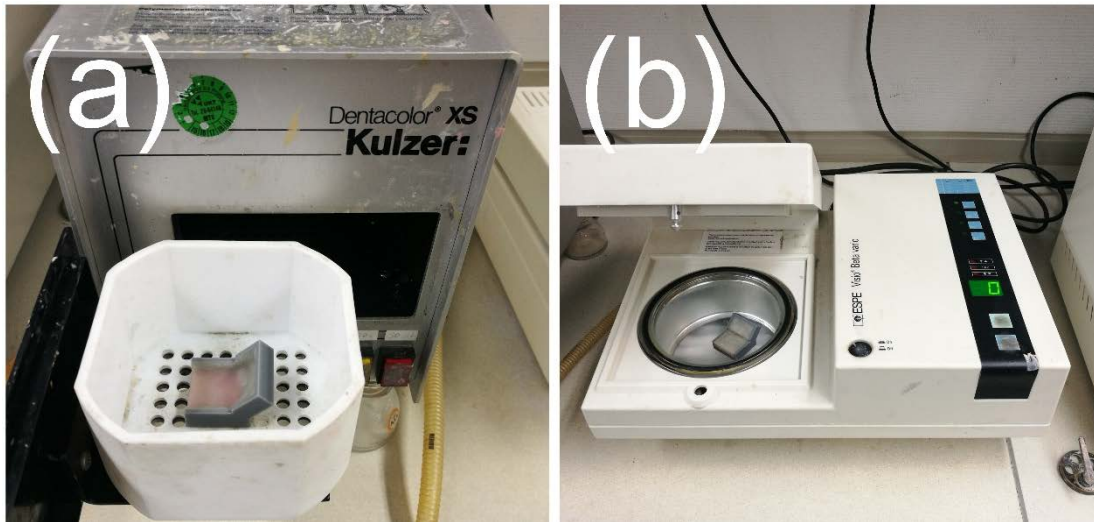


Figure 25: The UV-light curing of the reference test block. (a) The first resin layer was cured by the UV-light device “Dentacolor XS”; (b) Rest of the resin layers were cured by the UV-light device “LML2000”.

After UV-light curing, the reference test blocks were removed out from the mold. The outline of the centered hole was delineated using a marker pen guided by a premade locating paper (Figure 26).

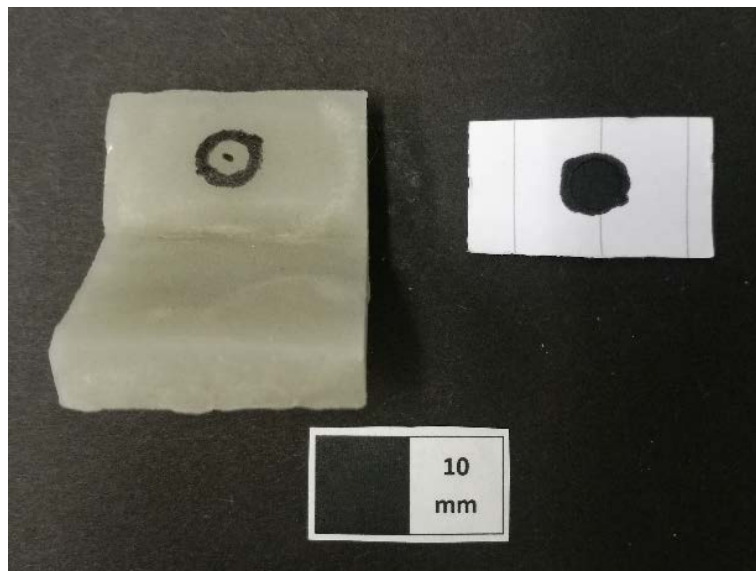


Figure 26: Marking the centered hole (white scale: 10 mm).

Then, the marked reference test block was fixed on a universal vice (Quick-action vice 3410000, Wolfcraft, Kempenich, Germany) (Figure 27a). A drilling machine (B 13S, Wörner, Denkendorf, Germany) equipped with a 4.5 mm drill bit was used to drill the

centered hole of each reference test block (Figure 27c). The quill travel was set to 49 mm, and the drilling speed was set to 488 revolutions per minute (Figure 27b).

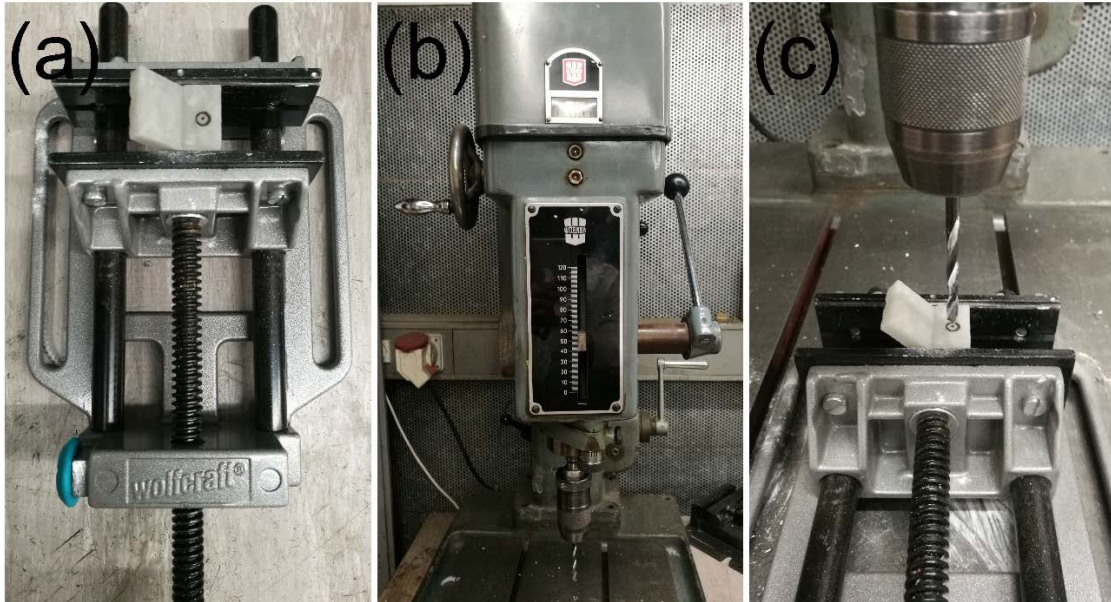


Figure 27: Drilling the centered hole of the reference test block. (a) Reference test block was fixed on a universal vice; (b) The parameter setting of the drilling machine “B 13S”; (c) The centered hole was being drilled.

After drilling, the debris was cleaned by compressed air. According to the normal clinical procedure, the wax residual of each reference test block was cleaned thoroughly by a steam jet cleaner (D-S 100 A, Harnisch + Rieth, Winterbach, Germany) and dried in air. The reference test blocks were then collected (Figure 28) and stored in black plastic bags.

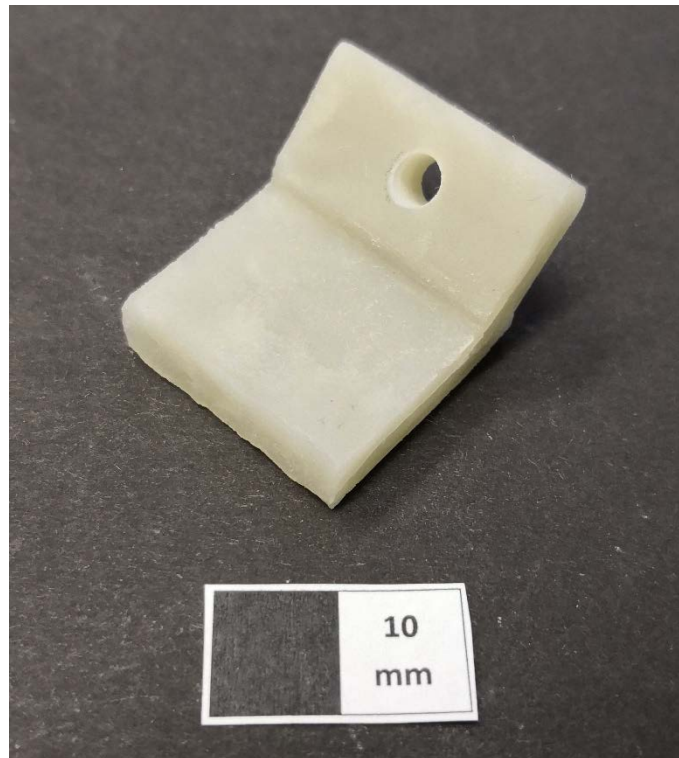


Figure 28: The fabricated reference test block.

2.4 CAD and AM of carrier

To ensure a reproducible impression depth of each test block in peel test, a carrier was designed using a CAD software (OpenSCAD, 2015.03-2 Windows, <http://www.openscad.org/>) (Figure 29a). The carrier consisted of three parts. Two lateral cubes with the dimension of $15.7 \text{ mm} \times 21 \text{ mm} \times 5.3 \text{ mm}$ (Figure 29b) were connected by an upper sheet. The central part of the sheet had a dimension of $25.4 \text{ mm} \times 19.75 \text{ mm} \times 2 \text{ mm}$, and the two lateral wings of the sheet had a dimension of $15.9 \text{ mm} \times 10 \text{ mm} \times 2 \text{ mm}$ (Figure 29c). The distance between the two cubes was 25.8 mm, which is slightly larger than the length of the test block base (25.4 mm) so that the carrier could accommodate the test block (Figure 29d).

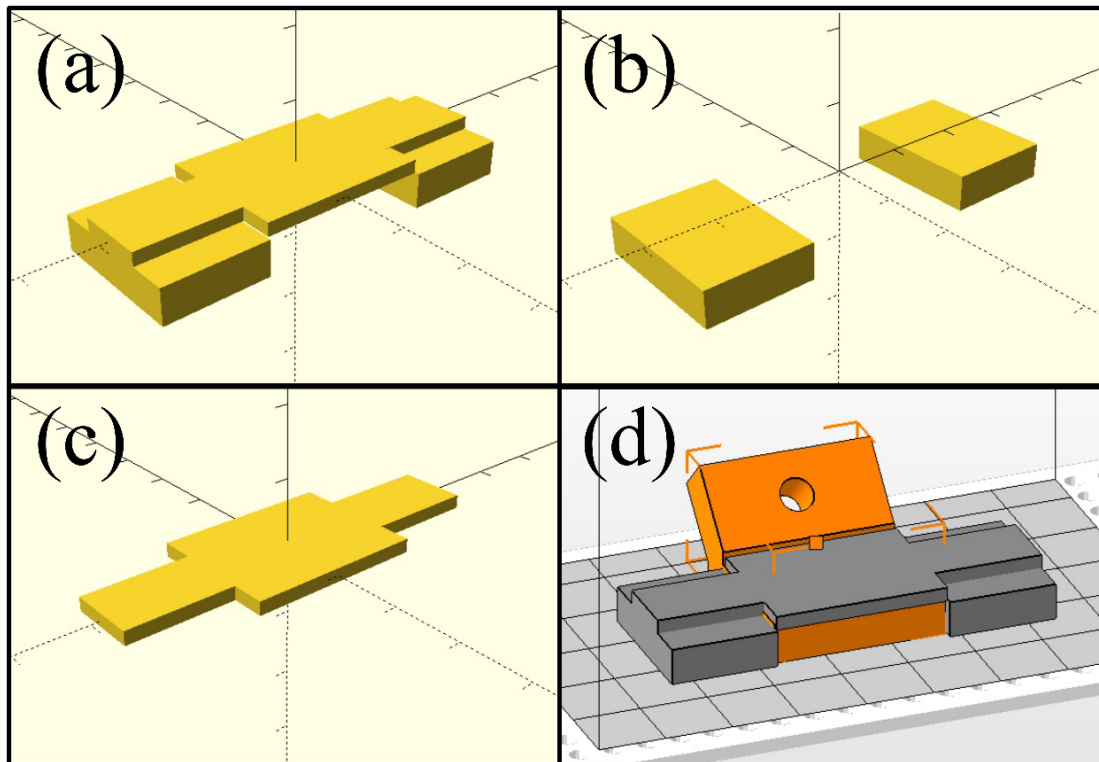


Figure 29: CAD of the carrier. (a) The CAD model of the carrier; (b) Two lateral cubes of the carrier; (c) Upper sheet of the carrier; (d) The central void part of the carrier could accommodate the test block base.

The CAD-designed carrier data were saved as STL file and sent to a 3D-printing preparing software (PreForm 2.18.0, Formlabs, Somerville, USA) for the SLA printer (Form 2, Formlabs, Somerville, USA). The printing direction and layout on the build platform are shown in Figure 30. Supporting materials were automatically generated by Preform with a height of 10 mm. The layer thickness was set to 50 μm . The carriers were printed using an engineering resin (Gery V4, Formlabs, Somerville, USA) which is suitable for repeatedly handling.



Figure 30: The printing direction and layout of the carrier.

Four carriers were printed each time for 2 hours and 47 minutes. The carriers were post-cleaned by IPA in Form Wash for 15 minutes and then exposed to 405 nm light at 60 °C for 30 minutes in Form Cure. Finally, the supporting materials were removed and the printed carriers were collected (Figure 31).

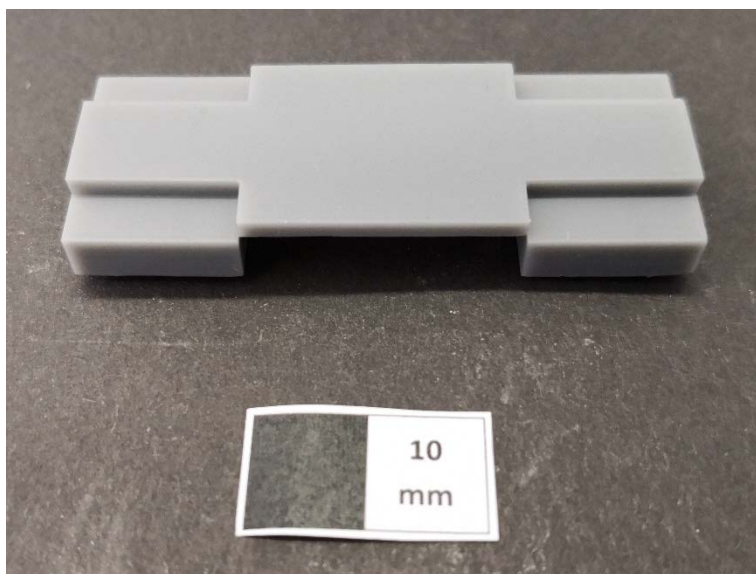


Figure 31: The SLA-printed carrier (white scale: 10 mm).

2.5 SEM analysis

In order to analyze the surface topography of the 3D-printed custom tray materials, one sample of each material group was sputtered by a sputter coater (SCD 050, BAL-TEC,

Pfaeffikon, Switzerland) and observed in an SEM (Leo 1430, Zeiss, Jena, Germany). Photos of the sputter coater and the SEM system are shown in Figure 32 and Figure 33 respectively.



Figure 32: Sputter coater “BAL-TEC SCD 050”.

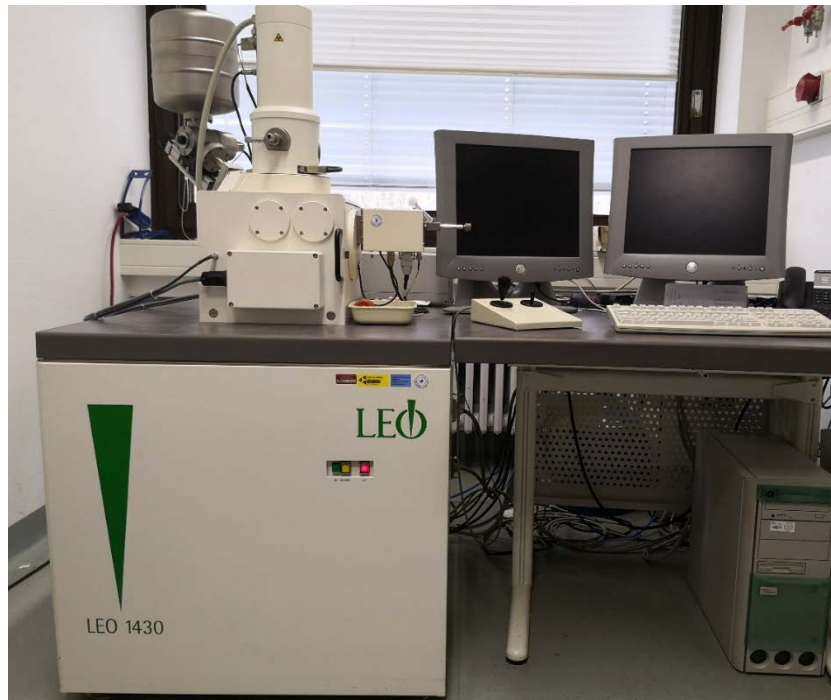


Figure 33: SEM system “Zeiss LEO 1430”.

For sample preparation, the handle of each test block was firstly removed by a saw, so that the test block could be fixed on holders with the test surfaces placed horizontally upwards. Since the test blocks were made from non-conductive polymers, liquid silver paint (Silberleitlack, Plano, Wetzlar, Germany) was applied to connect the holder and the test surface of each sample. After drying for 30 minutes, all samples were placed in the chamber of the sputter coater (Figure 34a). The chamber of the sputter coater was then purged with Argon to replace air and pumped down to the working pressure of 0.05 mbar. With the current of 61 mA, Au-Pd alloy (SCD 050, BAL-TEC, Luebeck, Germany) was sputtered onto the test surface of each sample for 120 seconds to form a 20 nm thick Au-Pd coating (Figure 34b).

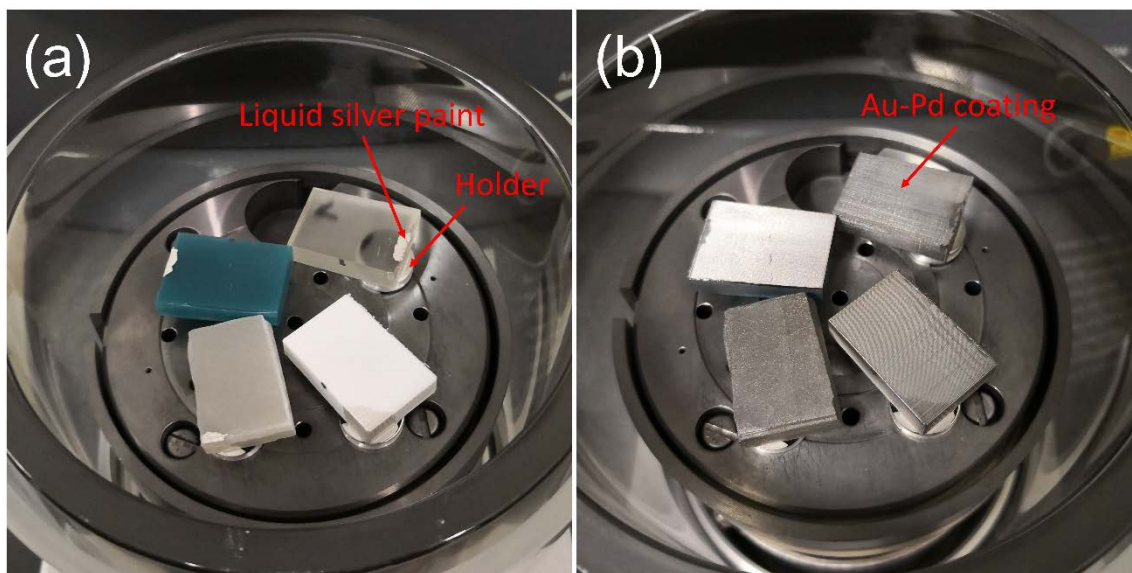


Figure 34: Sample sputtering before SEM analysis. (a) The test surface and holder were connected with liquid silver paint to conduct electricity; (b) Au-Pd coating was sputtered on the test surface of each sample.

Afterward, the sputtered samples were placed in the chamber of the SEM. The air pressure in the chamber was pumped down to vacuum. At the acceleration voltage of 10 kV, representative images of the test surfaces were taken with the magnification of 100 \times , 500 \times , 1000 \times , and 2000 \times .

2.6 Roughness measurement

The tilt of test blocks was firstly corrected by a leveling device (Schliffpresse, Leitz, Wetzlar, Germany) so that the test surface could be horizontally upward (Figure 35a). Seven samples of each tray material were measured by a profilometer (S6P, Mahr, Goettingen, Germany) (Figure 35b). The profilometer was equipped with a stylus, whose diameter and angle were 2 μm and 90°, respectively. When the profilometer performed a surface topography measurement, the stylus tip moved in contact with the measured surface to physically trace surface profiles. In an area of 3 mm x 3 mm on the test surface, 121 profiles with a length of 3 mm were recorded.

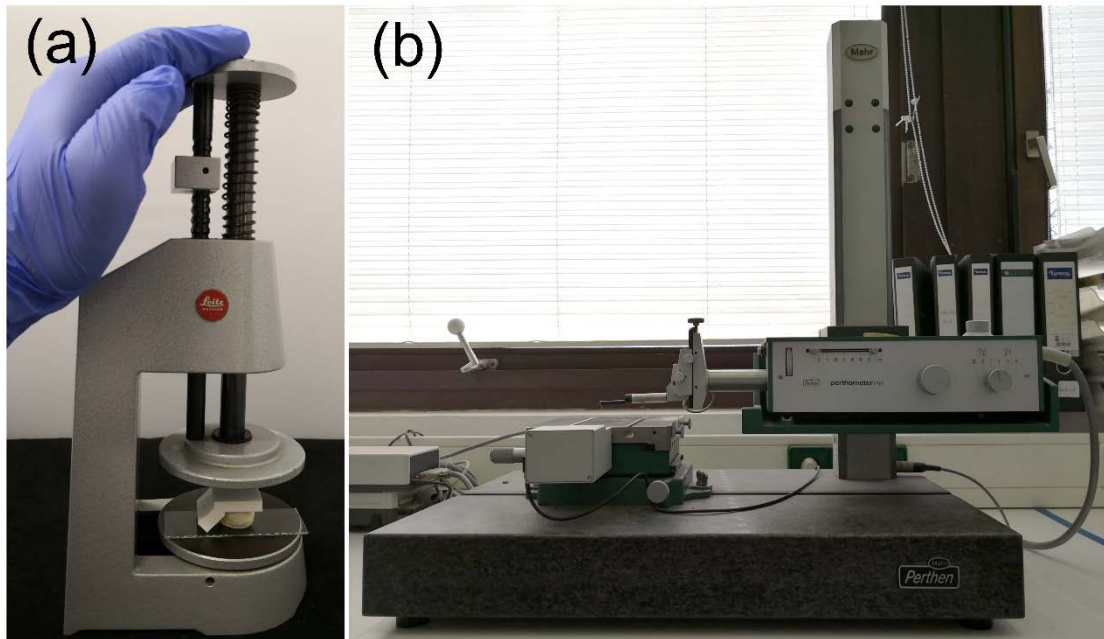


Figure 35: Devices used for roughness measurement. (a) The leveling device “Leitz Schliffpresse”; (b) The profilometer “Mahr S6P”.

After measuring, the data were analyzed in a roughness analysis software (MountainsMap Universal 7.3, Digital Surf, Besancon, France). The measured area was leveled in the software to correct tilt again. The roughness of the profiles was then filtered from waviness and form by a Robust Gaussian Filter (ISO 16610-71) with the cut-off value of 0.6 mm. Five three-dimensional roughness parameters that might be

able to disclose the correlations between the surface roughness and the peel bond strength were calculated, i.e., Sa, Ssk, Vvc, Vvv, and Sdr. Finally, the three-dimensional views of the test surfaces were reconstructed to visualize the surface topographies.

2.7 Peel bond strength test

The present study investigated the peel bond strength between three selected 3D-printing custom tray materials (Dental LT, FREEPRINT tray, and PLA), which were respectively printed by three AM technologies (SLA, DLP, and FFF), and three commonly used impression/adhesive systems (VSXE, VPS, and PE). A conventional light-curing resin was investigated as the reference custom tray material. Therefore, there were 12 groups with 144 samples in total ($n = 12$) (Figure 36).

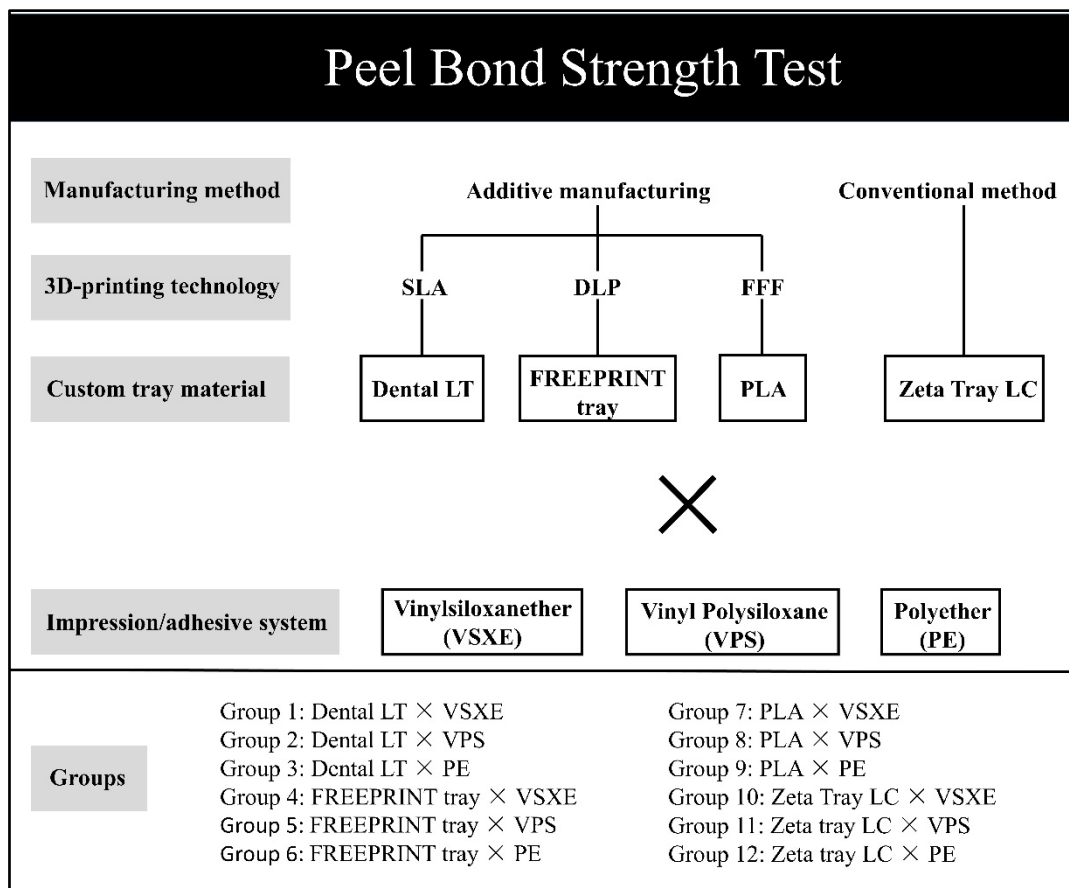


Figure 36: Grouping of peel bond strength test.

To retain the impression material, a universal adaptor was prepared as the following

steps. First, three screws were inserted into the adaptor (Figure 37a). The filling material, addition-vulcanising vinyl-polysiloxane (Dublisil 30, Dreve Dentamid, Unna, Germany), was then filled in the universal adaptor by a mixing device (Dosper evo, Dreve Dentamid, Unna, Germany) to the pre-marked line, which was 3 mm from the top edge of the adaptor (Figure 37b). After 45 minutes of setting, the filling material polymerized and was thus fixed by the screws. The reserved 3 mm thick space above the filling material would be used to retain the impression material and standardize its thickness.

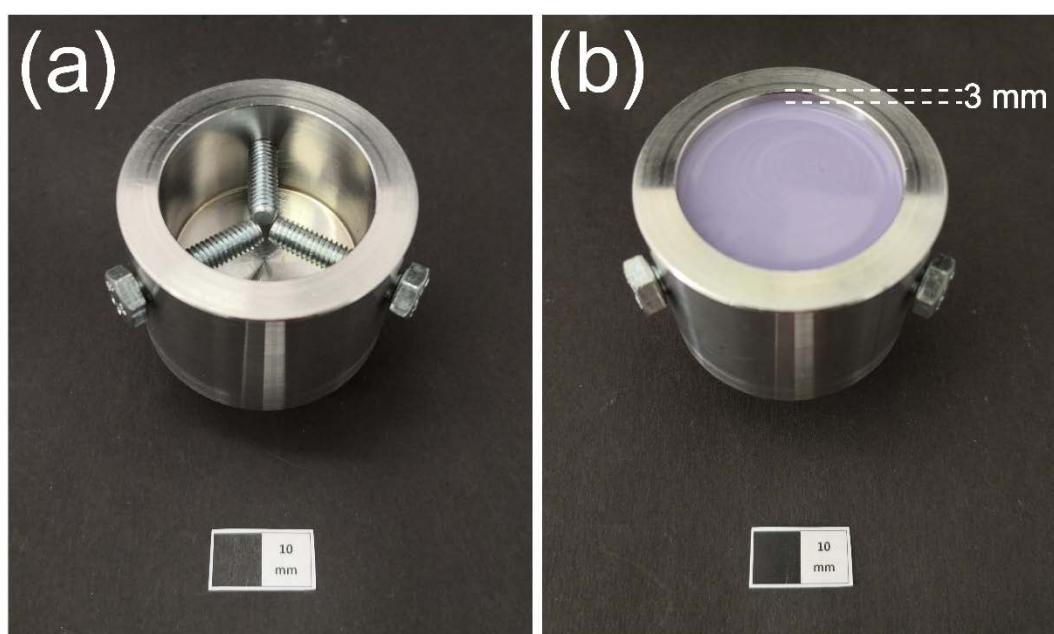


Figure 37: Preparation of the universal adaptor. (a) Three screws were inserted into the adaptor; (b) The filling material was 3 mm from the top edge of the adaptor (white scale: 10 mm).

Test blocks of each material group were cleaned by a steam jet machine (D-S 100 A, Harnisch + Rieth, Winterbach, Germany) and dried in air. Vaseline was applied to the surrounding walls around the test surface (Figure 38a). Afterward, the carrier was bonded to each test block by molten adhesive wax (Supradent-Wachs, Oppermann, Bonn, Germany) to construct a text complex (Figure 38b). The adhesive was then smeared on the test surface and dried in air (Figure 38c). With the use of an automatic mixing unit (Pentamix 2, 3M ESPE, Seefeld, Germany), the impression material was

uniformly dispensed in the adaptor, and the excessive impression material was removed by a dental mixing knife.

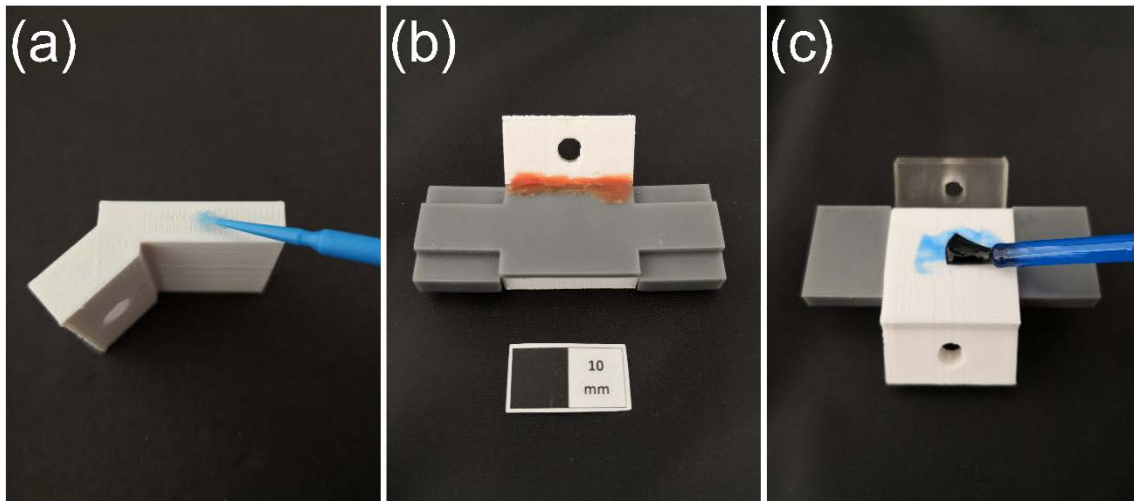


Figure 38: Preparation of the test block. (a) Vaseline was applied to the surrounding walls around the test surface; (b) The carrier and the test block were bonded by molten adhesive wax to construct a test complex; (c) A thin layer of the adhesive was smeared on the test surface (white scale: 10 mm).

Next, the test complex was placed in the center of the adaptor with impression material underneath at 23 °C room temperature and then fixed by a custom-made loading device in a 37 °C incubator (B 6200 (I), Heraeus, Hanau, Germany) (Figure 39b). A perpendicular weight of 1.4 kg was applied onto the center of the test complex to mimic the compressive force during the impression taking. Since the two lateral cubes of the carrier contacted the border of the adaptor, a reproducible impression depth of each test block was standardized (Figure 39a). The controlled temperature of 23 °C and 37 °C was used to simulate the extraoral and intraoral environment respectively. The adhesive drying time, extraoral working time, and intraoral set time of each impression/adhesive system were strictly executed according to the manufacturer's instructions (Table 3).

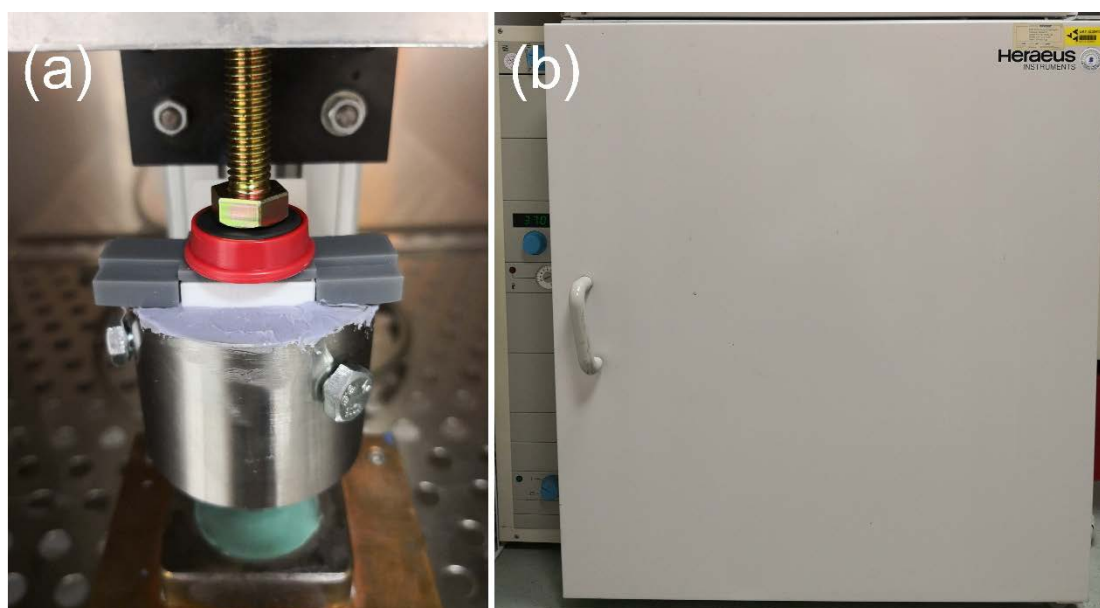


Figure 39: The impression setting in the peel bond strength test. (a) The test complex was fixed by a custom-made loading device with a perpendicular weight of 1.4 kg; (b) The custom-made loading device was enclosed in a 37 °C incubator to simulate the intraoral temperature.

Table 3: Impression/adhesive systems used in the present study.

Trade name	Identium Heavy (5:1)	Flexitime Heavy Tray Dynamix	Impregum Penta H Duo Soft
Chemical component	Vinylsiloxanether (VSXE)	Vinyl Polysiloxane (VPS)	Polyether (PE)
Impression type	Type 1, Heavy body	Type 1, Heavy body	Type 1, Heavy body
Adhesive	Identium Adhesive	Universal Adhesive	Polyether Adhesive
Manufacturer	Kettenbach, Eschenburg, Germany	Kulzer, Hanau, Germany	3M Deutschland, Neuss, Germany
Adhesive drying time	5 min	2 min	1 min
Impression working time (23 °C)	2 min	2 min	2:30 min

(continued)

(continued)

Impression intraoral set time (37 °C)	2:30 min	2:30 min	3:30 min
Total set time	4:30 min	4:30 min	6 min

After impression setting, the carrier was removed. With the separating effect of vaseline, the excessive impression material around the test block was effortlessly detached and cut off by a sharp scalpel, making the bonding only exist between the test surface and the impression material. The adaptor was then fixed in a universal testing machine (Z010, Zwick, Ulm, Germany) (Figure 40a). A tensile load at a crosshead speed of 300 mm/min was applied to the test block through a hook connected with a metal wire to produce a peeling force between the test block and the impression material (Figure 40b). The force and distance were dynamically recorded by the universal testing machine until the failure between the test block and the impression material occurred (Figure 40c).

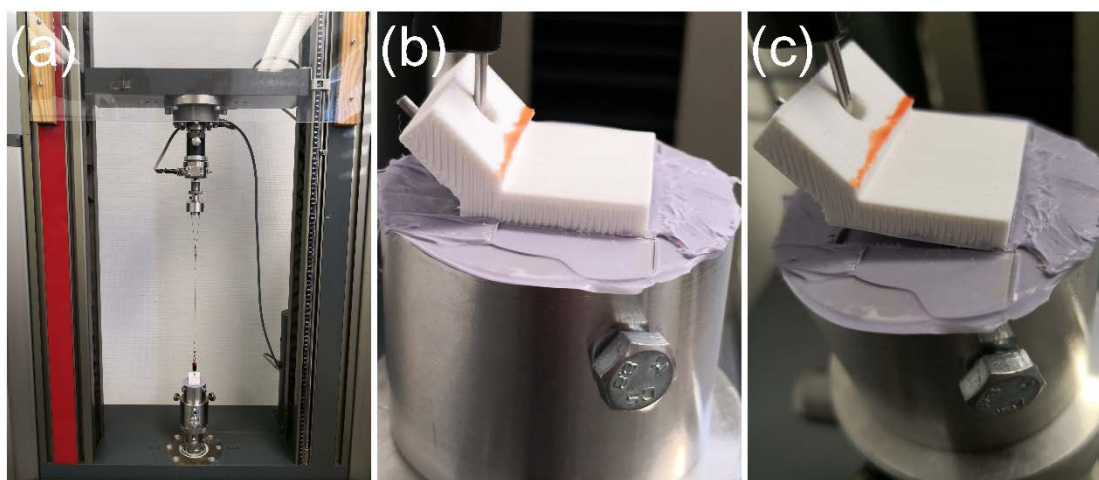


Figure 40: Peel bond strength test. (a) The universal testing machine; (b) A tensile load at a crosshead speed of 300 mm/min was applied to the test block; (c) The test block was detached from the impression material after peeling.

The force and distance data were then transferred to an analysis software (OriginPro 8,

OriginLab, Northampton, USA) to plot the force-distance curve. The width and length of each test surface were measured by a digital caliper (DIGI-MET, PREISSER, Gammertingen, Germany). The area of each test surface was calculated by Equation (1):

$$A = W \times L \quad (1)$$

where A is the area (m^2), W represents the width (m), and L represents the length (m) of each test surface. The formula of line peel bond strength was given by Equation (2):

$$\sigma_1 = F/W \quad (2)$$

where σ_1 is the line peel bond strength (N/m), F is the force at failure (N), and W is the width (m) of each test surface. The areal peel bond strength of each test block was determined by Equation (3):

$$\sigma_2 = F/A \quad (3)$$

where σ_2 is the areal peel bond strength (Pa), F is the force at failure (N), and A represents the area (m^2) of each test surface.

2.8 Failure mode analysis

After peeling, test surfaces were examined using a microscope (M400, Wild, Heerbrugg, Switzerland) with $6.3 \times$ and $32 \times$ magnification. The failure mode was recorded as adhesive failure, mixed failure, and cohesive failure. The definition of each failure mode used in this study is shown in Table 4.

Table 4: Classification and definition of the failure mode.

Failure mode	Definition
Adhesive failure	The detachment occurred between the impression material and the test block. No impression material residual could be found on the test block after peeling.

(continued)

(continued)

Mixed failure	The detachment occurred partly between the impression material and the test block, and partly within the impression material. Punctiform or flaky impression material residuals can be found on the peeled test surface.
Cohesive failure	The detachment occurred within the impression material. A large lump of integrated impression material could be found on the peeled surface of the test block.

To identify the rupture site of adhesive failure, the peeled test surfaces and impressions were further inspected and compared microscopically. The possible rupture sites were pre-classified as: at the adhesive-impression material interface, at the adhesive-tray material interface, and within the adhesive layer.

2.9 Statistical analysis

All data were first checked for normal distribution. The mean differences in roughness parameters including Sa, Ssk, Vvc, Vvv, and Sdr among the four custom tray materials were determined using one-way analysis of variance (ANOVA) followed by Tukey's range test for multiple comparisons. A two-way ANOVA was performed to examine the effect of tray material and impression/adhesive system on peel bond strength. In the following simple main effect analysis, Tukey's test was conducted for post hoc comparisons. GraphPad Prism (Prism 6.01 for Windows, GraphPad Software, San Diego, USA) was used for all statistical analyses. Differences were considered to be statistically significant when the p value was less than 0.05.

3. Results

3.1 SEM

As shown in Figure 41, the SLA-printed Dental LT test block exhibited a relatively smooth and flat surface except for some scratches with no specific direction. At higher magnifications, it was observed that the scratches were mainly composed of irregular micro ridges and prominences.

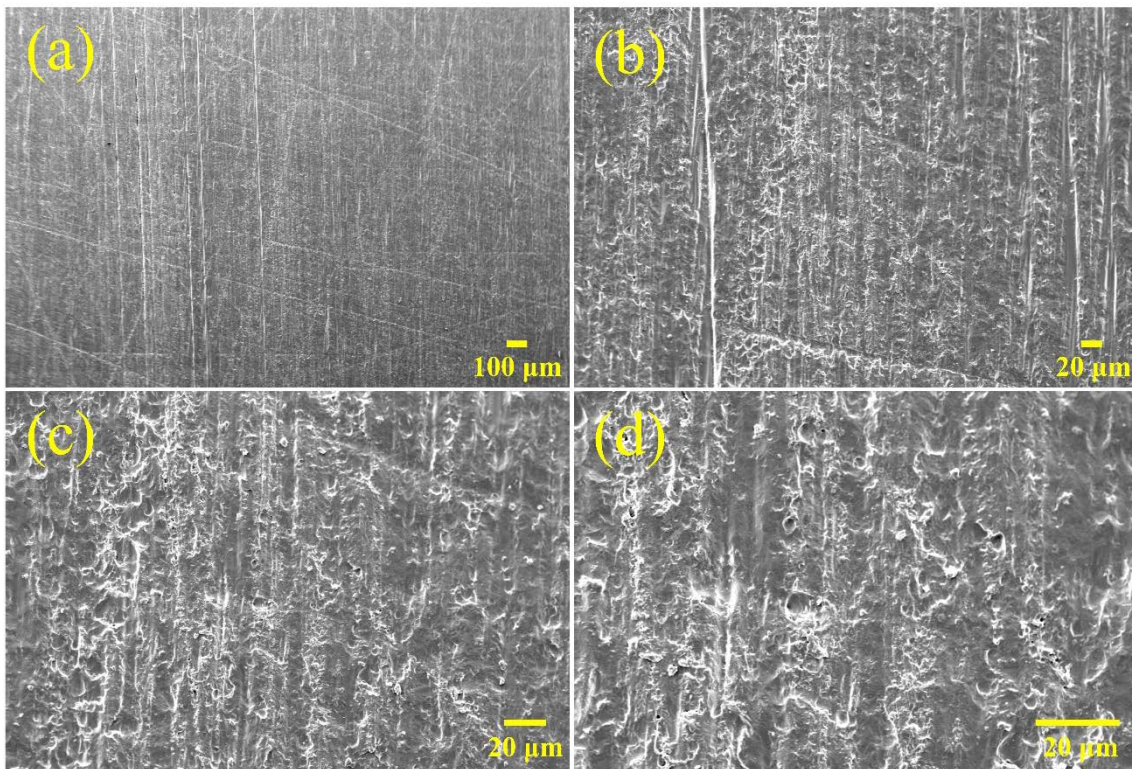


Figure 41: SEM images of the test surface of the SLA-printed Dental LT test block. (a) $100 \times$ magnification; (b) $500 \times$ magnification; (c) $1000 \times$ magnification; (d) $2000 \times$ magnification.

On the surface of the DLP-printed FREEPRINT tray test block, a surface texture composed of numerous regular valleys and peaks was clearly observed (Figure 42), the direction of which was consistent with the printing direction of the test block on the 3D printer's build platform. The SEM images with $1000 \times$ and $2000 \times$ magnifications further showed the microroughness structures: the peaks consisted of fibrous polymer strips, on which small particles could be found. Presumably, the formed microroughness

structures were related to the chemical polymerization of the resin.

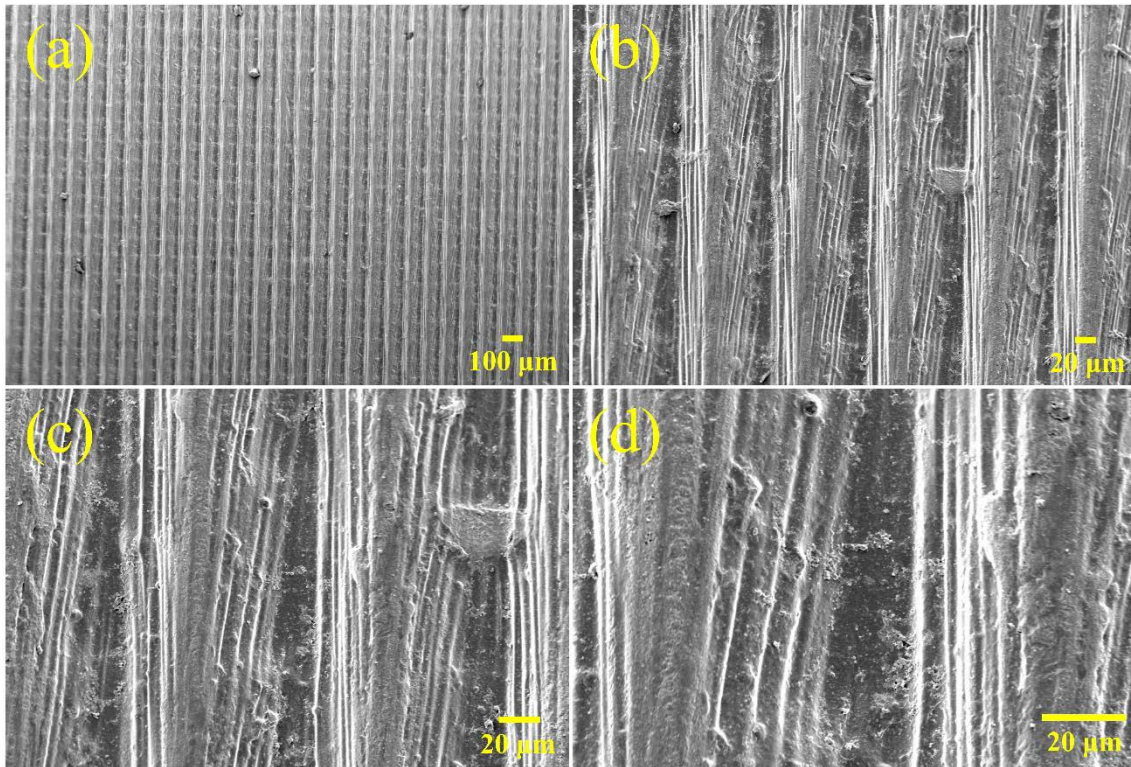


Figure 42: SEM images of the test surface of the DLP-printed FREEPRINT tray test block. (a) $100 \times$ magnification; (b) $500 \times$ magnification; (c) $1000 \times$ magnification; (d) $2000 \times$ magnification.

Similarly, a wavy surface was observed on the FFF-printed PLA test block (Figure 43). However, the surface texture direction of the FFF-printed test block was perpendicular to the printing direction, and the diameter of the FFF-printed peak ($170 \mu\text{m}$) was significantly greater than that of the DLP-printed one ($80 \mu\text{m}$). The high-magnification SEM images showed that the PLA-printed peaks were semispherical and smooth, on which few microroughness structures could be observed.

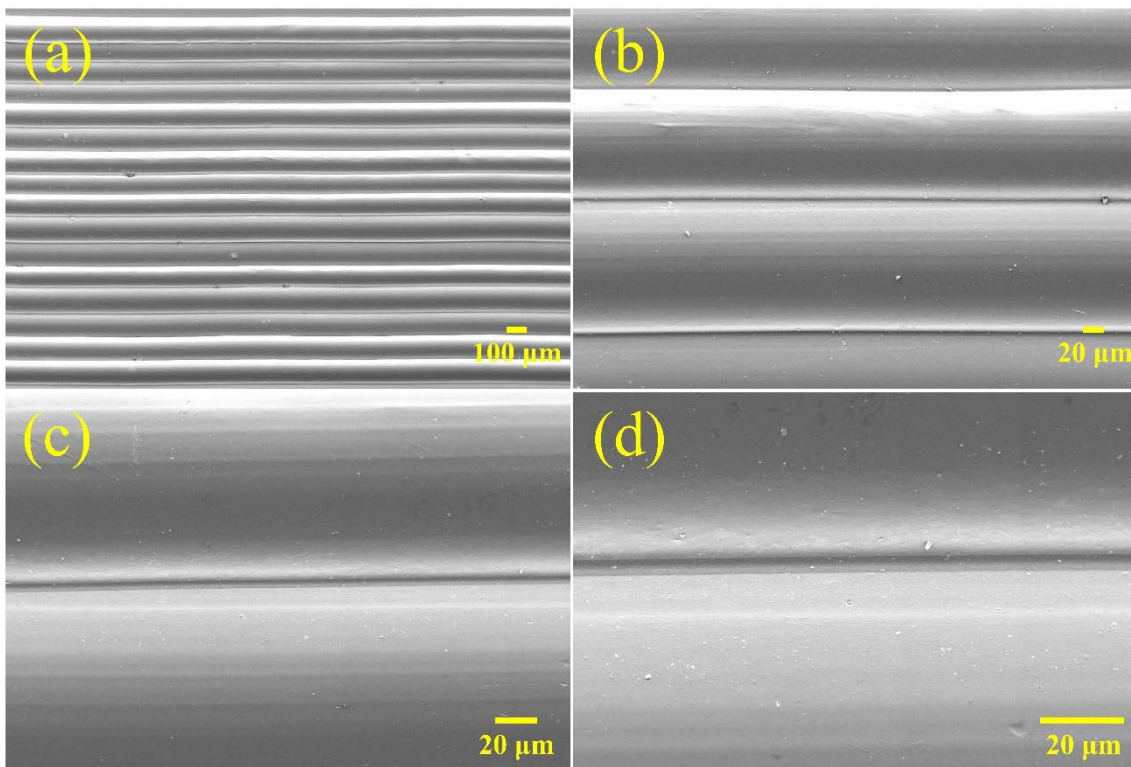


Figure 43: SEM images of the test surface of the FFF-printed PLA test block. (a) $100 \times$ magnification; (b) $500 \times$ magnification; (c) $1000 \times$ magnification; (d) $2000 \times$ magnification.

As Figure 44 indicates, the conventional light-curing resin, Zeta tray LC, showed a plane surface with few peaks. Numerous irregular pores, pits, and fissures were observed with uneven sizes, which ranged approximately from $10 \mu\text{m}$ to $100 \mu\text{m}$. Some of these recessed structures existed alone, while the others were connected, resulting in the formation of the larger cracks. The $1000 \times$ and $2000 \times$ magnified SEM images showed that spheres with a diameter from $2 \mu\text{m}$ to $20 \mu\text{m}$ were embedded in the surface. The wax residual was cleaned thoroughly by the steam and could not be found. The pores and pits were formed by the interruption of the plane surface, in which irregular walls could be observed. However, the SEM failed to detect the bottom of the valley, signifying the pores and pits possessed a certain depth.

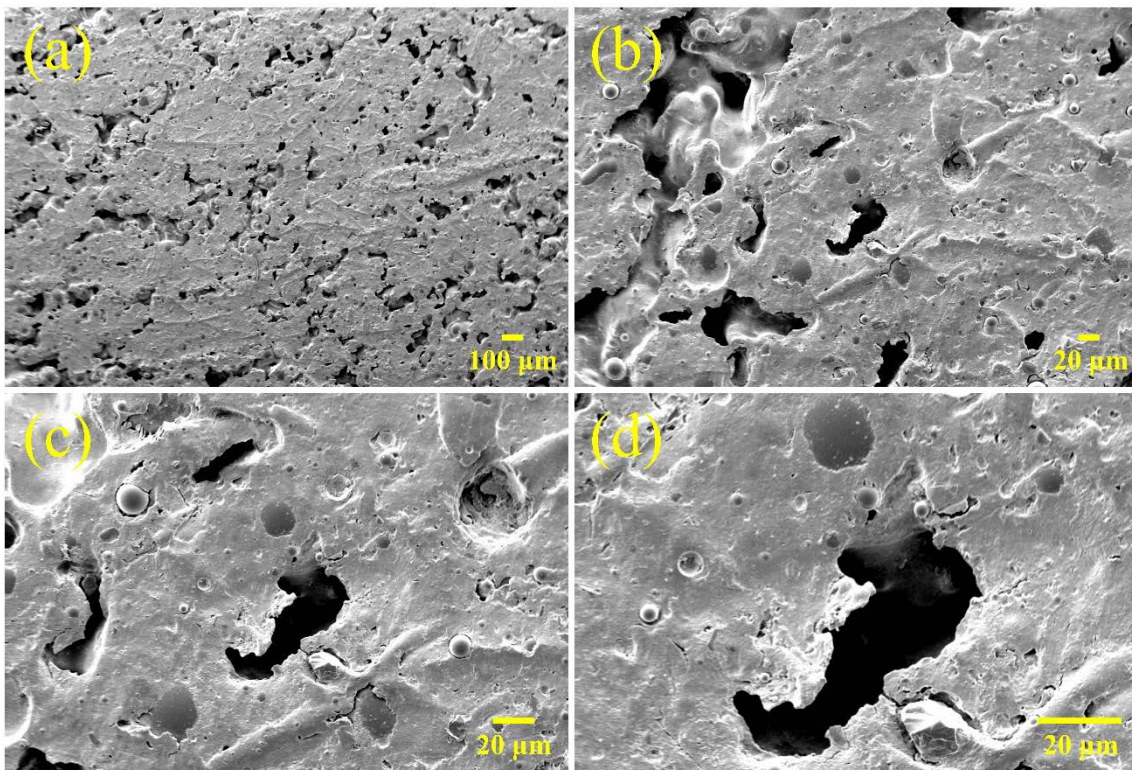


Figure 44: SEM images of the test surface of the conventionally light-cured Zeta tray LC test block. (a) 100 × magnification; (b) 500 × magnification; (c) 1000 × magnification; (d) 2000 × magnification.

3.2 Roughness measurement

As shown in Figure 45, the Sa value of the PLA group was the highest and statistically higher than that of the other three material groups, followed by the FREEPRINT tray and the reference group, which did not statistically differ. The Dental LT group showed the lowest Sa value, which was significantly lower than that of the other groups. The PLA group had the highest standard deviation (2.65), indicating that the consistency in Sa value among the PLA samples was relatively low.

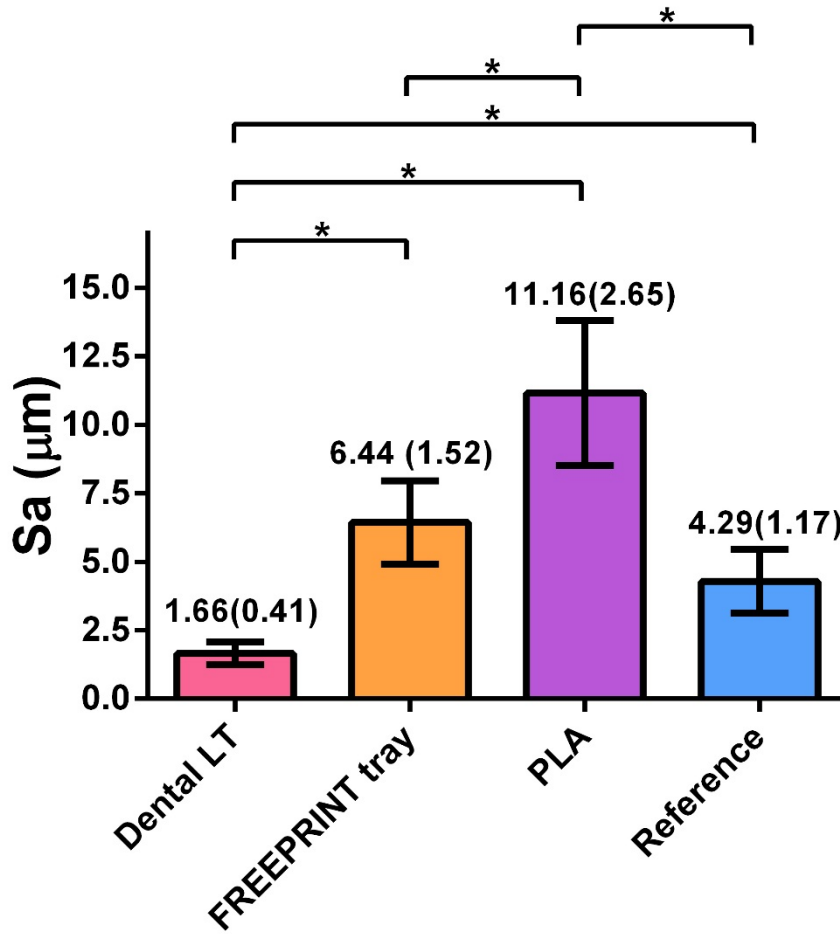


Figure 45: Mean (standard deviation) Sa values of all material groups (n = 7). * represents a statistically significant difference.

As Figure 46 indicates, the mean Ssk values of the four investigated material groups were all negative. Among them, the Ssk value of the reference group was the lowest, which statistically differed from that of the other material groups. Then came the Dental LT group, whose Ssk value was statistically lower than that of the PLA and the FREEPRINT tray group. The Ssk values of the PLA and the FREEPRINT tray group were similar and close to zero, statistically significant difference could not be observed between them. With a standard deviation of 0.81, the Dental LT samples showed a relatively high degree of dispersion in Ssk.

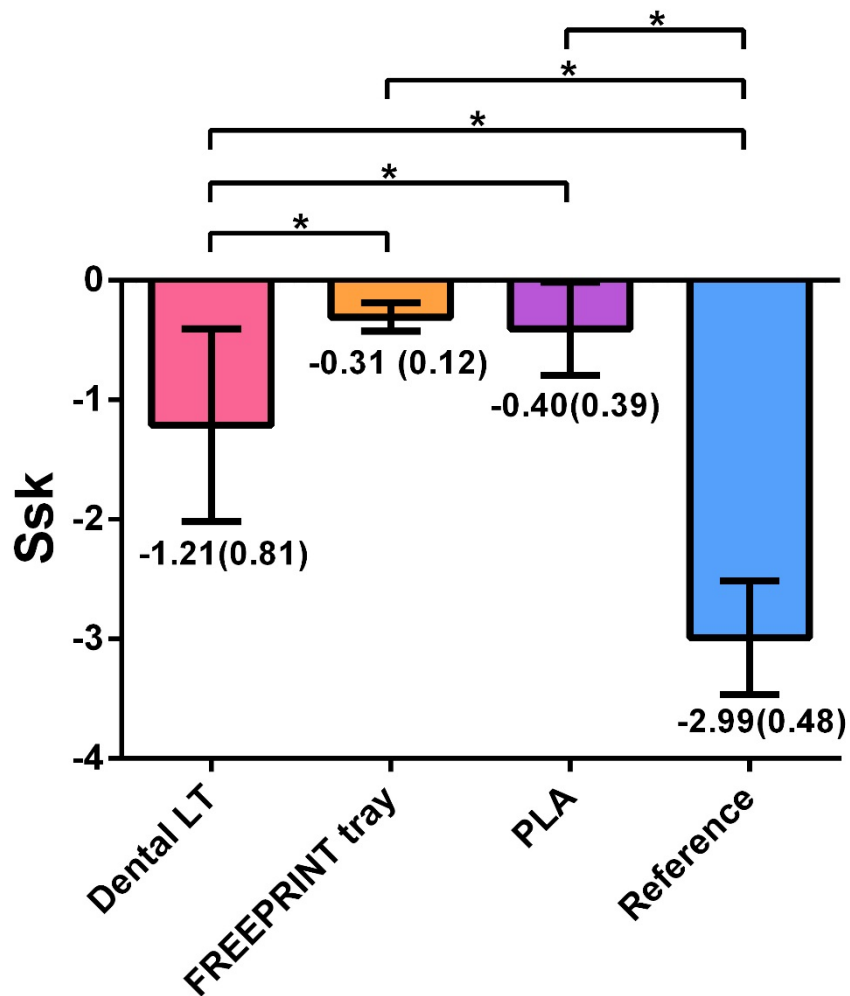


Figure 46: Mean (standard deviation) Ssk values of all material groups ($n = 7$). * represents a statistically significant difference.

As illustrated by Figure 47, the PLA group exhibited the highest Vvc value, which showed significant difference with that of any other material group, followed by the FREEPRINT tray group, whose Vvc value was approximately half of that of the PLA group but statistically higher than that of the Dental LT and the reference group. The mean Vvc value of the reference group was slightly higher than that of the Dental LT group, but no statistically significant difference could be found between them.

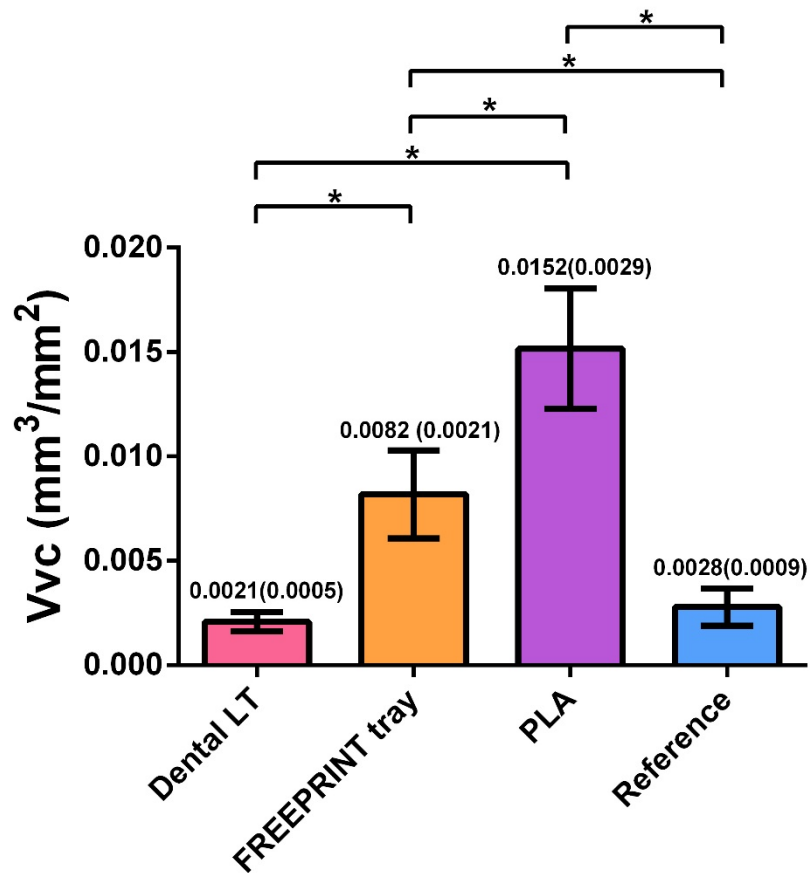


Figure 47: Mean (standard deviation) Vvc values of all material groups (n = 7). * represents a statistically significant difference.

As shown in Figure 48, the Vvv values of the PLA and the reference group were significantly higher than that of the Dental LT and the FREEPRINT tray group. Statistical differences could not be observed both between the PLA and the reference group and between the Dental LT and the FREEPRINT tray group. Compared with other material groups, the standard deviation of the PLA group was relatively high (0.0006).

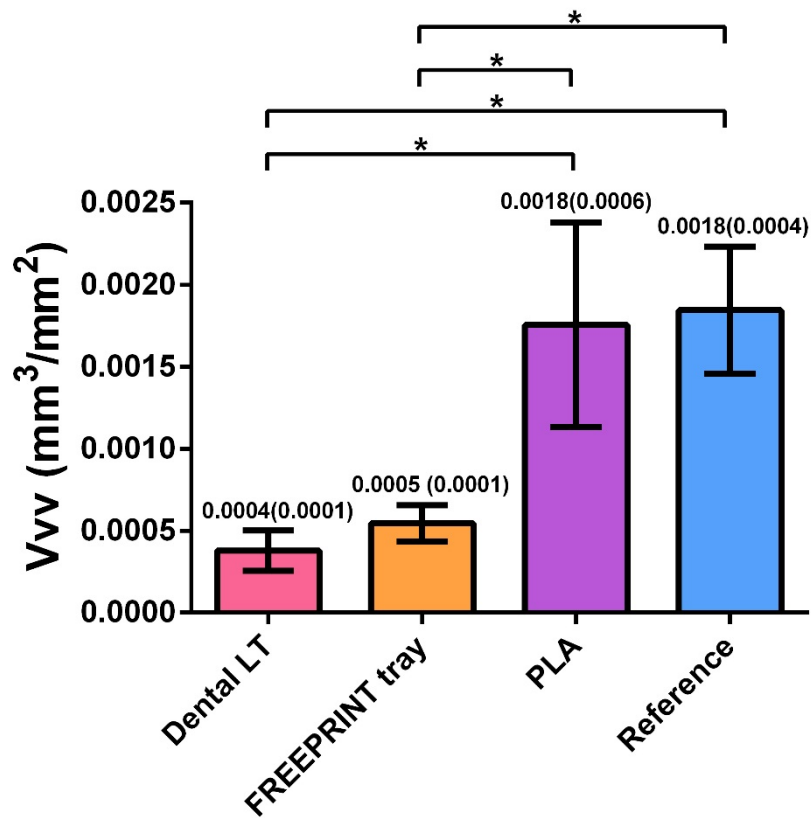


Figure 48: Mean (standard deviation) Vvv values of all material groups (n = 7). * represents a statistically significant difference.

As Figure 49 indicates, the statistical analysis result of Sdr was similar to that of Sa: the PLA group showed the highest Sdr value, which was significantly higher than that of the other groups. Then came the FREEPRINT tray and the reference group, between which no statistical difference could be found. The Dental LT group exhibited the lowest Sdr value, which statistically differed from that of the other groups. The Sdr values of the FREEPRINT tray group showed a relatively high degree of dispersion, which was presented by the standard deviation of 3.27.

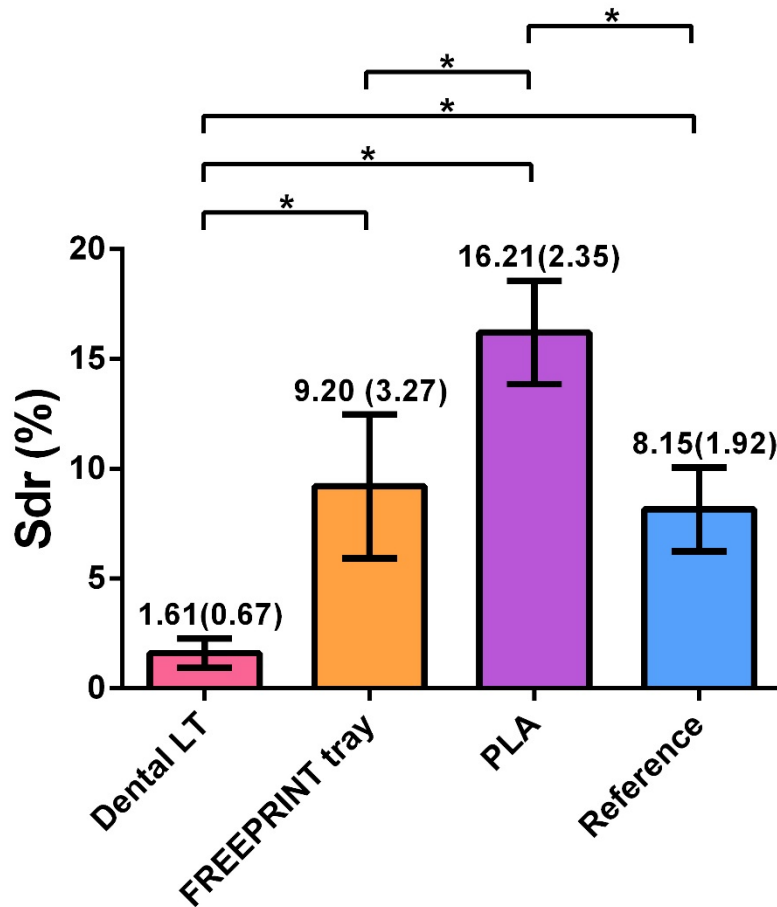


Figure 49: Mean (standard deviation) Sdr values of all material groups ($n = 7$). * represents a statistically significant difference.

The 3D-reconstructed surface topographies of the four material groups are shown in Figure 50. The surface of the Dental LT test block (Figure 50a) was relatively smooth with no evident texture. In contrast, waveforms in presence of peaks and valleys could be easily identified on both surfaces of the FREEPRINT tray and the PLA test block (Figure 50b and 50c). By comparing the two wavy surfaces, it was found that the DLP-printed FREEPRINT tray surface was flatter with a more uniform peak-to-valley distance ranged from $10\ \mu\text{m}$ to $20\ \mu\text{m}$, while the FFF-printed PLA surface had a larger undulation, and the distance between the peaks and valleys ranged from $30\ \mu\text{m}$ to $70\ \mu\text{m}$. Besides, the directions of the two surface textures were opposite and perpendicular to each other. The conventionally fabricated reference test block presented a porous

surface without textures (Figure 50d). The pores had irregular sizes and shapes with depths ranging from about 20 μm to 80 μm . Few peaks could be observed on the reference surface, and if any, their heights were less than 10 μm .

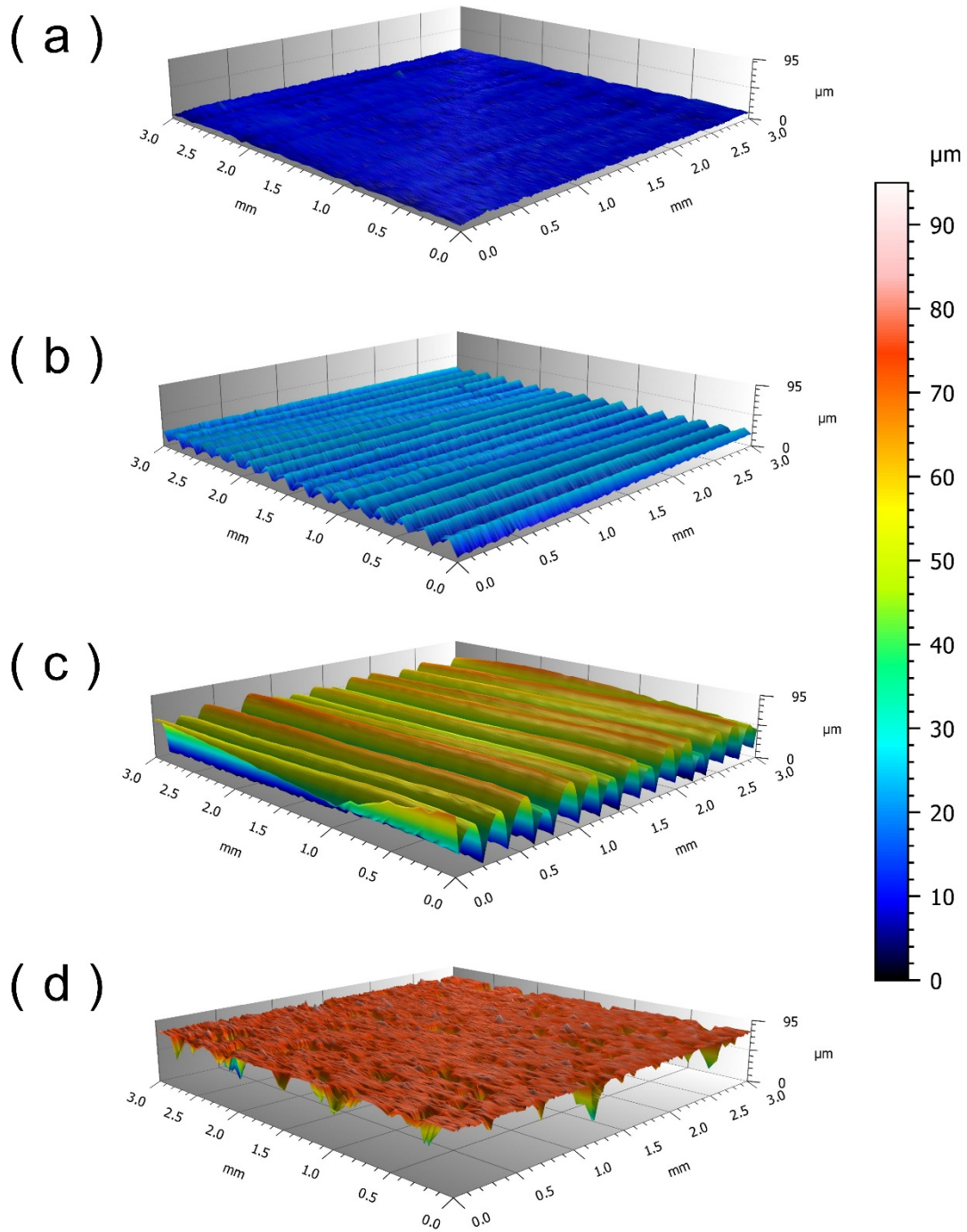


Figure 50: 3D-reconstructed surface topographies of the test blocks (15% vertical amplification). (a) Dental LT; (b) FREEPRINT tray; (c) PLA; (d) Reference.

3.3 Peel bond strength test

The profile of the peeling force-distance curve was found to be mainly affected by the impression/adhesive system and the failure mode. Figure 51 shows the representative curves of adhesive failure of each group. For peeling from the VSXE and VPS impression/adhesive systems, the curves ascended rapidly from the beginning point. After reaching the peak, the detachment between the test block and the impression occurred. The curves then dropped immediately and sharply until the universal testing machine automatically stopped.

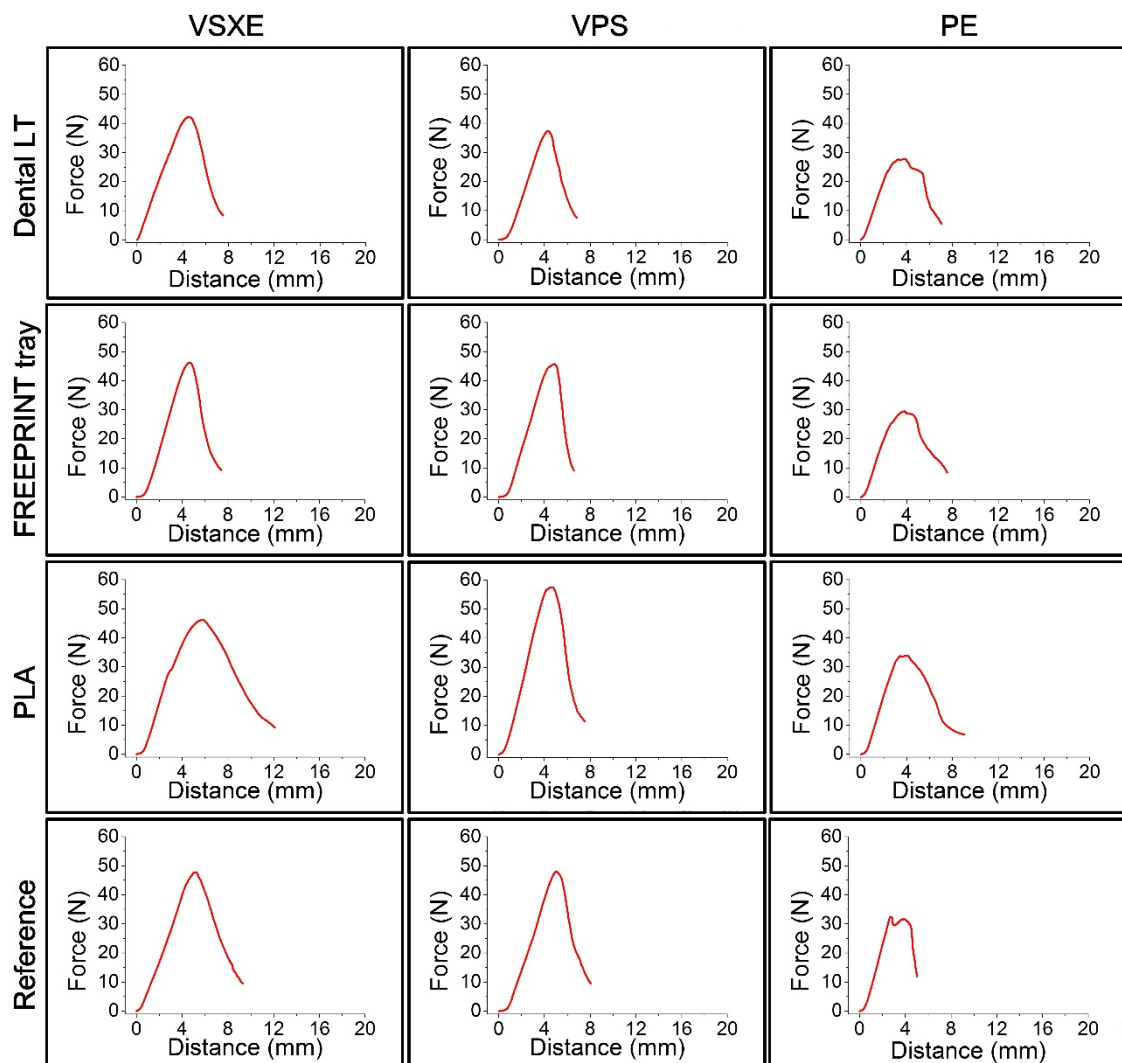


Figure 51: Representative peeling force-distance curves of adhesive failure of each tray-impression material combination.

However, for peeling from the PE impression/adhesive system, the curves dropped gently after the first peak, and a fluctuated plateau with a distance of about 2 mm was observed. Such plateau could hardly be found in the curves of VSXE and VPS impression/adhesive systems, or only a few tenths of a millimeter if any.

As shown in Figure 52, the curves of mixed failure showed a similar profile to that of the adhesive failure. However, it was found in some curves that the plateau was extended so that it could be identified more easily, such as the FREEPRINT tray-VPS combination in Figure 52, but such finding was not general.

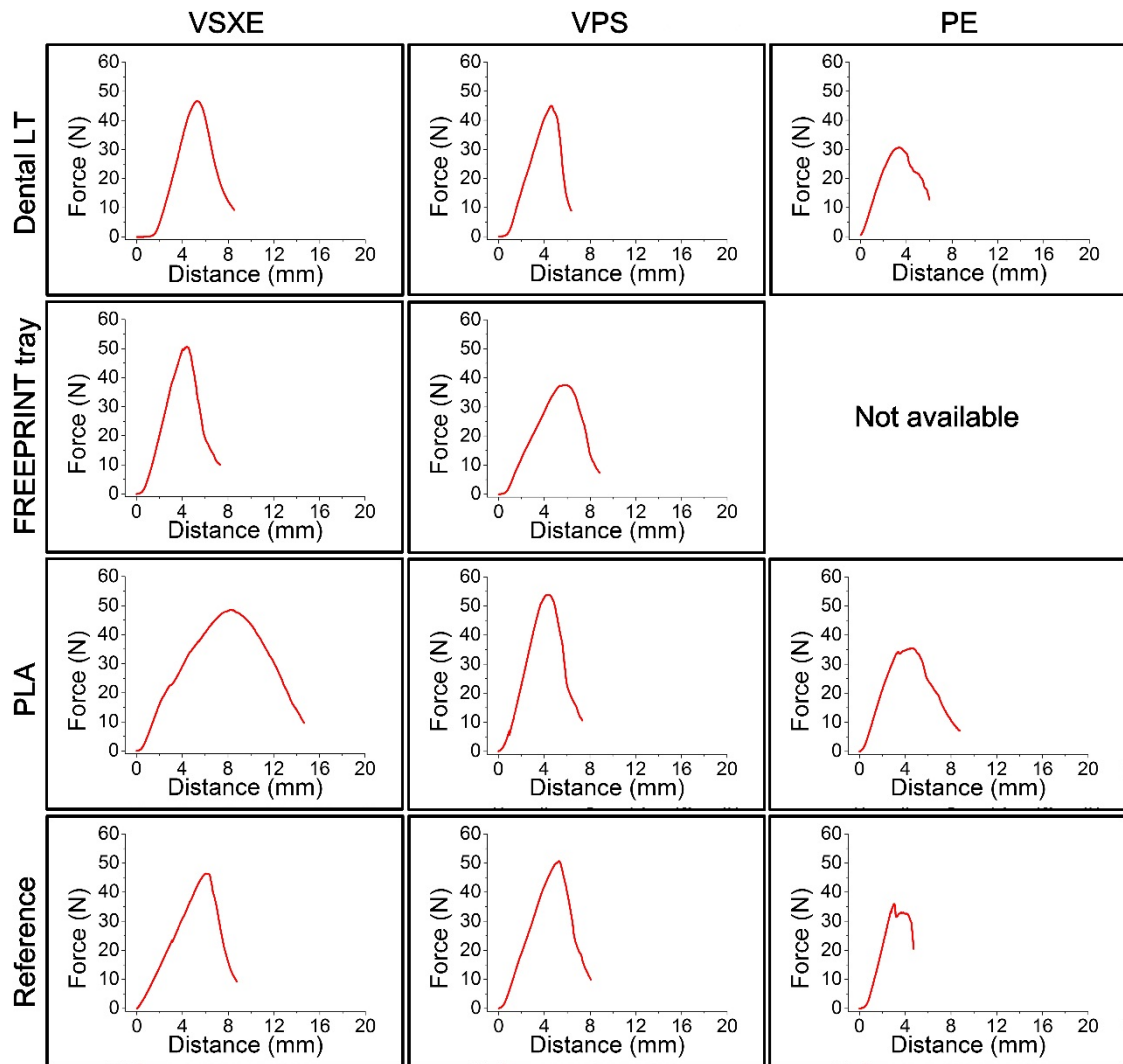


Figure 52: Representative peeling force-distance curves of mixed failure of each tray-impression material combination.

In contrast, the curves of cohesive failure exhibited a significant difference (Figure 53). After reaching the first peak, the curves dropped rapidly until the valley point, where the rupture started to occur within the impression. Afterward, the curves rose slowly, exceeded the first peak, and then fell gently, during which no obvious peak could be observed, and the failure site was always inside the impression material. In this study, cohesive failures only could be found in the Dental LT-VSXE, PLA-VSXE, and reference-VSXE groups.

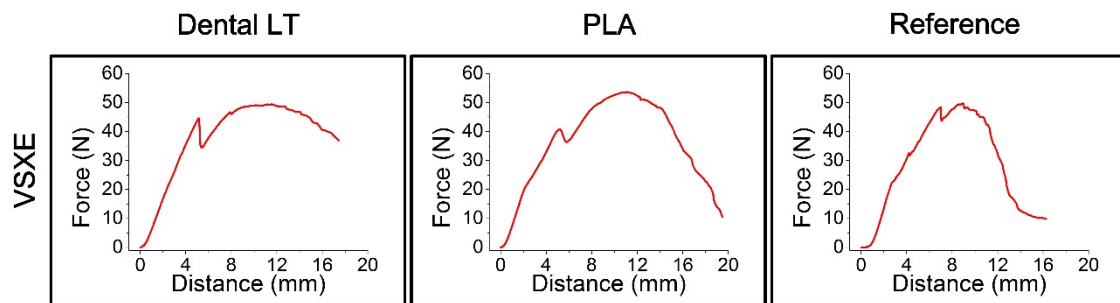


Figure 53: Representative peeling force-distance curves of cohesive failure of each tray material-VSXE combination.

Table 5 gives the mean and standard deviation of line and areal peel bond strength of each group. The results of two-way ANOVA indicated that type of tray materials, type of impression/adhesive systems, and their interaction were statistically significant (Table 6). The results of the following simple main effect analysis were illustrated in Figure 54 and 55, respectively. The line and areal peel bond strength showed similar statistical results since if the length of each test block was standardized, they should only differ in a scale factor. However, in this study, the accurate length of each test block was measured by a digital caliper, and the length values had slight differences in decimal places. To be rigorous, the line and areal peel bond strength were shown separately but not in a figure with two Y-axes.

Table 5: Mean (standard deviation) line peel bond strength (N/m) and areal peel bond strength (kPa) of each group (n = 12).

	VSXE	VPS	PE
Dental LT	1809.73 (152.86) N/m 71.05 (6.08) kPa	1680.53 (277.63) N/m 66.05 (10.83) kPa	1175.43 (126.46) N/m 46.11 (5.02) kPa
FREEPRINT tray	1835.51 (151.91) N/m 71.20 (5.91) kPa	1714.17 (228.90) N/m 67.63 (9.10) kPa	1206.19 (125.04) N/m 47.77 (4.94) kPa
PLA	1911.82 (159.42) N/m 75.31 (6.27) kPa	2173.24 (312.86) N/m 85.87 (12.35) kPa	1324.605 (140.74) N/m 52.21 (5.47) kPa
Reference	1880.79 (246.32) N/m 74.31 (9.81) kPa	2034.85 (149.47) N/m 80.34 (5.91) kPa	1199.56 (284.48) N/m 47.10 (11.10) kPa

Table 6: Two-way ANOVA of peel bond strength.

	SS	DF	MS	F (DFn, DFd)	P value
Interaction	934897	6	155816	F (6, 132) = 3.6	0.0023
IAS ^a	1.371e+007	2	6.856e+006	F (2, 132) = 159.9	< 0.0001
TM ^b	1.407e+006	3	468992	F (3, 132) = 10.9	< 0.0001
Residual	5.660e+006	132	42883		

a. IAS = Impression/adhesive system

b. TM = Tray material

As Figure 54 indicates, the four custom tray materials did not statistically differ in peel bond strength with VSXE and PE. However, for the bonding with VPS, the peel bond strength of PLA and reference was statistically higher than that of Dental LT and FREEPRINT tray. Statistical difference in peel bond strength with VPS could not be found either between PLA and reference or between Dental LT and FREEPRINT tray.

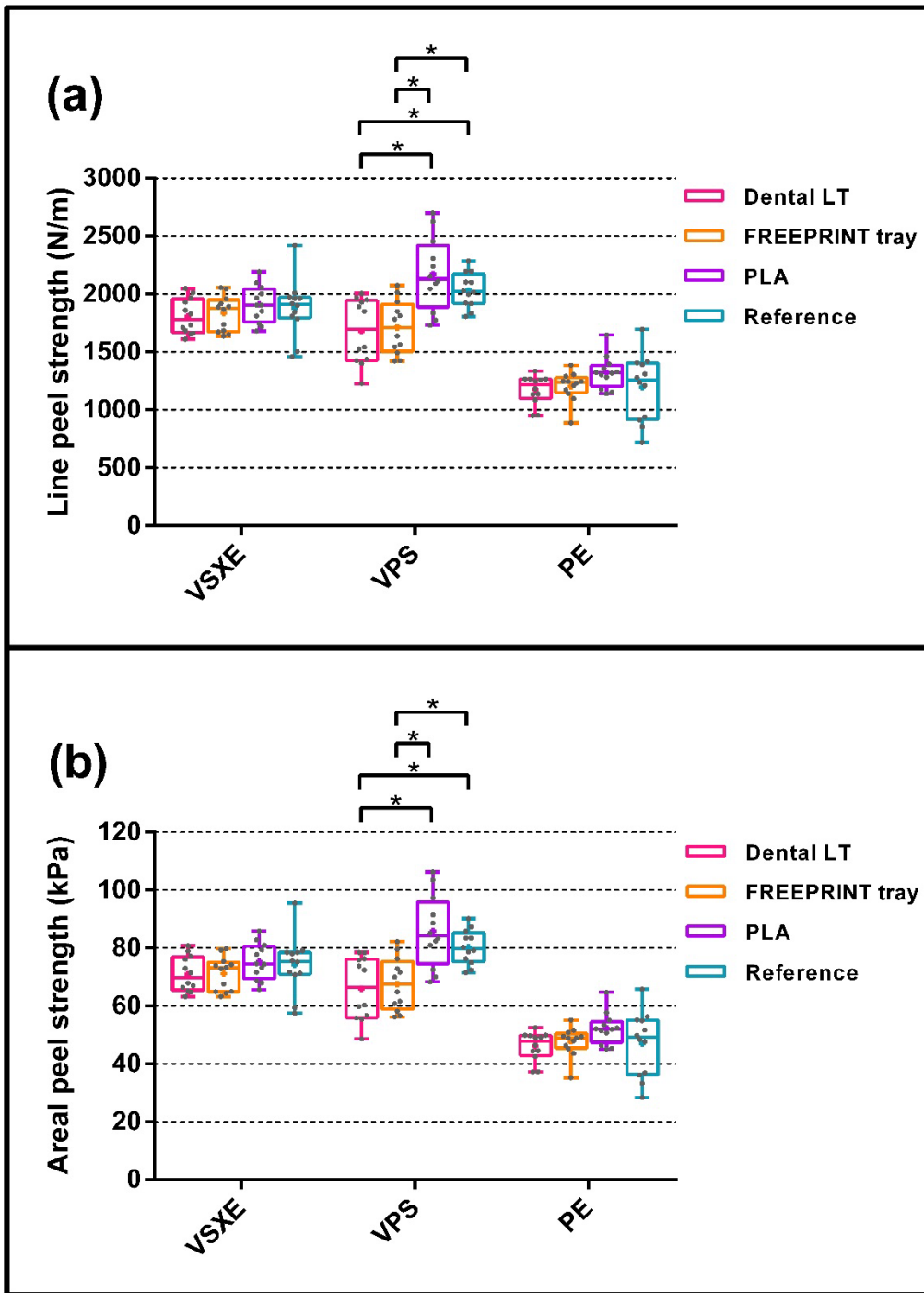


Figure 54: Peel bond strength of each tray-impression material combination (grouped by impression/adhesive system, box plot, n = 12). + represents the mean value of each group. (a) Line peel bond strength; (b) Areal peel bond strength.

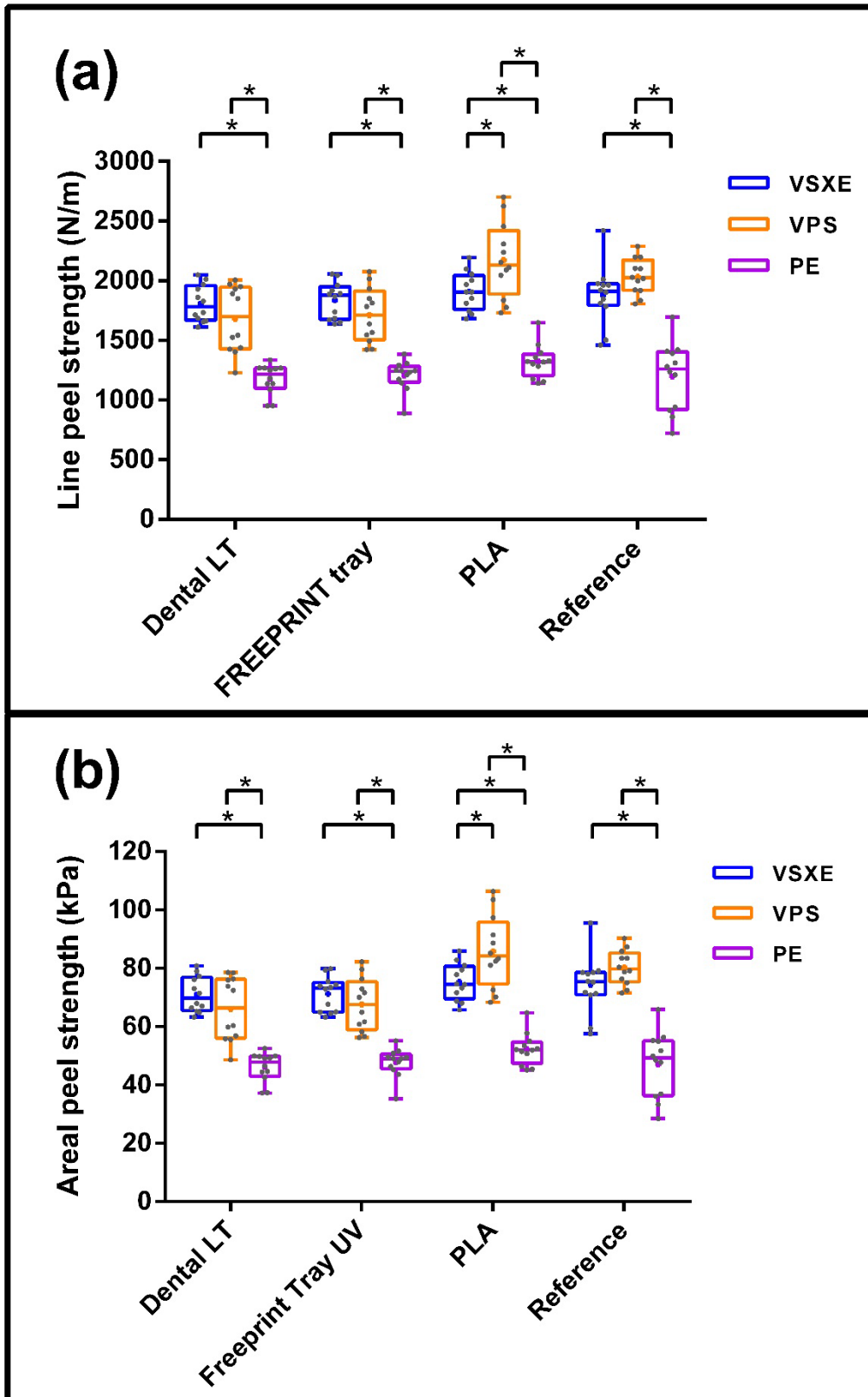


Figure 55: Peel bond strength of each tray-impression material combination (grouped by tray material, box plot, $n = 12$). + represents the mean value of each group. (a) Line peel bond strength; (b) Areal peel bond strength.

As illustrated by Figure 55, for the bonding to Dental LT, FREEPRINT tray and reference, VSXE and VPS showed significantly higher peel bond strength than PE, but no statistical difference could be found between them. For the bonding to PLA, VPS showed the highest peel bond strength, which was statistically higher than that of VSXE and PE, followed by VSXE, whose peel bond strength statistically differed from the lowest strength of PE.

3.4 Failure mode

By inspecting the peeled surfaces of test blocks microscopically, it was found that adhesive failure was the most common failure mode and existed in all groups. As shown in the low-magnification images of Figure 56, no impression material residuals could be observed on the peeled surfaces of adhesive failure. In the high-magnification images, it can be seen that a thin layer of adhesive remained. The surface texture of PLA and FREEPRINT tray became blurred or disappeared since the adhesive was filled in the texture valleys.

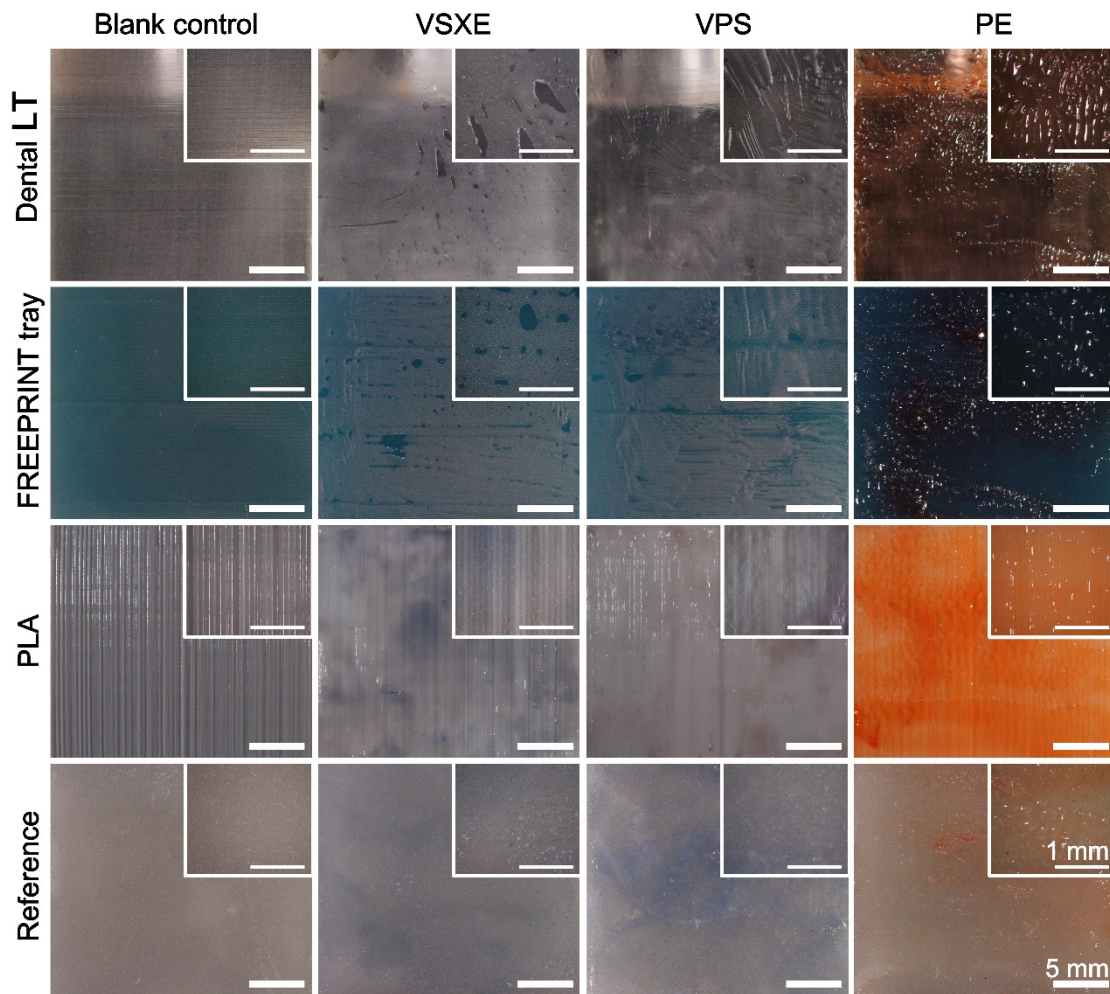


Figure 56: Representative light-microscopical images of test surfaces that adhesively failed after peeling ($6.3\times$ and $32\times$ magnification).

As figure 57 indicates, mixed failure was found in all groups except the FREEPRINT tray-PE combination. In addition to the remained adhesive, small dots or pieces of impression material residuals could be found on the peeled surfaces.

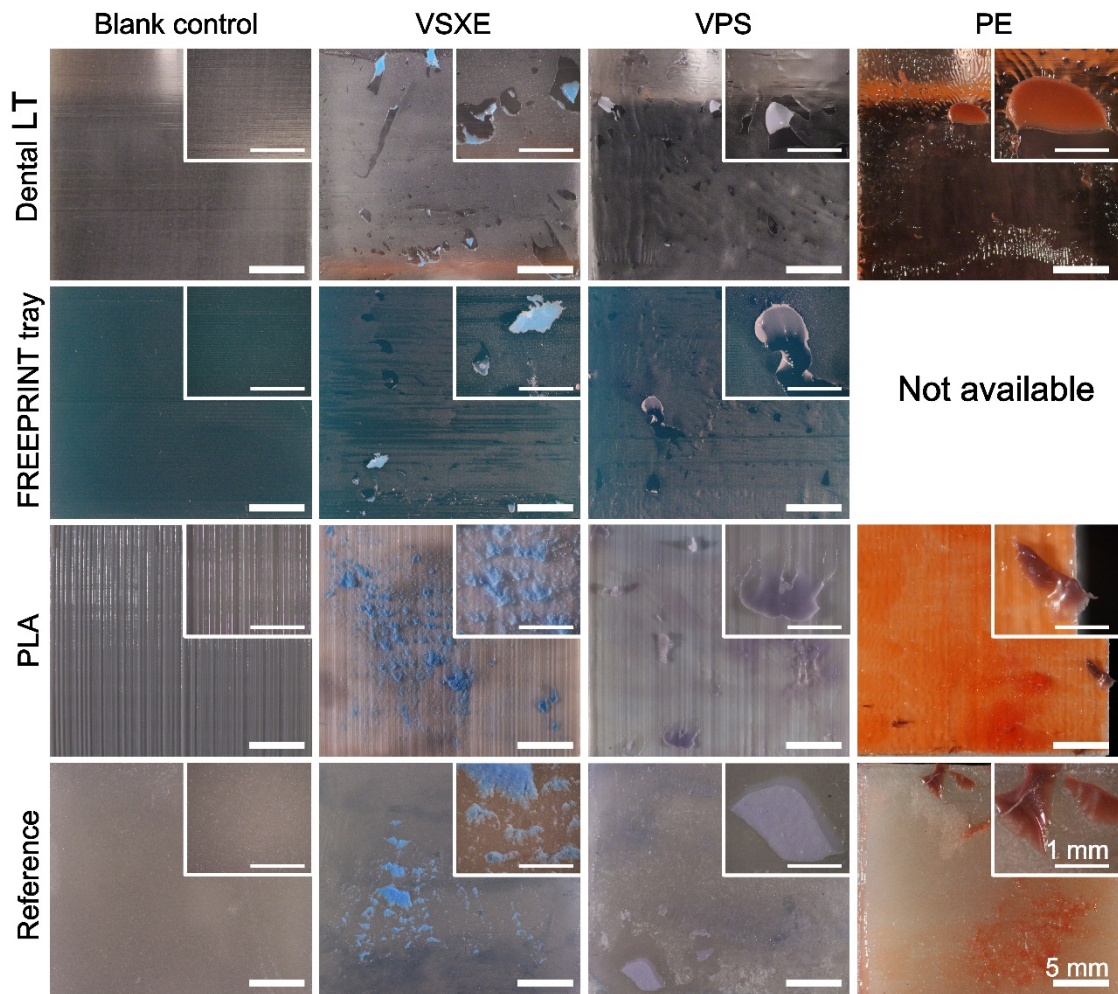


Figure 57: Representative light-microscopical images of test surfaces that mixedly failed after peeling ($6.3\times$ and $32\times$ magnification).

In this study, cohesive failure was the rarest and only existed in those VSXE groups, i.e., Dental LT-VSXE, PLA-VSXE, and reference-VSXE group (Figure 58). The failure occurred within the impression material, causing a large lump of impression material was torn off and integrally remained on the peeled surfaces.

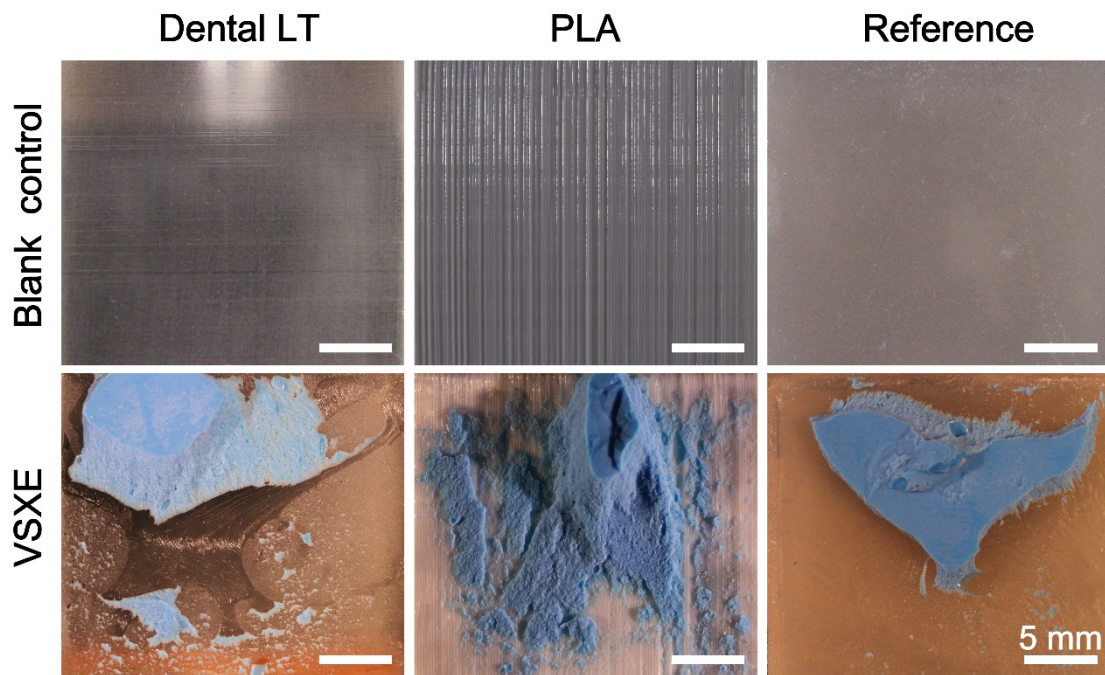


Figure 58: Representative light-microscopical images of test surfaces that cohesively failed after peeling ($6.3\times$ and $32\times$ magnification).

Figure 59 illustrates the constituent ratio of failure mode of each group. For VSXE and VPS impression/adhesive systems, the mixed failure ratios of PLA (66.67%) and reference (58.33%) were significantly higher than that of Dental LT (16.67%) and FREEPRINT tray (8.33%). Cohesive failures only occurred in those VSXE groups, and the cohesive failure ratios of PLA (16.67%) and reference (16.67%) were slightly higher than that of Dental LT (8.33%) and FREEPRINT tray (0%). For PE impression/adhesive system, the failure modes of the four tray material groups were similar dominated by adhesion failure, whose ratios ranged from 83.33% to 100%.

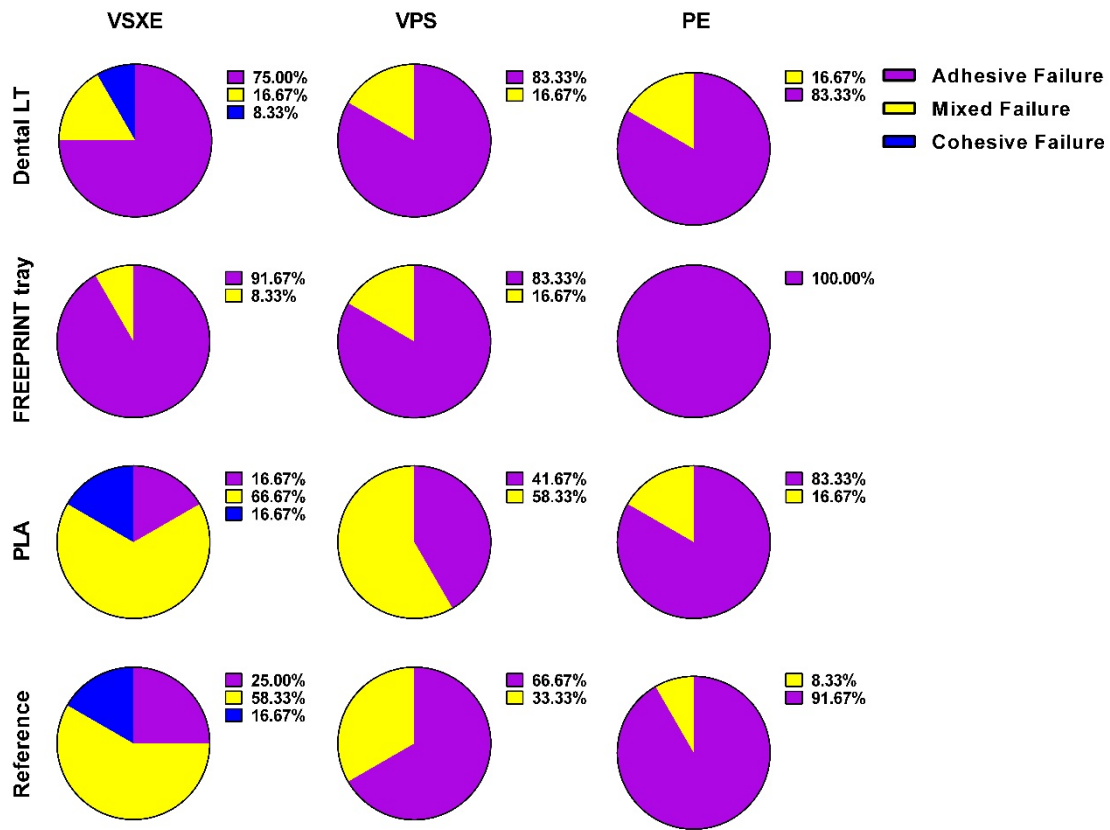


Figure 59: Constituent ratio of failure mode of each group (n = 12).

In this study, the rupture site of adhesive failure in all groups was partly within the adhesive layer, and partly at the adhesive-impression material interface, but never at the adhesive-tray material interface. A typical example is given in Figure 60. On the peeled surfaces of impression and tray material, numerous symmetrical geometry patterns could be found (Figure 60a and 60b, red dotted frame). At high magnification, these geometry patterns presented to be defective on the impression surface and raised on the tray material surface (Figure 60c and 60d). The bottom of the defect on the impression surface was the exposed impression material (Figure 60c, red arrow), while the corresponding raised pattern on the tray material surface was the adhesive that was integrally remained and highly transparent, indicating in these areas, the rupture site was at the adhesive-impression material interface. In areas outside the geometry patterns, remained adhesive could be found on both sides, which appeared granular on the impression surface (Figure 60c, green arrow) and frosted on the tray material surface

(Figure 60d, green arrow), demonstrating the rupture site was within the adhesive layer.

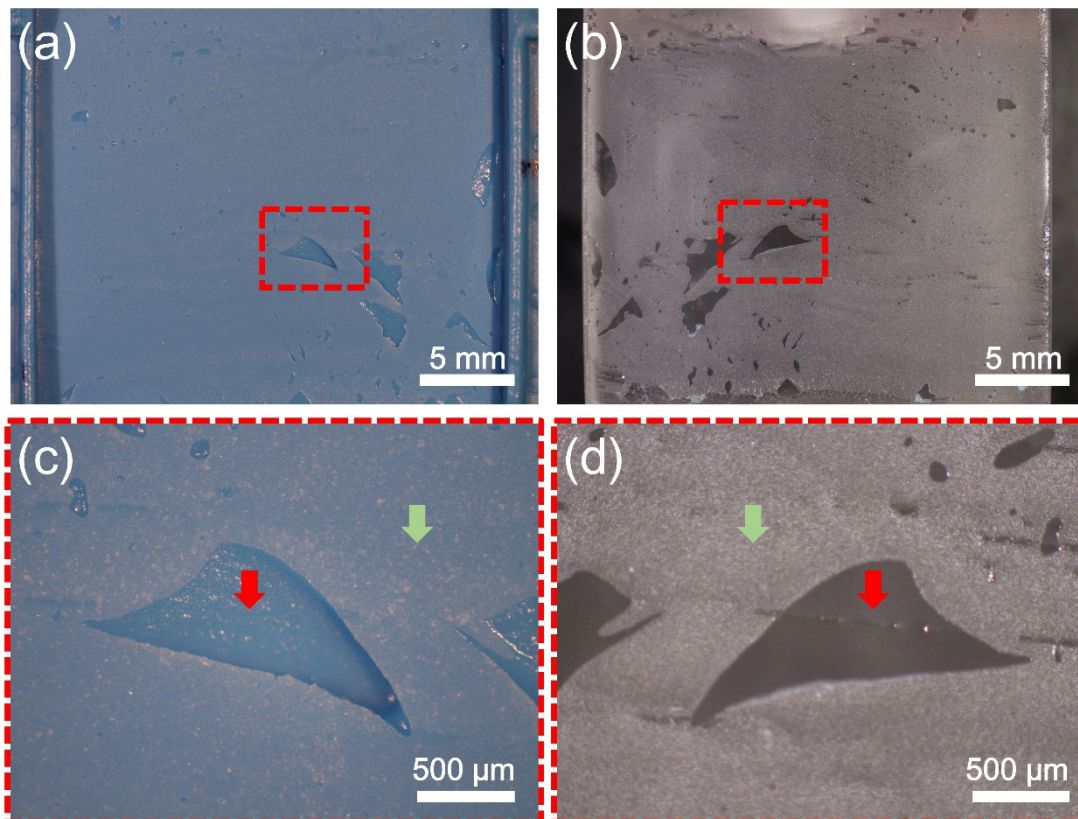


Figure 60: Representative light-microscopical images of adhesive failure between the VSXE impression and the Dental LT tray material ($6.3\times$ and $32\times$ magnification). (a) VSXE impression surface after peeling; (b) Dental LT surface after peeling; (c) The detachment between adhesive and impression material resulted in the defect on the peeled impression surface, exposing the subjacent impression material (red arrow). The rupture within the adhesive layer led the adhesive remain on the peeled impression surface (green arrow); (d) The adhesive debonded with impression material integrally remained on the peeled tray material surface, which presented to be raised and highly transparent (red arrow). The ruptured adhesive remained on the peeled tray material surface and presented to be frosted (green arrow).

The above results indicated that both the tray materials and the impression/adhesive systems had an impact on the peel bond strength. The tray materials influenced the bonding physically but not chemically.

Therefore, both null hypotheses were rejected.

4. Discussion

In this study, the layer thickness of all 3D-printed test blocks was standardized to 100 microns, and all test blocks were printed in the same direction. However, differences were found in surface topographies among test blocks manufactured by each 3D printing technology. The SEM images and 3D reconstructed surface topographies indicated that the SLA-printed Dental LT test block had the best surface finish. Despite some tiny scratches, no distinct surface texture could be observed. This is due to the working principle of SLA. The SLA 3D printer used in this study solidified the pattern of each layer by a 140-micron laser spot, whose direction was precisely guided by two numerically controlled motors, namely galvanometers. Due to the tininess of the laser spot and the accuracy of the guidance, good XY resolution was achieved within each layer, and almost no unfilled areas were found between the solidified layers (Figure 61).

In contrast, since the molten plastic flow cannot fully fill the area between each layer, the surface of FFF-printed PLA test block possessed a clear surface texture, which consisted of numerous peaks and valleys. The void space between two adjacent peaks was the unfilled area between two FFF-deposited layers (Figure 61). Thus, the orientation of the FFF-printed surface texture was perpendicular to the build direction of the test block [28].

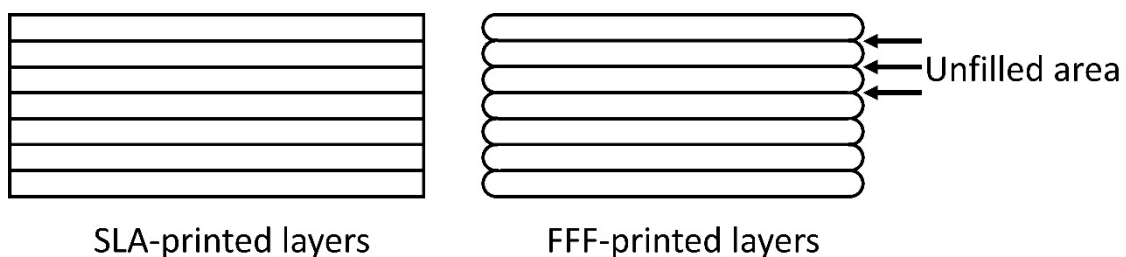


Figure 61: Coronal section of SLA- and FFF-printed layers. The unfilled areas existed between the FFF-printed layers.

Both the DLP-printed FREEPRINT tray test block and the FFF-printed PLA test block

showed a wavy surface, but the texture orientations of the two were opposite and perpendicular to each other (Figure 42, 43, 50b and 50c). The surface texture orientation of the FREEPRINT tray test block was along the build direction of the test block. As introduced in Section 1.2.4.2, the DLP 3D printers project the laser beam into the image of each layer, thus solidifying a whole layer at a time. The projected image of each layer is pixelated by the DMD, which is made of over a million rectangular micromirrors. Each micromirror represents a pixel. As shown in Figure 62, since each pixel is rectangular, the pixelation process can turn the edge from straight to stepped. The stepped edge of each layer successively accumulates along the build direction, eventually generating the DLP-printed surface texture, whose orientation is therefore the same as the build direction. Since the micromirrors are very small, the amplitude and wavelength of the DLP-printed surface texture are significantly lower than that of the FFF-printed one.

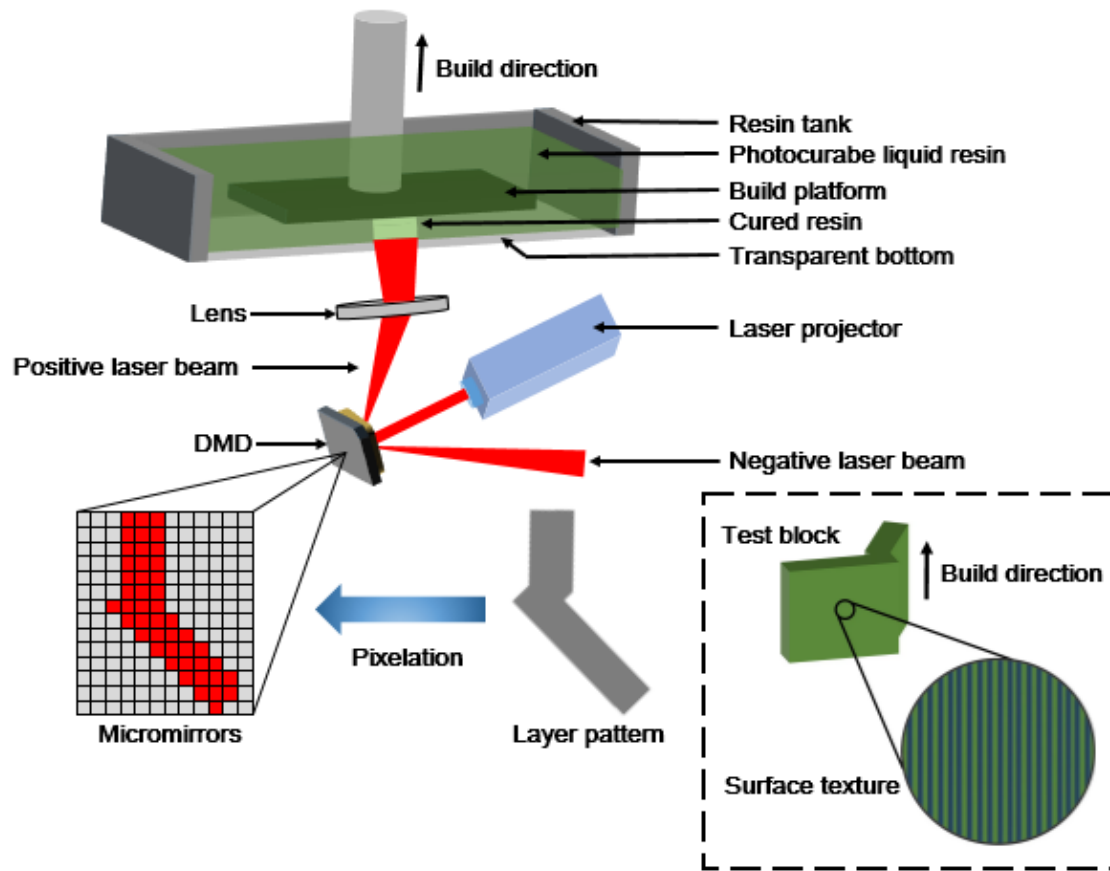


Figure 62: The generation of DLP-printed surface texture. The pattern of each layer is pixelated by the DMD. During this process, the edge could be turned from straight to stepped. Successive stepped edges accumulate layer by layer along the build direction, generating the observed surface texture on the test block. The orientation of the DLP-printed surface texture is the same as the build direction of the test block.

The reference tray material investigated in this study is a conventional light-curing resin, namely Zeta tray LC. Few peaks and numerous pores could be observed on its surface. The size and depth of the irregular pores varied greatly, from 10 μm to 100 μm and 20 μm to 80 μm , respectively. In engineering, this type of surface topography is suitable for wearing since the existence of pores and valleys improves the lubricant retention ability. As for bonding with impression/adhesive systems, it means more adhesive and impression material might be retained on the surface. It should be noted that not all conventional light-curing resins have a porous surface topography. For instance, another light-curing resin, Lichtwachs, exhibited a surface without pores. Instead, various

semi-spherical prominences were observed [28]. Presumably, the possible reason might be the different ingredients of the light-curing resins lead to the difference in radical polymerization.

In previous bonding studies, the tray material surfaces were usually post-processed to standardize the roughness and eliminate the difference in surface topography. Examples can be found by polishing the tray material surface using silicon carbide paper [41,50,56] or white diamond [43]. However, the roughness standardization might lead to deviations from clinical practice, since differences in surface topography do exist among trays made by different materials and methods, and such differences are likely to affect the bonding with the impression/adhesive system. In the present study, the surface topographies of all tray materials were not standardized. The AM tray materials were printed, post-cleaned and post-cured in strict accordance with the manufacturers' instructions, while the conventional light-curing was allowed to polymerize against wax sapper and cleaned by steam to simulate the laboratory conditions. Therefore, the surface topographies of all tray materials were in the state before clinical use, so the peel bond strength measured in this study was thought to be more clinically relevant. Instead of standardizing roughness, this study evaluated the surface topography of tray materials and analyzed its effect on the bonding with impression/adhesive systems.

The roughness parameters provide quantitative analysis for the surface topography. However, due to the complexity of surface topography, each roughness parameter can only provide limited information. Therefore, to find the parameter that is most related to the bonding becomes the main concern. Xu et al. indicated that S_{vi} might be related to the bonding between custom trays and impression/adhesive systems [28]. S_{vi} is a functional parameter defined in EUR 15178 EN [62]. However, in the new ISO 25178-2 standard, S_{vi} has been replaced by V_{vv} since V_{vv} can provide the same type of information, and it is more sensitive to different roughness levels [63]. Therefore, this

study investigated the surface topographies of all tray materials using the improved and updated 3D roughness parameters, i.e. Sa, Ssk, Vvc, Vvv and Sdr.

Sa is the most commonly used 3D roughness parameter which provides the amplitude-related information, that is, the average of the vertical distance of each point to the centered plane [64]. The results of Sa in this study indicated the four materials exhibited three levels of surface height: the highest for PLA, followed by FREEPRINT tray and reference, which did not statistically differ, and the lowest for Dental LT.

Ssk assesses the symmetry bias of surface topography about the centered plane. This parameter has no units and can be positive, negative or zero. A negative Ssk value indicates that the height distribution is skewed above the centered plane, where the surface exhibits few peaks and relatively deep valleys [65]. The more negatively Ssk skews, the more asymmetrical surface height distribution is. In the present study, all of the four investigated tray materials showed negative Ssk values. Among them, FREEPRINT tray and PLA showed slight skewness, whose Ssk values were close to zero. Dental LT had a moderate negative skewness and exhibited a certain degree of asymmetry. The reference surface was highly negatively skewed, signifying the lack of peaks and the existence of deep valleys, which could be further confirmed by the 3D-reconstructed surface topography (Figure 50d). It should be noted that Ssk can only assess the degree of bias. To further characterize the fluid retention ability of all tray materials, functional parameters Vvc and Vvv are required.

The 3D roughness parameters Vvc and Vvv evaluate the void volume of the material surface [63]. If the material ratio from 0% to 100% corresponds to surface height from the highest peak to the deepest valley, then according to the default value of ISO 25178-2, Vvc represents the void volume between two cutting planes at the heights that respectively correspond to 10% and 80% material ratio, while Vvv is the void volume

between two planes that correspond to 80% and 100% material ratio, respectively (Figure 63). Therefore, V_{vc} evaluates the void volume at the core zone, and V_{vv} assesses the void volume at the valley zone. Larger V_{vv} and V_{vc} values indicate that the material surface can retain more fluid in the corresponding area.

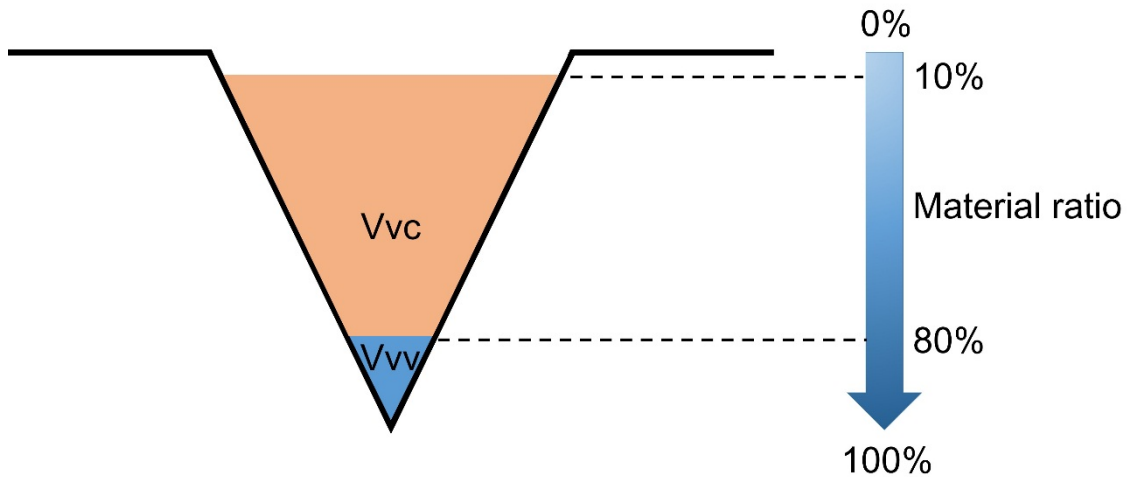


Figure 63: The schematic of V_{vc} and V_{vv} .

Because of the good surface finish, the V_{vc} and V_{vv} values of Dental LT were the lowest among the four investigated tray materials. The V_{vc} value of FREEPRINT tray was significantly higher than that of Dental LT due to the existence of surface texture, but the V_{vv} values of the two did not statistically differ. In contrast, due to the greater surface texture, the V_{vc} and V_{vv} values of PLA were the highest among the four groups. The reference material had a low V_{vc} value and a high V_{vv} value, indicating that the valleys on its surface were relatively narrow.

The 3D roughness parameter S_{dr} is a measure of surface complexity, which is unit-less and usually given as a percentage. For a surface with perfect smoothness, the S_{dr} equals to 0%. In this study, the results of S_{dr} were similar to that of S_a , indicating that the two parameters might have some degree of correlation, but this inference needs further study to confirm.

In the present study, a profilometer equipped with a stylus was utilized for roughness measurement. When the measurement was being performed, the stylus tip kept in contact with the sample surface and moved transversely across the test area to record a profile [24]. Limited by its diameter, the stylus tip could not fully enter every pit and fissure on the test surface, resulting in the reduction in accuracy of the results. The use of optical scanning instruments can compensate this shortcoming and improve the data accuracy for future studies.

Different test methods were utilized in previous studies to investigate the bonding between tray materials and impression/adhesive systems, including tensile test, shear test, and peel test. Although the tensile test is utilized by most of the studies [44,57,60,66], the peel test is thought to be more clinically relevant [45]. For instance, if the tray is withdrawn by a tensile force which is perpendicularly applied on the center of the tray, tensile stress will be produced in the central area, and shear stress will be generated between the walls of the tray and the impression material. However, in clinical situation, removing the tray from oral cavity is usually achieved by applying an upward or downward force to the tray handle, which would cause the initial detachment between impression and oral tissues always occur at either front or back side [28]. Therefore, the peel test modality is considered to be closer to the process of impression removal. For the above reasons, the present study utilized peel test for investigation. To focus more on clinical application and mimicry, the test blocks geometry was designed as the molded tray, and the peel test was different from a systematic fashion.

For a typical peel test, the peel strength is calculated by the average load per unit width of the bonding line, where the angle of separation can be different degrees, and the unit of peel strength is N/m or lb/in. However, the previous relevant peeling studies utilized the areal peel strength to investigate the bonding between tray materials and

impression/adhesive systems. Grant et al. compared the tensile and peel bond strength of nine impression/adhesive systems to an acrylic resin, in their study the peel bond strength was calculated using the areal stress with the unit of lb/in^2 or kg/cm^2 [45]. MacSween et al. measured the peel bond strength of five impression/adhesive systems to a perforated or non-perforated acrylic resin, in their study the unit of the peel bond strength was kg/cm^2 [46]. In addition, Tjan et al. [54] cited the study of Grant et al., and the peel bond strength was expressed by lb/in^2 . It was also found that a recently published paper cited the data of MacSween et al., whose unit was transformed from kg/cm^2 to MPa so that it could be compared with their results of tensile bond strength [56]. The reason for the previous studies using areal stress might be due to the experimental stress transmission was different from that in a standard peel test. Unlike the typical peel test (Figure 64a), the impression material from which the test block was peeled off was elastic. When the test block was being peeled, the impression material could be slightly deformed to cause energy stored, and stress might be transmitted to the remaining bonded interface through the elastic impression material, resulting in the peel force applied not only to the bonding line but also to the bonding area (Figure 64b).

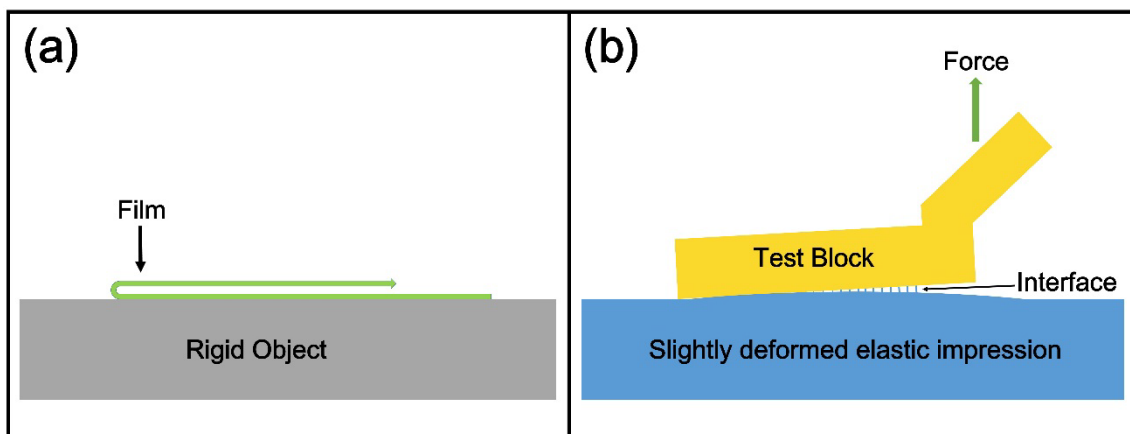


Figure 64: Comparison of peel tests. (a) An example of standard peel test: a film is peeled from a rigid object; (b) The peel test performed between test block and elastic impression.

The above analysis could be further supported by the force-distance curves of the peel

test in this study. It is known that the force-distance curve of a standard peel test would have a fluctuated plateau after the first peak. However, in the force-distance curves of the VSXE and VPS groups, such plateaus could only maintain a few tenths of a millimeter, and then the peeling passed into a catastrophic failure by complete disruption of the compound. Presumably, the highly elastic impression materials stored a lot of energy at the entire interface, and the release of the stored energy caused the peeling force transmitted to the bonding area. The force-distance curves of the PE groups had a relatively obvious plateau, which maintained a distance of about 2 mm, indicating the peeling behavior of the PE groups was more typical. This might be due to the fact that PE is the most rigid elastomeric impression material [67], whose high elastic modulus [68] and low flexibility resulted in the reduced storage and release of energy during the peeling process. In addition, it was observed in the peel bond test that the adhesive of PE had a higher elongation. The PE adhesive that was pulled into filaments but still bonded to both impression and tray material could be found behind the peeling frontier (Figure 65), which may also contribute to the extension of the plateau in the force-distance curve of the PE groups.

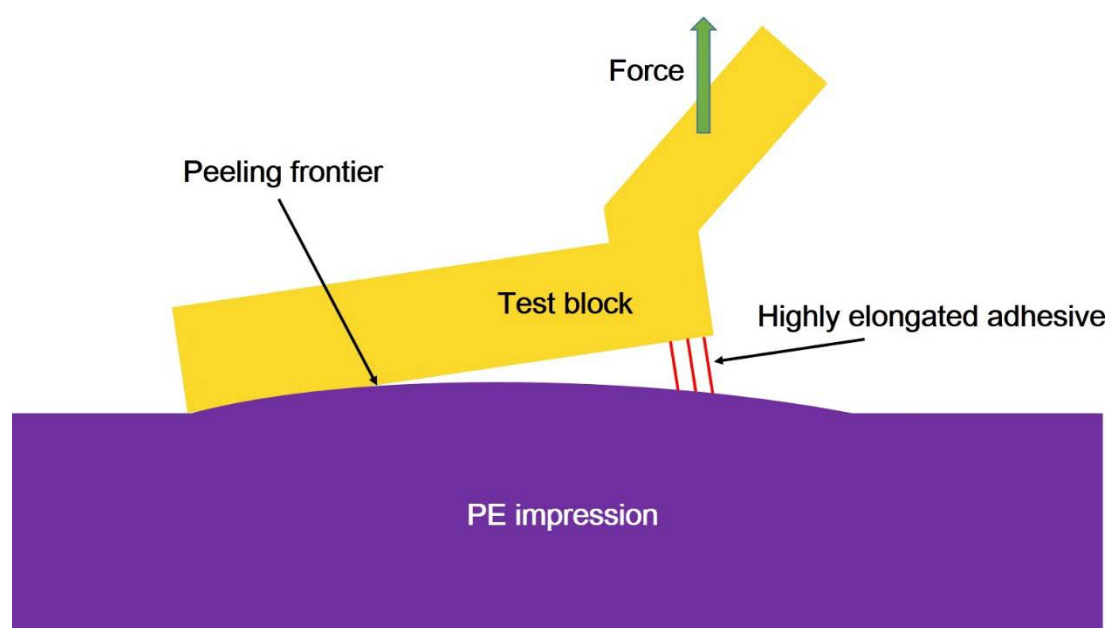


Figure 65: The adhesive of PE has a high elongation, which leads to the adhesive to be pulled into filament behind the peeling frontier.

A similar experimental design can be found in the study reported by Leung et al. [69], who claimed the test method was a cleavage test rather than a peel test. As mentioned in their article, cleavage test and peel test are similar, but the main difference between the two is that the adherend in a peel test is elastic, while that in a cleavage test is rigid. However, for the bonding between tray and impression material, the latter is a highly elastic adherend which would undergo unavoidable deformation during the test. Therefore, it is controversial to regard the test method as a cleavage test. The present study holds the view that the term of the test method should be peel test, although it is different from a systematic fashion. For the peel test in this study, undoubtedly, the highest stress occurs primarily at the bonding line. However, due to the elasticity of impression material, the peel stress is also thought to be related to the bonding area. Therefore, both line and areal stress were used to characterize the peel bond strength. For analyzing the areal peel stress, since the force is applied at the edge of the test block, the stress is unevenly distributed onto the bonding area. It is difficult to use a single formula to express the areal stress, nor did the early studies give any available equation [45,46]. Leung et al. [70] tried to develop a mathematic model, but the derivation process seems unconvincing. To accurately analyze the areal peel stress, Finite Element Analysis (FEA) might be a reasonable method, but this is beyond the scope of the present study. Therefore, the areal peel stress in this study was directly characterized by the most commonly used force-area formula, namely F/A .

In previous studies, different crosshead speeds have been utilized to investigate the bonding between the tray materials and impression/adhesive systems. The used crosshead speeds ranged from as low as 5 mm/min [71] to as high as 508 mm/min [43]. Table 7 shows the crosshead speeds used in the related studies. The effect of crosshead speed on the bond strength is controversial. Wilson et al. compared the tensile bond strength at crosshead speeds of 10 mm/min and 60 mm/min, and Ellam et al. calculated

the bond strength at crosshead speeds of 60 mm/min and 500 mm/min. Both studies claimed the bond strength increased with the increase of crosshead speed [72,73, quoted in 58]. However, Chai et al. reported the bond strength measured at crosshead speeds of 127 mm/min and 508 mm/min did not statistically differ [43]. Bindra et al. repeated the experiments of the above three studies, but their conclusions were opposite to that of each study [58]. Nevertheless, since the strain rate may influence the bond strength, setting a crosshead speed that is close to the material application would be more meaningful. In this study, the crosshead speed was set to 300 mm/min, which was thought to be a speed close to the clinical impression removal [28].

Table 7: Different crosshead speeds used in the related studies.

Authors	Year	Type of bond strength	Crosshead speed
Grant et al. [45]	1988	Peel	25.4 mm/min
Davis et al. [40]	1976	Tensile	508 mm/min
Chai et al. [43]	1991	Tensile	127, 508 mm/min
Dixon et al. [71]	1993	Tensile	5 mm/min
Bindra et al. [58]	1997	Tensile and shear	10, 60, 150, 300, 500 mm/min

According to manufacturer's instructions, the impression set time is divided into working time at 23 °C (room temperature) and intraoral set time at 37 °C, but most of the relevant studies were performed only at room temperature and ignored the simulation of the intraoral temperature. However, since the tray and impression materials have different coefficients of thermal expansion, the 14 °C thermal difference between intraoral and extraoral environment may result in the inconsistent volume contraction of the two after the impression removal. This inconsistency in volume contraction may further cause the generation of stress at the tray-impression interface. Therefore, the compatibility in thermal-induced volume change between tray and impression materials may be an important factor that affects the bonding, but this speculation has not been explored and needs further investigation. In this study, the intraoral temperature was simulated during impression setting, which was thought to be

an improvement of previous test methods and closer to clinical practice. Therefore the obtained results might be more clinically relevant. However, all laboratory studies cannot fully duplicate the real clinical situation. For instance, this study did not consider the intraoral moisture, which is one of the experimental limitations.

Since few studies utilized peel test to investigate the bonding between tray and impression materials, and the early studies did not give the formula used for calculating areal peel stress, the available data for parallel comparison are limited. The VPS impression/adhesive system showed generally higher peel bond strength in all tray material groups than the PE, which was supported by the results reported by MacSween et al. [46] and Grant et al. [45]. However, the tensile bond strength of VPS and PE was generally reported to be similar [39,43,45,48], indicating that the PE might have reduced resistance to peeling load. The line peel stress of VSXE, VPS and PE ranged between 1810-1911 N/m, 1681-2173 N/m and 1175-1325 N/m respectively, which were generally higher than that of a C-silicone impression/adhesive system (379-671 N/m) investigated in the author's previous publication [28], and higher than that of an alginate impression/adhesive system (1077 N/m) reported by Lung et al. [70], indicating that acceptable peel bond strength might have been achieved in all experimental groups.

When the impression-adhesive-tray bonding system is subjected to separation force, failure is most likely to occur at the weakest structures, which include within the impression material, at the adhesive-impression material interface, within the adhesive, and at the adhesive-tray material interface. In previous studies, the terms of failure mode were used loosely without clear definition and classification. For instance, Chai et al. defined adhesive failure as the failure occurred at the adhesive-impression material interface or adhesive-tray material interface [43], but they may neglect the fact that adhesive failure might result from the rupture within the adhesive. Davis et al. described cohesive failure as the failure appeared within the impression material [40]. However,

when only tiny amounts of impression material residuals were observed on the debonded tray material surface, Nicholson et al. equalized it as a cohesive failure [53, quoted in 43], whereas Kawamura et al. categorized it as a mixed failure [74, quoted in 43]. Therefore, to clarify the terms of failure modes, the present study made a categorization which may help future studies in standardization.

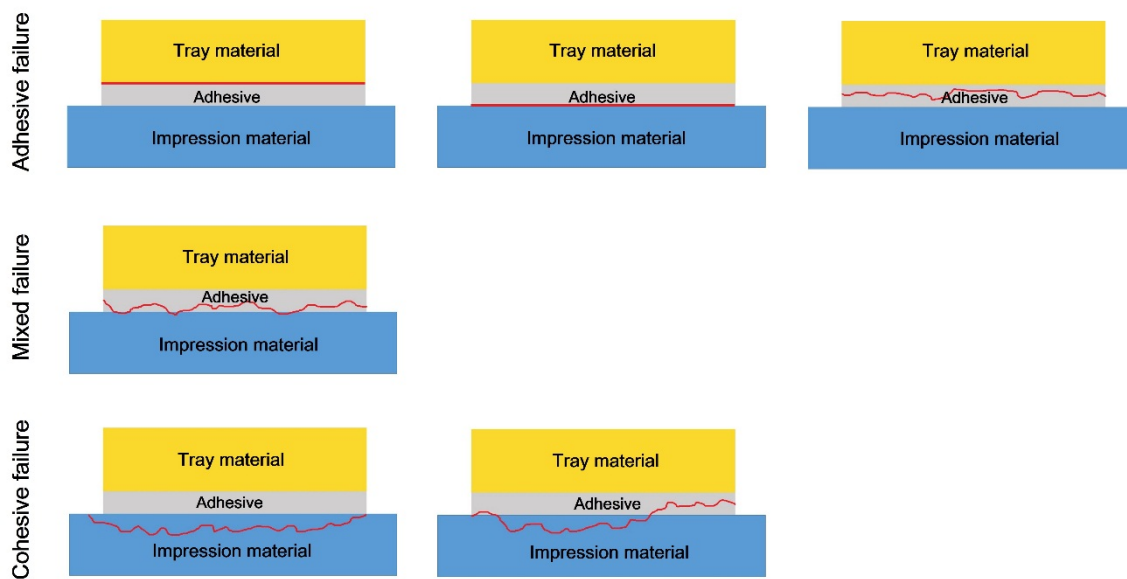


Figure 66: Categorization of failure modes between tray and impression material.

As shown in Figure 66, for adhesive failure, no impression material residuals can be found on the debonded tray material surface, the rupture site can be at the adhesive-tray material interface, within the adhesive, at the adhesive-impression material interface, a mixing of any two sites, or a mixing of the three. Concerning mixed failure, tiny amounts of impression material residuals present in dots or flakes can be found on the tray material surface after detachment, only a small portion of rupture site is inside the impression material. With regard to cohesive failure, a relatively large lump of integrated impression material can be observed on the detached tray material surface, the rupture mostly occurs within the impression material.

In this study, the failure mode of PE impression/adhesive system was mostly adhesive failure. This finding was similar to that reported by MacSween et al. [46], who indicated that the failure mode of PE impression/adhesive system was pure adhesive failure in peel test, but contradictory with that reported by Grant et al. [45], who found that PE impression/adhesive system failed cohesively. The failure modes of VSXE and VPS impression/adhesive systems varied with tray materials, the mixed failure ratios of PLA and reference were significantly higher than those of Dental LT and FREEPRINT tray. In previous studies, the failure mode of VPS impression/adhesive system was reported to be adhesive failure by Grant et al. [45] and cohesive failure by MacSween et al. [46]. Since VSXE is a relatively new elastomeric impression material, its relevant bonding study is still lacking.

Accurate identification of the rupture site in adhesive failure was longly considered difficult [45]. Previous studies usually roughly reported the rupture site as a single mode. The present study provided a reliable method for the precise identification, that is, comparatively examining both detached impression and tray material surfaces microscopically. The results showed that the rupture site of adhesive failure in all groups was not a single mode, but a mixing of two modes (partly at adhesive-impression material interface and partly within the adhesive). However, the rupture at the adhesive-tray material interface was never observed, indicating the actual peel bond strength between tray material and adhesive was higher than what has been measured. Since the bonding between the adhesive and impression material provided by the same manufacturer are almost pre-determined to be good, it is reasonable to conclude all the investigated tray materials achieved good chemical compatibility with the adhesives and satisfied the requirements of clinical success. The results of two-way ANOVA indicated that tray material had a statistically significant effect on the peel bond strength. If the chemical factor of tray material is excluded, it is therefore the surface topography of the tray materials affected the peel bond strength. The previous

study showed the roughness parameter V_{vv} might be related to the peel bond strength [28]. However, in this study, V_{vv} could only be related to the peel bond strength of those VPS groups, while other investigated roughness parameters showed no correlation to the bonding. The possible reason is speculated as follows: V_{vv} evaluates the ability of fluid retention in the valley zone. Since PLA and reference had higher V_{vv} values than Dental LT and FREEPRINT tray, the impression material can be better retained on their surfaces. Even so, higher V_{vv} values may not directly result in higher mixed failure ratios, because the failure modes may also be affected by the tear strength of the three investigated impression materials. PE may have the highest tear strength because the detachment between PE and PLA or between PE and reference occurred outside the PE impression material. Since the failure modes between PE and the four tray materials were mainly adhesive failure and did not show a significant difference, the peel bond strength between PE and the four tray materials did not statistically differ. VPS may have a lower tear strength, which caused the debonding between VPS and PLA and between VPS and reference occur partly inside the VPS impression material. Therefore, for peeling from VPS, the mixed failure ratios of PLA and reference group were significantly higher than those of Dental LT and FREEPRINT tray group, so was the peel bond strength. VSXE may have the lowest tear strength, in addition to the high mixed failure ratios found in the PLA and reference group, cohesive failures were also observed. However, the peeling force required for debonding may not significantly increase due to the low tear strength of VSXE, so the peel bond strength of PLA and reference group were slightly higher than that of Dental LT and FREEPRINT tray group but with no statistically significant difference.

The minimum clinically required bond strength between tray and impression is unknown [33,46,60,75]. Also, the force needed for impression removal was reported inconsistently, values as low as 19.9 N to 36.3 N [76] or as high as 224.3 N to 514.0 N [77] have been reported. In the clinical situation, the actually required impression

removal force might be determined by various factors, such as the size and number of undercuts, the rigidity of impression and tray material, the tray removal method, and the angulation of dental implants [48,70,76]. Nevertheless, it would be prudent to choose a tray-impression combination with the optimum bond strength to avoid the possible detachment. The results of this study indicated that for the VSXE and PE impression/adhesive systems, choosing any of the four tray materials could achieve similar peel bond strength, but for the bonding with the VPS impression/adhesive system, PLA or reference might be a better choice (Figure 54). For Dental LT, FREEPRINT tray, and reference tray material, selecting the VSXE or VPS impression/adhesive systems may generate higher peel bond strength than choosing PE. However, for PLA, the best choice in bonding might be the VPS impression/adhesive system (Figure 55).

Accurately locating the rupture site may contribute to the future reinforcement of the weakest structure in the impression-adhesive-tray bonding system. For instance, the bonding between FREEPRINT tray and PE failed adhesively with the rupture sites found partly at the adhesive-impression interface, and partly within the adhesive, attempts should be focused on strengthening the adhesive and its bonding with the impression to increase the bond strength. In this study, all tray materials have achieved good chemical compatibility with the adhesives, but the reduced surface roughness (V_{vv}) may decrease the peel bond strength, especially in bonding with the VPS impression/adhesive system. Therefore, roughening the tray material surface, especially increasing the V_{vv} value, may increase the bond strength with VPS, but this needs further investigation.

5. Conclusion

The present study assessed the bonding between three 3D-printing custom tray materials (Dental LT, FREEPRINT tray, and PLA), which were respectively manufactured by three AM technologies (SLA, DLP, and FFF), and three elastomeric impression/adhesive systems (VSXE, VPS, and PE) by peel test. The peel bond strength of the 3D-printing custom tray materials was compared with that of a conventional light-curing resin (Zeta Tray LC). Through SEM analyses and roughness measurements, the surface topographies of the four tray materials were investigated qualitatively and quantitatively. Additionally, the failure mode and rupture site of each group were inspected microscopically to study the chemical compatibilities between the tray materials and the adhesives, and to disclose the possible correlations between the tray surface roughness and the peel bond strength. The SEM analyses and roughness measurements showed each investigated tray material had a featured surface topography. Dental LT showed a smooth surface with the best surface finish. Due to the working principle of DLP and FFF, surface textures could be found on both surfaces of FREEPRINT tray and PLA, but the texture orientations of the two were opposite and perpendicular to each other. The reference light-curing resin exhibited a porous surface with numerous valleys and few peaks. The result of peel test indicated the four tray materials did not statistically differ in peel bond strength with VSXE and PE, but PLA and reference showed higher peel bond strength with VPS than Dental LT and FREEPRINT tray. For bonding with Dental LT, FREEPRINT tray and reference, the peel bond strength of VSXE and VPS showed no significant difference, but both were higher than that of PE. For bonding with PLA, VPS showed the highest peel bond strength, followed by that of VSXE, and the peel bond strength of PE was the lowest. The failure mode depended on both tray material and impression/adhesive system. For peeling from VSXE and VPS, the mixed failure ratios of PLA and reference were higher than those of Dental LT and FREEPRINT tray. For peeling from PE, the failure modes of the four tray materials were all mostly adhesive failure. Cohesive failures could only

be found in the VSXE groups. The rupture site of adhesive failure in all groups was partly at the adhesive-impression material interface, and partly within the adhesive, but never at the adhesive-tray material interface, indicating good chemical compatibility between the 3D-printed tray materials and the adhesives were achieved. The surface topographies of the tray materials influenced the peel bond strength. However, since the peel bond strength was also affected by the impression material, no direct correlations to the peel bond strength were achieved by the investigated roughness parameters except V_{vv} , which could be partly related, especially in the VPS groups.

To sum up, the 3D-printed tray materials could be good alternatives to the conventional light-curing resin when the VSXE or PE impression/adhesive system is used. For bonding with the VPS impression/adhesive system, PLA seems an ideal tray material, whereas Dental LT and FREEPRINT tray may need further surface roughening.

6. Summary

The present study aimed to evaluate the bonding between three 3D-printing custom tray materials and three elastomeric impression/adhesive systems by peel test. The peel bond strength of the 3D-printed custom tray materials was compared with that of a conventional light-curing resin.

CAD-designed test blocks were printed by stereolithography (SLA), digital light processing (DLP), and fused filament fabrication (FFF) using the corresponding tray materials Dental LT, FREEPRINT tray, and polylactide (PLA), and the reference test blocks were conventionally fabricated with a light-curing resin ($n = 12$). Through SEM analyses and roughness measurements, the surface topographies of the four tray materials were investigated qualitatively and quantitatively. The force at failure in the peel test was recorded to calculate the bond strength between each tray material and impression/adhesive system. The failure mode and rupture site were identified by comparatively examining the peeled surfaces of tray and impression material using a microscope.

The result showed that Dental LT had a smooth surface with the best surface finish. Surface textures could be found on both surfaces of FREEPRINT tray and PLA, but the texture orientations of the two were opposite and perpendicular to each other. The reference light-curing resin exhibited a porous surface with numerous valleys and few peaks. The four tray materials did not statistically differ in peel bond strength with VSXE and PE, but PLA and reference showed higher peel bond strength with VPS than Dental LT and FREEPRINT tray. For bonding with Dental LT, FREEPRINT tray and reference, the peel bond strength of VSXE and VPS showed no significant difference, but both were higher than that of PE. For bonding with PLA, VPS showed the highest peel bond strength, followed by that of VSXE, and the peel bond strength of PE was the lowest. For peeling from VSXE and VPS, the mixed failure ratios of PLA and reference

were higher than those of Dental LT and FREEPRINT tray. For peeling from PE, the failure modes of the four tray materials were all mostly adhesive failure. Cohesive failures could only be found in the VSXE groups. The rupture site of adhesive failure in all groups was partly at the adhesive-impression material interface and partly within the adhesive, but never at the adhesive-tray material interface.

In summary, a good chemical compatibility between the 3D-printed tray materials and the adhesives was achieved. The surface topographies of the tray materials influenced the peel bond strength, but only the roughness parameter dales void volume (V_{vv}) could be partly related to the peel bond strength. The 3D-printed tray materials could be good alternatives to the conventional light-curing resin when the VSXE or PE impression/adhesive system is used. For bonding with VPS impression/adhesive system, PLA seems an ideal tray material, whereas Dental LT and FREEPRINT tray may need further surface roughening.

7. Zusammenfassung

Die vorliegende Studie zielte darauf ab, die Verbindung zwischen drei mittels additiver Fertigungsverfahren hergestellten individuellen Abformlöffeln und drei Abform-Elastomeren im Abzugstest zu untersuchen. Die Haftfestigkeit der Materialien für den 3D-Druck wurde mit der eines herkömmlichen lichthärtenden Polymers verglichen.

CAD-gestaltete Testblöcke wurden mittels Stereolithographie (SLA), digitaler Lichtverarbeitung (DLP) und Fused Filament Fabrication (FFF) unter Verwendung der entsprechenden Löffelmaterialien Dental LT, FREEPRINT tray und Polylactid-Filament (PLA) und der Referenztestblöcke gedruckt bzw. konventionell mit einem lichthärtenden Polymer ($n = 12$) hergestellt. Durch REM-Analysen und Rauheitsmessungen wurden die Oberflächentopografien der vier Materialien qualitativ und quantitativ untersucht. Die Kraft beim Versagen im Abzugstest wurde aufgezeichnet, um die Haftfestigkeit zwischen jedem Löffelmaterial und dem Abform-/Klebstoffsystem zu berechnen. Die Versagensart und die Bruchstelle wurden durch vergleichende Untersuchung der abgezogenen Oberflächen der Prüfkörper und des Abformmaterials unter Verwendung eines Mikroskops identifiziert.

Das Ergebnis zeigte, dass Dental LT eine glatte Oberfläche mit der besten Oberflächengüte hatte. Oberflächentexturen waren auf beiden Oberflächen von FREEPRINT tray und des PLA-Filaments zu finden, die Texturorientierungen der beiden Gruppen waren jedoch entgegengesetzt und rechtwinklig zueinander. Das lichthärtende Referenzharz zeigte eine poröse Oberfläche mit zahlreichen Tälern und wenigen Peaks. Die vier Löffelmaterialien unterschieden sich nicht statistisch in der Abziehfestigkeit von VSXE und PE, aber PLA und die Referenz zeigten eine höhere Schälfestigkeit mit VPS als die mit Dental LT und FREEPRINT tray. Bei der Verbindung mit Dental LT, FREEPRINT tray und dem Referenzmaterial zeigte die

Haftfestigkeit von VSXE und VPS keinen signifikanten Unterschied, beide waren jedoch höher als die von PE. Für das Verbinden mit dem PLA-Material zeigte VPS die höchste Abziehfestigkeit, gefolgt von der von VSXE, und die Abziehfestigkeit von PE war die niedrigste. Beim Abschälen von VSXE und VPS waren die gemischten Versagensraten bei PLA und der Referenz höher als bei Dental LT und FREEPRINT tray. Beim Ablösen von PE waren die Versagensarten der vier Löffelmaterialien überwiegend adhäsives Versagen. Kohäsive Ausfälle konnten nur in den VSXE-Gruppen gefunden werden. Die Bruchstelle des Klebstoffversagens lag in allen Gruppen teilweise an der Grenzfläche zwischen Klebstoff und Abdruckmaterial und teilweise innerhalb des Klebstoffs, jedoch niemals an der Grenzfläche zwischen Klebstoff und Probe.

Zusammenfassend wurde eine gute chemische Kompatibilität zwischen den 3D-gedruckten Abformmaterialien und den Klebstoffen erzielt. Die Oberflächentopografien der Löffelmaterialien beeinflussten die Haftfestigkeit der Schälverbindung, jedoch konnte nur der Rauheitsparameter (V_{vv}) teilweise mit der Haftfestigkeit der Schälverbindung in Zusammenhang gebracht werden. Die 3D-gedruckten Löffelmaterialien könnten eine gute Alternative zum herkömmlichen lichthärtenden Polymer sein, wenn das VSXE- oder PE-Abform-/Klebstoffsystem verwendet wird. Für das Verkleben mit dem VPS-Abform-/Klebstoffsystem scheint PLA ein ideales Löffelmaterial zu sein, wohingegen die Dental LT- und FREEPRINT tray Materialien möglicherweise eine weitere Oberflächenaufrauung erfordern.

8. References

1. Terry DA, Tric O, Blatz M, Burgess JO. The custom impression tray: Fabrication and utilization. *Dent Today*. 2010;29:132–4.
2. Kanazawa M, Iwaki M, Arakida T, Minakuchi S. Digital impression and jaw relation record for the fabrication of CAD/CAM custom tray. *J Prosthodont Res*. 2018;62(4):509–13.
3. Krishna CH, Mahendranadh Reddy K, Gupta N, Mahadev Shastry Y, Chandra Sekhar N, Aditya V, Reddy GVK. Fabrication of customized sectional impression trays in management of patients with limited mouth opening: a simple and unique approach. *Case Rep Dent*. 2013;2013.
4. Bomberg TJ, Hatch RA, Hoffman W. Impression material thickness in stock and custom trays. *J Prosthet Dent*. 1985;54(2):170–2.
5. Thongthammachat S, Moore BK, Barco MT, Hovijitra S, Brown DT, Andres CJ. Dimensional accuracy of dental casts: influence of tray material, impression material, and time. *J Prosthodont*. 2002;11(2):98–108.
6. Christensen GJ. The state of fixed prosthodontic impressions. *J Am Dent Assoc*. 2005;136(3):343–6.
7. Al-Namel H. Beginner Guide to Impression Trays in Dentistry [Internet]. 2015. Available on 29.04.2019 from: <https://www.slideshare.net/AsadiUsama/beginner-guide-to-impression-trays-in-dentistry>
8. Chen H, Yang X, Chen L, Wang Y, Sun Y. Application of FDM three-dimensional printing technology in the digital manufacture of custom edentulous mandible trays. *Sci Rep*. 2016;6:19207.
9. Shillingburg HT, Hatch RA, Keenan MP, Hemphill MW. Impression Materials and Techniques Used for Cast Restorations in Eight States. *J Am Dent Assoc*. 1980;100(5):696–9.
10. Strub JR, Rekow ED, Witkowski S. Computer-aided design and fabrication of dental restorations: current systems and future possibilities. *J Am Dent Assoc*. 2006;137(9):1289–96.
11. Huang Z, Wang X, Hou Y. Novel Method of Fabricating Individual Trays for Maxillectomy Patients by Computer - Aided Design and Rapid Prototyping. *J Prosthodont*. 2015;24(2):115–20.
12. Wei L, Chen H, Zhou YS, Sun YC, Pan SX. Evaluation of production and clinical working time of computer-aided design/computer-aided manufacturing (CAD/CAM) custom trays for complete denture. *J Peking Univ Heal Sci*. 2017;49(1):86–91.
13. Sun Y, Chen H, Li H, Deng K, Zhao T, Wang Y, Zhou Y. Clinical evaluation of final impressions from three-dimensional printed custom trays. *Sci Rep*. 2017;7(1):14958.
14. Qu F, Du X, Liu W-C. 3D-printed custom trays with a Gothic arch for centric relation recording and definitive impression making for complete dentures: A

- dental technique. *J Prosthet Dent.* 2019;121(1):32–6.
15. Revilla-León M, Sánchez-Rubio JL, Oteo-Calatayud J, Özcan M. Impression technique for a complete-arch prosthesis with multiple implants using additive manufacturing technologies. *J Prosthet Dent.* 2017;117(6):714–20.
 16. van Noort R. The future of dental devices is digital. *Dent Mater.* 2012;28(1):3–12.
 17. Ford S, Despeisse M. Additive manufacturing and sustainability: an exploratory study of the advantages and challenges. *J Clean Prod.* 2016;137:1573–87.
 18. Groth C, Kravitz ND, Jones PE, Graham JW, Redmond WR. Three-dimensional printing technology. *J Clin Orthod.* 2014;48(8):475–85.
 19. Gebhardt A. 3D-Drucken: Grundlagen und Anwendungen des additive manufacturing (AM). Carl Hanser Verlag GmbH Co KG; 2016. 1-3 p.
 20. Bhargav A, Sanjairaj V, Rosa V, Feng LW, Fuh YH J. Applications of additive manufacturing in dentistry: A review. *J Biomed Mater Res Part B Appl Biomater.* 2018;106(5):2058–64.
 21. Stansbury JW, Idacavage MJ. 3D printing with polymers: Challenges among expanding options and opportunities. *Dent Mater.* 2016;32(1):54–64.
 22. Barazanchi A, Li KC, Al - Amleh B, Lyons K, Waddell JN. Additive Technology: Update on Current Materials and Applications in Dentistry. *J Prosthodont.* 2016;26(2):156–63.
 23. Okwuosa TC, Stefaniak D, Arafat B, Isreb A, Wan K-W, Alhnan MA. A Lower Temperature FDM 3D Printing for the Manufacture of Patient-Specific Immediate Release Tablets. *Pharm Res.* 2016;33(11):2704–12.
 24. Alsoufi MS, Elsayed AE. How Surface Roughness Performance of Printed Parts Manufactured by Desktop FDM 3D Printer with PLA+ is Influenced by Measuring Direction. *Am J Mech Eng.* 2017;5(5):211–22.
 25. Ituarte IF, Chekurov S, Salmi M, Tuomi J, Partanen J. Post-processing opportunities of professional and consumer grade 3D printing equipment: a comparative study. *Int J Rapid Manuf.* 2015;5(1):58–75.
 26. Krishnan SP, Dawood A, Richards R, Henckel J, Hart AJ. A review of rapid prototyped surgical guides for patient-specific total knee replacement. *J Bone Joint Surg Br.* 2012;94-B(11):1457–61.
 27. Fortin T, Champleboux G, Lormée J, Coudert JL. Precise Dental Implant Placement in Bone Using Surgical Guides in Conjunction With Medical Imaging Techniques. *J Oral Implantol.* 2000;26(4):300–3.
 28. Xu Y, Unkovskiy A, Klaue F, Rupp F, Geis-Gerstorfer J, Spintzyk S. Compatibility of a Silicone Impression/Adhesive System to FDM-Printed Tray Materials—A Laboratory Peel-off Study. *Materials (Basel).* 2018;11(10).
 29. Zhang X, Jiang XN, Sun C. Micro-stereolithography of polymeric and ceramic microstructures. *Sensors Actuators A Phys.* 1999;77(2):149–56.
 30. Keyhan SO, Ghanean S, Navabazam A, Khojasteh A, Iranq MHA. Three-Dimensional Printing: A Novel Technology for Use in Oral and Maxillofacial Operations. In: *A Textbook of Advanced Oral and Maxillofacial*

- Surgery Volume 3. IntechOpen; 2016.
31. Hornbeck LJ. Digital Light Processing and MEMS: an overview. In: Digest IEEE/Leos 1996 Summer Topical Meeting Advanced Applications of Lasers in Materials and Processing. IEEE; 1996. p. 7–8.
 32. Kocovic P. 3D Printing and Its Impact on the Production of Fully Functional Components: Emerging Research and Opportunities: Emerging Research and Opportunities. IGI Global; 2017. 42 p.
 33. Abdullah MA, Talic YF. The effect of custom tray material type and fabrication technique on tensile bond strength of impression material adhesive systems. *J Oral Rehabil.* 2003;30(3):312–7.
 34. Carotte P V, Johnson A, Winstanley RB. The influence of the impression tray on the accuracy of impressions for crown and bridge work--an investigation and review. *Br Dent J.* 1998;185(11):580.
 35. Fehling AW, Hesby RA, Pelleu GB. Dimensional stability of autopolymerizing acrylic resin impression trays. *J Prosthet Dent.* 1986;55(5):592–7.
 36. Goldfogel M, Harvey WL, Winter D. Dimensional change of acrylic resin tray materials. *J Prosthet Dent.* 1985;54(2):284–6.
 37. Thongthammachat S, Moore BK, Barco MT, Hovijitra S, Brown DT, Andres CJ. Dimensional accuracy of dental casts: Influence of tray material, impression material, and time. *J Prosthodont.* 2002;11(2):98–108.
 38. Wirz J, Jaeger K, Schmidli F. Light-polymerized materials for custom impression trays. *Int J Prosthodont.* 1990;3(1):64–71.
 39. Maruo Y, Nishigawa G, Oka M, Minagi S, Irie M, Suzuki K. Tensile bond strength between custom tray and elastomeric impression material. *Dent Mater J.* 2007;26(3):323–8.
 40. Davis GB, Moser JB, Brinsden GI. The bonding properties of elastomer tray adhesives. *J Prosthet Dent.* 1976;36(3):278–85.
 41. Ashwini BL, Manjunath S, Mathew KX. The Bond Strength of Different Tray Adhesives on Vinyl Polysiloxane to Two Tray Materials: An In Vitro Study. *J Indian Prosthodont Soc.* 2014;14(1):29–37.
 42. Yi M-H, Shim J-S, Lee K-W, Chung M-K. Drying time of tray adhesive for adequate tensile bond strength between polyvinylsiloxane impression and tray resin material. *J Adv Prosthodont.* 2009;1(2):63–7.
 43. Chai JY, Jameson LM, Moser JB, Hesby RA. Adhesive properties of several impression material systems: Part I. *J Prosthet Dent.* 1991;66(2):201–9.
 44. Samman JM, Fletcher A. A study of impression tray adhesives. *Quintessence Int.* 1985 Apr;16(4):305–9.
 45. Grant BE, Tjan AHL. Tensile and peel bond strengths of tray adhesives. *J Prosthet Dent.* 1988;59(2):165–8.
 46. MacSween R, Price RB. Peel bond strengths of five impression material tray adhesives. *J Can Dent Assoc.* 1991;57(8):654–7.
 47. Rathee S, Eswaran B, Eswaran M, Prabhu R, Geetha K, Krishna G, Jagadeshwari. A Comparison of Dimensional Accuracy of Addition Silicone of Different

- Consistencies with Two Different Spacer Designs - In-vitro Study. *J Clin Diagn Res.* 2014;8(7):ZC38-ZC41.
48. Payne JA, Pereira BP. Bond strength of two nonaqueous elastomeric impression materials bonded to two thermoplastic resin tray materials. *J Prosthet Dent.* 1995;74(6):563–8.
 49. Marafie Y, Looney S, Nelson S, Chan D, Browning W, Rueggeberg F. Retention strength of impression materials to a tray material using different adhesive methods: an in vitro study. *J Prosthet Dent.* 2008;100(6):432–40.
 50. Peregrina A, Land MF, Wandling C, Johnston WM. The effect of different adhesives on vinyl polysiloxane bond strength to two tray materials. *J Prosthet Dent.* 2005;94(3):209–13.
 51. Ona M, Takahashi H, Sato M, Igarashi Y, Wakabayashi N. Effect of reactive adhesives on the tensile bond strength of polyvinyl siloxane impression materials to methyl methacrylate tray material. *Dent Mater J.* 2010;29(3):336–40.
 52. Lakshmi CBS, Umamaheswari B, Devarhubli AR, Pai S, Wadambe TN. An evaluation of compatibility of three different impression materials to three different tray acrylic materials using tray adhesives: An In vitro Study. *Indian J Dent Sci.* 2018;10(1):37–41.
 53. Nicholson JW, Porter KH, Dolan T. Strength of tray adhesives for elastomeric impression materials. *Oper Dent.* 1985;10(1):12–6.
 54. Tjan AHL, Whang SB. Comparing effects of tray treatment on the accuracy of dies. *J Prosthet Dent.* 1987;58(2):175–8.
 55. Bomberg TJ, Goldfogel MH, Hoffman W, Bomberg SE. Considerations for adhesion of impression materials to impression trays. *J Prosthet Dent.* 1988;60(6):681–4.
 56. Kumar S, Gandhi UV, Banerjee S. An In Vitro Study of the Bond Strength of Five Adhesives Used for Vinyl Polysiloxane Impression Materials and Tray Materials. *J Indian Prosthodont Soc.* 2014;14(1):61–6.
 57. Ramdev P, PA J. Influence of adhesives on the bond strength of Vinylpolysiloxane to acrylic tray material. *Int J Contemp Dent.* 2011;2(2):57–60.
 58. Bindra B, Heat J. Adhesion of elastomeric impression materials to trays. *J Oral Rehabil.* 1997;24(1):63–9.
 59. Dixon DL, Breeding LC, Brown JS. The effect of custom tray material type and adhesive drying time on the tensile bond strength of an impression material/adhesive system. *Int J Prosthodont.* 1994;7(2):129–33.
 60. Payne JA, Pereira BP. Bond strength of three nonaqueous elastomeric impression materials to a light-activated resin tray. *Int J Prosthodont.* 1992;5(1):55–8.
 61. Craig RG, Powers JM. Restorative dental materials. 11th editi. Mosby St. Louis (MO); 2001. 330-389 p.
 62. Stout K, Sullivan P, Dong W, Mainsah E, Luo N, Mathia T, Zahouani H. The development of methods for the characterization of roughness in three dimensions. London: Penton Press; 1993. 234-240 p.
 63. Jiang X, Blunt L, Stout K. Comparison study of areal functional parameters for

- rough surfaces [Internet]. Poster presented at: Annual Metrology - Analysis and Modeling. Nashville: Proc ASPE; 2000. Available on 29.04.2019 from: http://www.aspe.net/publications/Annual_2000/PDF/POSTERS/METROL/ANALYSIS/JIANG.PDF
64. Deltombe R, Kubiak KJ, Bigerelle M. How to select the most relevant 3D roughness parameters of a surface. *Scanning J Scanning Microsc.* 2014;36(1):150–60.
 65. Leach R. *Characterisation of areal surface texture*. Springer; 2013. 20 p.
 66. Hogans III WR, Agar JR. The bond strength of elastomer tray adhesives to thermoplastic and acrylic resin tray materials. *J Prosthet Dent.* 1992;67(4):541–3.
 67. Rubel BS. *Impression Materials: A Comparative Review of Impression Materials Most Commonly Used in Restorative Dentistry*. *Dent Clin North Am.* 2007;51(3):629–42.
 68. Jamani KD, Harrington E, Wilson HJ. Rigidity of elastomeric impression materials. *J Oral Rehabil.* 1989;16(3):241–8.
 69. Leung KCM, Chow TW, Woo ECW, Clark RKF. Effect of adhesive drying time on the bond strength of irreversible hydrocolloid to stainless steel. *J Prosthet Dent.* 1999;81(5):586–90.
 70. Leung KCM, Chow TW, Woo CW, Clark RKF. Tensile, shear and cleavage bond strengths of alginate adhesive. *J Dent.* 1998;26(7):617–22.
 71. Dixon DL, Breeding LC, Bosser MJ, Nafso AJ. The effect of custom tray material type and surface treatment on the tensile bond strength of an impression material/adhesive system. *Int J Prosthodont.* 1993;6(3):303–6.
 72. Ellam AH, Smith DC. The relative effectiveness of adhesives for polysulphide impression materials. *Br Dent J.* 1966;120(3):135.
 73. Wilson HJ. The bonding of alginate impression materials to impression trays. *Br Dent J.* 1963;115:291–4.
 74. Kawamura M. The bonding of rubber impression materials to tray materials. *J Osaka Odontol Soc.* 1970;33:359.
 75. Moergeli Jr JR, Vermilyea SG. Changes in pH of irreversible hydrocolloid impression materials during setting. *J Prosthet Dent.* 1986;56(3):342–3.
 76. Sotiriou M, Hobkirk JA. An in vivo investigation of seating and removal forces associated with recording impressions in dentate patients. *J Prosthet Dent.* 1995;74(5):455–62.
 77. Dixon DL, Breeding LC, Moseley JP. Custom impression trays. Part II: Removal forces. *J Prosthet Dent.* 1994;71(3):316–8.

Unpublished findings: part of the present study is being prepared for journal and conference publication.

Appendix

Statistical analysis tables

Table 8: Shapiro-Wilk normality test of Sa (n = 7).

	Dental LT	FREEPRINT tray	PLA	Reference
W	0.930	0.833	0.838	0.924
P value	0.547	0.085	0.094	0.498
Sum	11.590	45.050	78.140	30.040

Table 9: Shapiro-Wilk normality test of Ssk (n = 7).

	Dental LT	FREEPRINT tray	PLA	Reference
W	0.932	0.858	0.980	0.884
P value	0.565	0.146	0.960	0.242
Sum	-8.475	-2.149	-2.827	-20.920

Table 10: Shapiro-Wilk normality test of Vvc (n = 7).

	Dental LT	FREEPRINT tray	PLA	Reference
W	0.960	0.861	0.900	0.913
P value	0.822	0.156	0.333	0.416
Sum	0.015	0.057	0.106	0.019

Table 11: Shapiro-Wilk normality test of Vvv (n = 7).

	Dental LT	FREEPRINT tray	PLA	Reference
W	0.925	0.947	0.915	0.895
P value	0.509	0.699	0.428	0.303
Sum	0.003	0.004	0.012	0.013

Table 12: Shapiro-Wilk normality test of Sdr (n = 7).

	Dental LT	FREEPRINT tray	PLA	Reference
W	0.887	0.846	0.830	0.937
P value	0.257	0.113	0.080	0.611
Sum	11.260	64.420	113.500	57.060

Table 13. Shapiro-Wilk normality test of line peel strength (n = 12).

		W	P value	Sum
VSXE	Dental LT	0.921	0.291	21717
	FREEPRINT tray	0.905	0.184	22026
	PLA	0.974	0.950	22942
	Reference	0.899	0.153	22569
VPS	Dental LT	0.871	0.067	20166
	FREEPRINT tray	0.931	0.395	20570
	PLA	0.955	0.709	26079
	Reference	0.968	0.891	24418
PE	Dental LT	0.882	0.092	14105
	FREEPRINT tray	0.887	0.107	14474
	PLA	0.915	0.249	15895
	Reference	0.948	0.608	14395

Table 14. Shapiro-Wilk normality test of areal peel strength (n = 12).

		W	P value	Sum
VSXE	Dental LT	0.919	0.276	852.6
	FREEPRINT tray	0.900	0.158	854.5
	PLA	0.976	0.959	903.7
	Reference	0.904	0.179	891.7
VPS	Dental LT	0.870	0.066	792.6
	FREEPRINT tray	0.930	0.382	811.6
	PLA	0.955	0.713	1030.0
	Reference	0.971	0.923	964.1
PE	Dental LT	0.886	0.104	553.4
	FREEPRINT tray	0.890	0.119	573.3
	PLA	0.914	0.243	626.6
	Reference	0.948	0.610	565.2

Table 15: One-way ANOVA of Sa.

	SS	DF	MS	F	P value
Between groups	340.1	3	113.4	41.78	< 0.0001
Within groups	65.12	24	2.713		
Total	405.2	27			

Table 16: Tukey's multiple comparisons test of Sa (n = 7).

		Mean Diff.	95% CI of diff.	P value
Dental LT	FREEPRINT tray	-4.780	-7.209 to -2.351	< 0.0001
	PLA	-9.507	-11.940 to -7.078	< 0.0001
	Reference	-2.636	-5.065 to -0.207	0.0299
FREEPRINT tray	PLA	-4.727	-7.156 to -2.298	< 0.0001
	Reference	2.144	-0.285 to 4.573	0.0971
PLA	Reference	6.871	4.443 to 9.300	< 0.0001

Table 17: One-way ANOVA of Ssk.

	SS	DF	MS	F	P value
Between groups	32.39	3	10.80	41.78	< 0.0001
Within groups	6.258	24	0.2607		
Total	38.65	27			

Table 18: Tukey's multiple comparisons test of Ssk (n = 7).

		Mean Diff.	95% CI of diff.	P value
Dental LT	FREEPRINT tray	-0.904	-1.657 to -0.151	0.0145
	PLA	-0.807	-1.560 to -0.054	0.0325
	Reference	1.778	1.025 to 2.531	< 0.0001
FREEPRINT tray	PLA	0.097	-0.656 to 0.850	0.9843
	Reference	2.682	1.929 to 3.435	< 0.0001
PLA	Reference	2.585	1.832 to 3.338	< 0.0001

Table 19: One-way ANOVA of Vvc.

	SS	DF	MS	F	P value
Between groups	7.695e-004	3	2.565e-004	74.55	< 0.0001
Within groups	8.257e-005	24	3.441e-006		
Total	8.520e-004	27			

Table 20: Tukey's multiple comparisons test of Vvc (n = 7).

		Mean Diff.	95% CI of diff.	P value
Dental LT	FREEPRINT tray	-0.006	-0.009 to -0.003	< 0.0001
	PLA	-0.013	-0.016 to -0.010	< 0.0001
	Reference	-0.001	-0.003 to 0.002	0.8920
FREEPRINT tray	PLA	-0.007	-0.010 to -0.004	< 0.0001
	Reference	0.005	0.003 to 0.008	< 0.0001
PLA	Reference	0.012	0.010 to 0.015	< 0.0001

Table 21: One-way ANOVA of Vvv.

	SS	DF	MS	F	P value
Between groups	1.268e-005	3	4.226e-006	29.82	< 0.0001
Within groups	3.401e-006	24	1.417e-007		
Total	1.608e-005	27			

Table 22: Tukey's multiple comparisons test of Vvv (n = 7).

		Mean Diff.	95% CI of diff.	P value
Dental LT	FPt ^a	-1.676e-004	-7.226e-004 to 3.875e-004	0.8384
	PLA	-1.378e-003	-1.933e-003 to -8.228e-004	< 0.0001
	Reference	-1.468e-003	-2.023e-003 to -9.128e-004	< 0.0001
FPt ^a	PLA	-1.210e-003	-1.765e-003 to -6.552e-004	< 0.0001
	Reference	-1.300e-003	-1.855e-003 to -7.452e-004	< 0.0001
PLA	Reference	-9.000e-005	-6.451e-004 to 4.651e-004	0.9695

a. FPt = FREEPRINT tray

Table 23: One-way ANOVA of Sdr.

	SS	DF	MS	F	P value
Between groups	750.9	3	250.3	49.25	< 0.0001
Within groups	122.0	24	5.082		
Total	872.9	27			

Table 24: Tukey's multiple comparisons test of Sdr (n = 7).

		Mean Diff.	95% CI of diff.	P value
Dental LT	FPt ^a	-7.594	-10.920 to -4.270	< 0.0001
	PLA	-14.610	-17.930 to -11.280	< 0.0001
	Reference	-6.543	-9.867 to -3.219	< 0.0001
FPt ^a	PLA	-7.011	-10.340 to -3.687	< 0.0001
	Reference	1.051	-2.273 to 4.376	0.8189
PLA	Reference	8.063	4.739 to 11.390	< 0.0001

a. FPt = FREEPRINT tray

Table 25: Tukey's multiple comparisons test of line peel strength among tray materials under each impression/adhesive system level (simple main effect analysis, n = 12).

			Mean Diff.	95% CI of diff.	P value
VSXE	Dental LT	FPt ^a	-25.8	-245.8 to 194.2	0.9901
		PLA	-102.1	-322.1 to 117.9	0.6231
		Reference	-71.1	-291.0 to 148.9	0.8350
	FPt ^a	PLA	-76.3	-296.3 to 143.7	0.8034
		Reference	-45.3	-265.3 to 174.7	0.9502
		PLA	Reference	31.0	-188.9 to 251.0
VPS	Dental LT	FPt ^a	-33.6	-253.6 to 186.3	0.9786
		PLA	-492.7	-712.7 to -272.7	< 0.0001
		Reference	-354.3	-574.3 to -134.3	0.0003
	FPt ^a	PLA	-459.1	-679.0 to -239.1	< 0.0001
		Reference	-320.7	-540.7 to -100.7	0.0013
		PLA	Reference	138.4	-81.6 to 358.4
PE	Dental LT	FPt ^a	-30.8	-250.7 to 189.2	0.9835
		PLA	-149.2	-369.2 to 70.8	0.2951
		Reference	-24.1	-244.1 to 195.8	0.9919
	FPt ^a	PLA	-118.4	-338.4 to 101.6	0.5012
		Reference	6.6	-213.4 to 226.6	0.9998
		PLA	Reference	125.0	-94.9 to 345.0

a. FPt = FREEPRINT tray

Table 26: Tukey's multiple comparisons test of line peel strength among impression/adhesive systems under each tray material level (simple main effect analysis, n = 12).

			Mean Diff.	95% CI of diff.	P value
Dental LT	VSXE	VPS	129.2	-71.2 to 329.6	0.2810
		PE	634.3	433.9 to 834.7	< 0.0001
FPt ^a	VSXE	VPS	505.1	304.7 to 705.5	< 0.0001
		PE	629.3	428.9 to 829.7	< 0.0001
PLA	VSXE	VPS	508.0	307.6 to 708.4	< 0.0001
		PE	848.6	648.2 to 1049.0	< 0.0001
Reference	VSXE	VPS	-154.1	-354.5 to 46.3	0.1663
		PE	681.2	480.8 to 881.6	< 0.0001
	VPS	PE	835.3	634.9 to 1036.0	< 0.0001

a. FPt = FREEPRINT tray

Table 27: Tukey's multiple comparisons test of areal peel strength among tray materials under each impression/adhesive system level (simple main effect analysis, n = 12).

			Mean Diff.	95% CI of diff.	P value
VSXE	Dental LT	FPt ^a	-0.2	-8.8 to 8.5	> 0.9999
		PLA	-4.3	-12.9 to 4.4	0.5768
		Reference	-3.3	-11.9 to 5.4	0.7612
FPt ^a	PLA	Reference	-4.1	-12.8 to 4.6	0.6068
		Reference	-3.1	-11.8 to 5.6	0.7875
		Reference	1.0	-7.7 to 9.7	0.9905
VPS	Dental LT	FPt ^a	-1.6	-10.2 to 7.1	0.9645
		PLA	-19.8	-28.5 to -11.2	< 0.0001
		Reference	-14.3	-23.0 to -5.6	0.0002
FPt ^a	PLA	Reference	-18.2	-26.9 to -9.6	< 0.0001
		Reference	-12.7	-21.4 to -4.0	0.0012
		Reference	5.5	-3.1 to 14.2	0.3484
PE	Dental LT	FPt ^a	-1.7	-10.3 to 7.0	0.9592
		PLA	-6.1	-14.8 to 2.6	0.2628
		Reference	-1.0	-9.6 to 7.7	0.9910
FPt ^a	PLA	Reference	-4.4	-13.1 to 4.2	0.5433
		Reference	0.7	-8.0 to 9.3	0.9970
		Reference	5.1	-3.5 to 13.8	0.4184

a. FPt = FREEPRINT tray

Table 28: Tukey's multiple comparisons test of line peel strength among impression/adhesive systems under each tray material level (simple main effect analysis, n = 12).

			Mean Diff.	95% CI of diff.	P value
Dental LT	VSXE	VPS	5.0	-2.9 to 12.9	0.2942
		PE	24.9	17.0 to 32.8	< 0.0001
	VPS	PE	19.9	12.1 to 27.8	< 0.0001
FPt ^a	VSXE	VPS	3.6	-4.3 to 11.5	0.5328
		PE	23.4	15.5 to 31.3	< 0.0001
	VPS	PE	19.9	12.0 to 27.8	< 0.0001
PLA	VSXE	VPS	-261.4	-461.8 to -61.0	0.0053
		PE	587.2	386.8 to 787.6	< 0.0001
	VPS	PE	848.6	648.2 to 1049.0	< 0.0001
Reference	VSXE	VPS	-6.0	-13.9 to 1.9	0.1695
		PE	27.2	19.3 to 35.1	< 0.0001
	VPS	PE	33.3	25.4 to 41.1	< 0.0001

a. FPt = FREEPRINT tray

Declaration of contribution

The present study was conceptualized by Prof. Dr. Jürgen Geis-Gerstorfer and Mr. Sebastian Spintzyk. This project was validated, administrated and supervised by Prof. Dr. Jürgen Geis-Gerstorfer.

The experiment methods were discussed and determined by Mr. Sebastian Spintzyk, Dr. Fabian Hüttig, and Yichen Xu. Part of the impression material was provided by Dr. Fabian Hüttig, and the other experiment materials were provided by Section of Medical Material Science and Technology, University Hospital Tübingen.

The original CAD file of the test block was provided by Mr. Felix Klaue, and Yichen Xu did the subsequent redesign by error correction. The CAD of reference test block mold, the wax spacer mold and the carrier was performed independently by Yichen Xu. All test blocks were either 3D-printed or manually fabricated by Yichen Xu.

The SEM analysis was executed by Mr. Ernst Schweizer (sample sputtering and SEM operation) and Yichen Xu (sample preparation). The roughness measurement was performed by Yichen Xu. The peel bond strength test was carried out by Ms. Christine Schille (universal testing machine operation) and Yichen Xu (sample preparation). Mr. Sebastian Spintzyk and Yichen Xu together defined the classification of the failure mode (Table 4). Yichen Xu performed the classification and microscopical analysis of the failure mode. All data processing, statistical analysis, and graph making were done by Yichen Xu.

The manuscript was written by Yichen and corrected by Prof. Dr. Jürgen Geis-Gerstorfer. The entire study was carried out in Section of Medical Material Science and Technology, University Hospital Tübingen. Therefore, I clarify that the present thesis is the original work of Yichen Xu. All assistance was gratefully acknowledged.

Tübingen
Yichen Xu

Acknowledgment

I would like to sincerely thank my supervisor, Prof. Dr. Jürgen Geis-Gerstorfer, for giving me a precious opportunity to study in Germany. In the past three years, Prof. Geis-Gerstorfer helped me both in my life and study patiently, kindly and selflessly, so that I could overcome the difficulties and finish my study. I have learned from him that one should keep a keen heart and a rigorous attitude towards science to pursue the truth from the nuances. What he taught me is the most precious treasure that I will hold in my hand to dedicate the rest of my life to dentistry.

I want to gratefully acknowledge my co-supervisor, Mr. Sebastian Spintzyk. From the beginning of touching the concept of 3D-printing to being familiar with various CAD software and AM technologies, Mr. Spintzyk brought me into this new field and patiently guided me step by step. I could benefit from every discussion with him due to his insightful scientific thoughts.

Many grateful thanks would be given to Dr. Fabian Hüttig, for his clinical suggestions and for providing the impression material; to Prof. Dr. Frank Rupp, for his guidance in surface topography; to Dr. Lutz Scheideler, for his advice in scientific writing; to Ms. Christine Schille, for her assistance in peel test; and to Mr. Ernst Schweizer, for his help in SEM analysis.

I desire to thank my colleagues Ms. Evi Kimmerle-Müller, Ms. Ingrid Stephan, Mr. Günter Wedenig, Ms. Marion Hampel, Ms. Zeqian Xu, Ms. Xingting Han, Mr. Ping Li, and Mr. Mohamed Younis, who gave me a lot of help and support. I appreciated the happy time working with them.

At last, I would like to thank the Chinese Scholarship Council for financial support (Grant 201606240087) and my parents for their encouragement.

Curriculum Vitae

Personal Information

Name: Yichen Xu

Gender: Male

Date of birth: 10.10.1988

Nationality: Chinese



Education

09. 2004 – 06. 2007	Chengdu No.7 Middle School, Sichuan Province
09. 2007 – 06. 2012	West China school of Stomatology, Sichuan University, Bachelor Degree (Dental Medicine)
09. 2013 – 06. 2016	West China school of Stomatology, Sichuan University, Master Degree (Dental Medicine)
Since 10. 2016	Department of Prosthodontics and Section “Medical Materials and Technology”, University Hospital Tuebingen, Doctor Degree (Dr. med. dent)

Science Experience and Scholarship

- Project: University Student Scientific Research Training Project.

Topic: Investigation of subjective demand of orthodontic treatment for middle school students in zones with different economic levels.

Year: 2009 - 2010
- Project: National Undergraduate Innovating Experiment.

Topic: A exploratory study on the relationship between 6 – 12 years old children’s dental anxiety disorder and parents’ factors.

Year: 2011 - 2012
- Project: The National Natural Science Foundation of China.

Topic: The modification of implant collar by anodizing and poly-dopamine coating.

Year: 2013 - 2014

- Project: In Vivo and in Situ Tissue Engineering Materials for Dental Application.
Topic: Fabrication of osteoplastic scaffold materials and exploration of controlled release of growth factors.
Year: 2014 – 2016
- Project: Investigation of additive manufacturing of individual trays for complete dentures.
Year: 2016 – 2019
- Project: A laboratory study on the accuracy and compressive strength of 3D-printed dental casts.
Year: Since 2018
- Project: The effect of post-processing on the cytotoxicity of a 3D-printing splint material for orthodontic application.
Year: Since 2019
- Scholarship from the Chinese Scholarship Council, 2016 – 2019

Publications

1. Xu, Y., Unkovskiy, A., Klaue, F., Rupp, F., Geis-Gerstorfer, J., & Spintzyk, S. (2018). Compatibility of a Silicone Impression/Adhesive System to FDM-Printed Tray Materials—A Laboratory Peel-off Study. *Materials*, 11(10), 1905.
2. Teng, F., Chen, H., Xu, Y., Liu, Y., & Ou, G. (2018). Polydopamine deposition with anodic oxidation for better connective tissue attachment to transmucosal implants. *Journal of periodontal research*, 53(2), 222-231.
3. Xu, Y., Ou, G. (2016). Research advances of hydrogels formed by Michael-Type addition reactions [article in Chinese]. *West China journal of stomatology*, 34(supplement), 260-265.

4. Xu, Y., Li, J., Luo, W., Chen, Z., Teng, F., Ou, G. (2015). The application of bone splitting for simultaneous placement of dental implant in aesthetical zones of maxillary [article in Chinese]. Chinese clinical annual book of implant dentistry, 86-93.
5. Xu, Y. (2011). The research progress in the influential factors of the bond strength of fiber posts [article in Chinese]. China modern doctor magazine, 49(23), 27-29.
6. Chen, G., Yin, B., Zhao, Q., Xu, Y., Huo, J., Li, Z., Meng, M., Chen, Y. (2012). Investigation of differences in subjective demand for orthodontic treatment of middle school students in zones with different economic levels [article in Chinese]. West China journal of stomatology, 30(4), 407-410.

Certificate

Dental practitioner's qualification certificate of People's Republic of China (licensed since 2014).